
CARLETON ELECTRONICS RESEARCH LABORATORY

Department of Electronics
Carleton University
Ottawa, Canada K1S 5B6

LINEARIZATION TECHNIQUES FOR
EFFICIENT UHF-SHF
SOLID-STATE POWER AMPLIFIERS

By
T. W. TARASCHUK

[Principal Investigator: R. G. HARRISON]

Technical Report No: **CERL - 85 - 01**

IC

D.O.C. Serial No. OSV83-00049
D.S.S. File No. 19SV.36100-3-0171

LINEARIZATION TECHNIQUES FOR
EFFICIENT UHF-SHF SOLID-STATE
POWER AMPLIFIERS

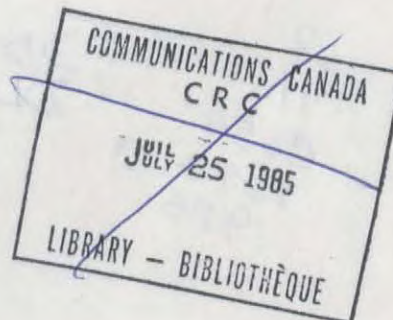
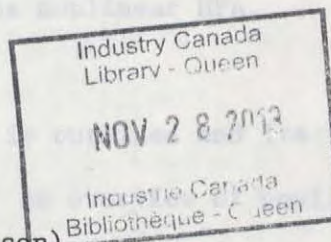
Interim Report

for the Department of Communications,
Communications Research Centre,
Ottawa, Ontario, Canada, K2H 8S2

Submitted according to the terms of
Department of Communications Contract Serial No. OSV83-00049,
Department of Supply and Services File No. 19SV.36100-3-0171.

Prepared by: T.W. Taraschuk
(Principal Investigator: R.G. Harrison)

Department of Electronics
Carleton University
Ottawa, Ontario, Canada
K1S 5B6

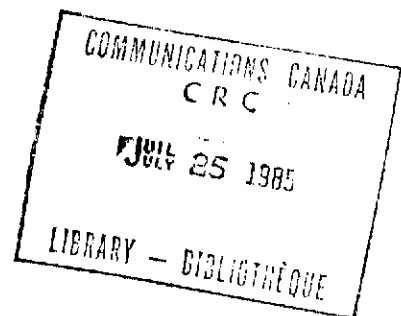


March 1985

ABSTRACT

The amplification of microwave signals is corrupted by nonlinearities present in typical high power amplifiers (HPA). Undesired intermodulation products and significant AM-to-AM and AM-to-PM conversion may result. A relatively simple remedy to this problem is the intentional predistortion of the input signal prior to amplification by the nonlinear HPA.

In this report, a 900 MHz, RF predistorter is outlined and its performance in an adaptive system is presented. An overview of nonlinear analysis methods suitable for modelling general nonlinear and predistortion processes is also included.



ACKNOWLEDGEMENTS

I am pleased to acknowledge my indebtedness and gratitude to Professor Robert Harrison. His supervision and careful review of this report are very much appreciated.

I wish to thank Dr. W.D. Hindson, Communications Research Centre, Shirley's Bay, for providing funding for this research. Without his efforts, this project would not have been possible.

I would also like to express my gratitude to Mr. Nagui Mikhail, Carleton University, whose technical aid was found to be invaluable.

Finally, I wish to thank the Faculty, staff and students of the Department of Electronics for their support and friendship.

TABLE OF CONTENTS

ABSTRACT		i
ACKNOWLEDGEMENTS		ii
LIST OF FIGURES		vi
LIST OF SYMBOLS		ix
CHAPTER 1	<u>AN OVERVIEW OF NONLINEAR SYSTEMS</u>	1
1.1	Introduction	1
1.2	Classification of Nonlinear Systems	2
1.2.1	Nonlinear systems without memory	2
1.2.2	Nonlinear systems effectively without memory	5
1.2.3	Nonlinear systems with memory	9
1.3	Analysis Methods for Nonlinearities	10
1.3.1	Introduction	10
1.3.2	Classical power series	10
1.3.3	Fourier methods	11
1.3.4	Chebyshev transform methods	13
1.3.5	A mathematical description of phase nonlinearities and resultant AM-to-PM conversion: nonlinear envelope modelling	16
1.3.6	Power series with frequency response	21
1.3.7	Volterra series	28
1.3.7.1	Volterra response for multiple sinusoidal inputs	30
CHAPTER 2	<u>CORRECTION METHODS FOR MICROWAVE AMPLIFIER NONLINEARITIES</u>	35
2.1	Introduction	35
2.1.1	Power back-off	36
2.1.2	Negative feedback	38
2.1.3	Feedforward	38
2.1.4	Predistortion/postdistortion techniques	40
2.1.5	Linear amplification with nonlinear components (LINC)	42

CHAPTER 3	<u>PREDISTORTION: CONCEPT AND THEORY</u>	46
	3.1 A Heuristic View of Predistortion	46
	3.1.1 Cascading of transfer functions	47
	3.1.2 Cascading of power series	51
	3.1.3 Envelope transfer function linearization: Cascading of the Chebyshev transform	54
	3.1.4 Cascaded Volterra series	59
	3.1.5 The creation of new nonlinear products for cascaded systems	68
	3.1.6 Predistortion system performance for upconverted systems	71
	3.1.7 Effect of predistortion on amplifier efficiency	75
	3.2 Summary of Theoretical Advancements	76
CHAPTER 4	<u>RF PREDISTORTER DESIGN</u>	78
	4.1 Introduction	78
	4.2 Proposed RF Predistortion System	78
	4.3 Development of an RF Predistorter	80
	4.4 A Proposed Concave, Convex Predistorter	113
CHAPTER 5	<u>AN ADAPTIVE COMPLEX RF PREDISTORTION SYSTEM</u>	117
	5.1 Introduction	117
	5.2 "In-Phase/Quadrature" System Realization	117
	5.3 Adaptive Control	123
CHAPTER 6	<u>EXPERIMENTAL RESULTS</u>	131
	6.1 Introduction	131
	6.2 Predistorter Results	131
	6.3 HPA Characteristics	139
	6.4 Predistortion System Performance	142
	6.4.1 System performance; optimization at 27 dBm	143
	6.4.2 System performance; optimization at 30 dBm	149
	6.4.3 Ideal predistorter transfer characteristics	156
	6.4.4 Three-tone intermodulation performance	160
CHAPTER 7	<u>CONCLUSIONS AND RECOMMENDATIONS FOR FUTURE WORK</u>	169
APPENDIX 1:	NOTES ON LINEAR INDEPENDENCE	172
APPENDIX 2:	SELECTED CHEBYSHEV TRANSFORMS	176
APPENDIX 3:	5080-3080 /5082-2810 DIODE SPECIFICATIONS	178

APPENDIX 4:	MEASUREMENT APPARATUS	183
APPENDIX 5:	AMPLIFIER SPECIFICATIONS	186
REFERENCES		188

LIST OF FIGURES

1.1a	Piecewise Linear Limiter	4
1.1b	Comparator	4
1.2	"In-phase/quadrature" representation	7
1.3	"In-phase/quadrature" representation	8
1.4	Fourier series representation	12
1.5	Periodic extension of Fourier representation	12
1.6	Power series with frequency response system block	22
2.1	Dual amplifier topology	37
2.2	Feedforward distortion reduction topology	39
2.3a	Predistortion system	41
2.3b	Predistortion system	41
2.4	"In-phase/quadrature" predistortion topology	43
2.5	LINC topology	44
3.1	Cascaded amplitude transfer functions	48
3.2	Cascaded phase transfer functions	50
3.3	Cascaded power series	52
3.4	Cascading of the Chebyshev transform	55
3.5	"In-phase/quadrature" predistortion system	60
3.6	Cascaded Volterra system	61
3.7	Power series with frequency response cascade	69
3.8	Cascaded third-order systems	70
3.9	Predistortion system with upconversion	72
4.1a	"In-phase/quadrature" predistorter	79
4.1b	Phase modulator predistorter	79
4.2	Anode to cathode nonlinear element	82
4.3	High frequency predistorter	83
4.4	Schottky diode model	85
4.5	Impedance contour of diode model with varying resistance	86
4.6	Resonated impedance contour	88
4.7	General nonlinear reflection network	89
4.8	Transformed Schottky diode pair	91
4.9	Transformed impedance contour	92
4.10	Voltage divider topology	94
4.11	Shunt PIN diode topology	95
4.12	General two-port network	96
4.13	RF predistorter topology	98
4.14	RF predistorter implementation	100
4.15	Analysis of the RF predistorter	102
4.16	Theoretical predistorter transfer characteristic, G varying	107
4.17	Theoretical predistorter transfer characteristic, V_{BIAS} varying	108
4.18	Microstrip structure for the predistorter	109
4.19	Detail of the predistorter elements	110
4.20	Predistorter bias structure	111

4.21	Predistortion system implementation	114
4.22	Predistorters with circulator isolators	115
4.23	Proposed concave-convex predistorter	116
5.1	Conceptual "in-phase/quadrature" system	118
5.2	Microwave "in-phase/quadrature" topology	120
5.3	45° reference "in-phase/quadrature" system	122
5.4a	Complex predistortion system	126
5.4b	Complex predistortion system	127
5.4c	Complex predistortion system	128
5.4d	Adaptive A/D, D/A boards	128
6.1	Predistorter amplitude characteristic, PIN current varying	133
6.2	Predistorter phase characteristic, PIN current varying	134
6.3	Predistorter amplitude characteristic, V_{BIAS} varying	135
6.4	Predistorter phase characteristic, V_{BIAS} varying	136
6.5	Predistorter amplitude characteristic, frequency varying	137
6.6	Predistorter phase characteristic, frequency varying	138
6.7	Static AM-to-AM HPA transfer characteristic	140
6.8	Static AM-to-PM HPA transfer characteristic	141
6.9	Static amplitude characteristics	144
6.10	Static phase characteristics	146
6.11	Third-order carrier to intermodulation ratios	147
6.12	Fifth-order carrier to intermodulation ratios	148
6.13	Two-tone intermodulation spectrum for the HPA	150
6.14	Two-tone intermodulation spectrum for the linearized HPA	151
6.15	Static amplitude characteristics	152
6.16	Static phase characteristics	153
6.17	Third-order carrier to intermodulation ratios	154
6.18	Fifth-order carrier to intermodulation ratios	155
6.19	Two-tone intermodulation spectrum for the HPA	157
6.20	Two-tone intermodulation spectrum for the linearized HPA	158
6.21	Ideal predistorter characteristics	159
6.22	HPA three-tone intermodulation spectrum. Output power = 27.07 dBm.	161
6.23	Linearized three-tone intermodulation spectrum. Output power = 27.09 dBm.	162
6.24	HPA three-tone intermodulation spectrum. Output power = 27.25 dBm.	163
6.25	Linearized three-tone intermodulation spectrum. Output power = 27.25 dBm.	164
6.26	HPA three-tone intermodulation spectrum. Output power = 27.66 dBm.	165
6.27	Linearized three-tone intermodulation spectrum. Output power = 27.66 dBm.	166
6.28	HPA three-tone intermodulation spectrum. Output power = 27.53 dBm.	167

6.29	Linearized three-tone intermodulation spectrum. Output power = 27.53 dBm.	168
7.1	Proposed predistortion system	171

LIST OF SYMBOLS

A	Amplitude of a sinusoidal signal.
A	Linear gain of an amplifier.
AM	Amplitude modulation.
a	Incident wave amplitude normalized to $\sqrt{Z_0}$.
a_n	Taylor series coefficient of order n.
$\alpha(t)$	Instantaneous phase of a sinusoidal signal.
B.P.F.	Bandpass filter.
BW	Bandwidth.
b	Reflected wave amplitude normalized to $\sqrt{Z_0}$.
$b(v_{IN})$	Voltage dependent reflected wave amplitude normalized to $\sqrt{Z_0}$.
b_ℓ	Fourier series coefficient of order ℓ .
b_m	Taylor series coefficient of order m.
C_{Bypass}	Bypass capacitor.
C_I	Diode junction capacitance.
C_P	Diode parasitic packaging capacitance.
$C_{xx}(t_1, t_2)$	Covariance function of process X.
C/I	Logarithmic carrier-to-intermodulation ratio.
D.C.	Direct current.
dB	Decibel.
dBm	Decibel referenced to 1 mW.
$E(X)$	Expected value of process X.
E_M	Maximum input amplitude of a sinusoidal signal.

E_q	Amplitude of sinusoidal signal at frequency ω_q .
ϵ_r	Relative dielectric constant.
$F(A)$	AM-to-PM coefficient.
$F(A, \omega)$	Frequency dependent AM-to-PM coefficient.
FM	Frequency modulation.
$f(v_{IN})$	A function of the input voltage.
f_c	Local oscillator frequency.
f_{IN}	Frequency of an input signal.
G	Linear gain of an amplifier.
G	Conductance.
$G(A)$	AM-to-AM coefficient
$G(A, \omega)$	Frequency dependent AM-to-AM coefficient.
$G_n(\omega_1, \dots, \omega_n)$	n^{th} -order Volterra frequency transfer function.
$g^{-1}(Ax)$	Mathematical inverse function of $g(Ax)$.
g_l	Taylor series coefficient of order l .
$\Gamma(v_{IN})$	Amplitude dependent reflection coefficient.
$\Gamma(n)$	Gamma function of n .
HPA	High power amplifier.
$H(\omega)$	Linear complex frequency response.
H_k	Volterra transfer function of order k .
$H_n(\omega_1, \dots, \omega_n)$	Volterra transfer function of order n .
h_l	Taylor series coefficient of order l .
$h_n(\tau_1, \dots, \tau_n)$	n^{th} -order impulse response.
IF	Intermediate frequency.
$I_m(x)$	Modified Bessel function of the first kind of order m .

i_D	Net anti-parallel diode current.
i_O	Single diode current.
$J_m(x)$	Bessel function of the first order of order m .
j	Imaginary operator, $\sqrt{-1}$.
$K(\omega)$	Linear complex frequency response.
$K_2(\omega_1, \omega_2)$	Volterra transfer function of order 2.
K_s	Diode saturation current.
L	Inductance.
L	Length of a transmission line.
LINC	Linear amplification with nonlinear components.
λ	Electrical wavelength.
λ	Semiconductor parameter, q/nKT
M	Frequency mix vector.
MHz	Standard unit of frequency.
M_{OUT}	Output frequency mix vector.
MSAT	Mobile satellite program.
m_k	Number of times that frequency component at ω_k appears in the frequency mix vector.
n	Semiconductor diode ideality factor.
Ω	Unit of resistance, Ohms.
ω	Angular frequency.
ω_M	Angular frequency given by the frequency mix vector.
ω_c	Angular frequency of the local oscillator.
ω_k	Angular frequency of the k^{th} component.
ω_o	Angular frequency of an input sinusoid.

ω_q	Angular frequency of the q^{th} sinusoid.
ω_{q_n}	Double-indexed angular frequency notation.
$P(A)$	In-phase component of an output signal.
PM	Phase modulation.
P_{DISS}	Power dissipated in a network.
P_{IN}	Power input to a network.
P_{out}	Output power from an HPA.
P_{REF}	Power reflected from a network.
$\phi(v_{\text{IN}})$	Amplitude dependent phase.
$\phi(\omega)$	Linear phase-frequency characteristic.
$\phi(t)$	Time-varying phase.
$\phi_{\text{OUT}_{\text{BP}}}$	Bandpass output phase.
ψ_1	Output phase from a nonlinear system.
ψ_2	Output phase from a nonlinear system.
$\psi(\omega)$	Linear phase-frequency characteristic.
$Q(A)$	Quadrature component of an output signal.
q	Unit of electrical charge.
R	Half period of a Fourier representation.
R	Resistance.
$R_{xx}(t_1, t_2)$	Correlation function of process X.
$R_{xy}(\tau)$	Cross-correlation function of processes X,Y.
RF	Radio frequency.
$S_{1a}(t)$	Input signal to LINC system.
S_{ij}	Scattering matrix notation.
$S_{xx}(\omega)$	Spectral density of process X.
$S_{xy}(\omega)$	Cross-power spectrum of processes X,Y.

T	Kelvin temperature.
TWT	Travelling wave tube.
t	Denotes time.
$\theta(y)$	Amplitude dependent phase.
$\theta(E)$	Amplitude dependent phase.
θ	Phase of an input sinusoid.
θ_q	Phase of the q^{th} sinusoid.
UHF	Ultra high frequency.
u	Instantaneous value of an input signal.
V_{BIAS}	DC bias voltage.
v	voltage.
v_{IN}	Input voltage.
$v_m(a)$	m^{th} -order Chebyshev transform for a nonlinearity.
v_O	Output voltage described by a Taylor series.
v_{OUT}	Output voltage of a nonlinear system.
$V_{\text{OUT BP}}$	Bandpass output voltage of a nonlinear system.
$v_o(A)$ FUNDAMENTAL	Fundamental output voltage of a nonlinear system.
$v_{o\text{BP}}$	Bandpass output voltage.
v_{ok}	Output voltage of cascaded Volterra nonlinearities.
v_{PK}	Peak voltage of a sinusoid.
w	Output of a memoryless nonlinearity.
$w(t)$	Output of a memoryless nonlinearity.
w_o	Output of a memoryless nonlinearity.
$w_{o\text{BP}}$	Bandpass output of a memoryless nonlinearity.
X	Reactance.

X	Random process.
$x(t)$	Input to a nonlinear system.
$y(t)$	Total output of a Volterra system.
y_D	Admittance of a Schottky diode.
$y_n(t)$	n^{th} -order output of a Volterra system.
$y_n(t;M)$	Total nonlinear output for frequency mix vector M.
y_{TOTAL}	Total RF admittance.
Z_{IN}	Input impedance of a Schottky diode.
Z_L	Load impedance.
Z_O	Characteristic impedance.
Z_{OQ}	Characteristic impedance of a quarter-wave section.
Z_p	In-phase nonlinearity
Z_q	Quadrature nonlinearity.
$z(t)$	Output of a nonlinear system.
!	Factorial.
	Denotes absolute value.
*	Denotes complex conjugate.
$\binom{n}{m}$	$n! / [(n-m)! m!]$
$(n;M)$	Multinomial coefficient.

CHAPTER 1

AN OVERVIEW OF NONLINEAR SYSTEMS1.1 Introduction

All amplifiers have inherent nonlinearities which limit their usefulness and range of applications. For example, in microwave HPAs,^{*} the input power level must be kept below a certain level to ensure operation in a region of sufficiently linear amplification. Ignoring this requirement leads to the generation of significant intermodulation products caused by amplitude and phase nonlinearities.

Alternatives to power back off exist, however, and some of the more popular methods of linearization will be outlined in a subsequent chapter.

A brief classification of types of nonlinear systems, and the effects they produce, is given below.

* High power amplifiers.

1.2 Classification of Nonlinear Systems

Nonlinear systems can be classified as belonging to one of three types [1]:

- (a) Nonlinear systems without memory,
- (b) Nonlinear systems effectively without memory,
- (c) Nonlinear systems with memory.

Each type of system produces distinct nonlinear effects. These three types of systems and their effects are characterized in the following subsections.

1.2.1 Nonlinear systems without memory

Systems belonging to this category have the following three characteristics:

- (1) The output instantaneously responds to the input.
- (2) The system does not have a frequency response.
- (3) There are no phase nonlinearities.

Nonlinearities without memory are sometimes called resistive nonlinearities. Indeed, a nonlinear circuit without energy storage elements cannot possess memory.

A mathematical description of members of this category follows.

If

$$v_{IN} = A \cos(\omega t + \theta) \tag{1}$$

then the bandpass (narrowband) component at the output would be

$$v_{\text{OUT}} = G(A) \cos (\omega t + \theta) \quad (2)$$

where $G(A)$ represents the AM-to-AM conversion coefficient (an envelope-dependent gain quantity). It should be understood that in general, an infinite number of harmonic products will also result.

A necessary requirement for inclusion in the memoryless category is that $G(A)$ should not depend upon frequency. Consequently a single AM-to-AM coefficient holds for any frequency present at the system input.

The effects of memoryless nonlinearities are:

- (1) Nonlinear amplitude distortion, i.e., AM-to-AM conversion.
- (2) The generation of frequencies not associated with the input, i.e., harmonics and intermodulation products.
- (3) A possible shift in the system's DC operating point for even-order nonlinearities.

Example of this type of nonlinearity are the piecewise-linear limiter and the comparator, as shown in Figure 1.1.

An appropriate representation for such characteristics is the relatively simple classical power (Taylor) series; for this reason, memoryless nonlinearities are often used in nonlinear modelling. It should be understood that no real system can ever be truly without memory because of the always-present reactive elements.

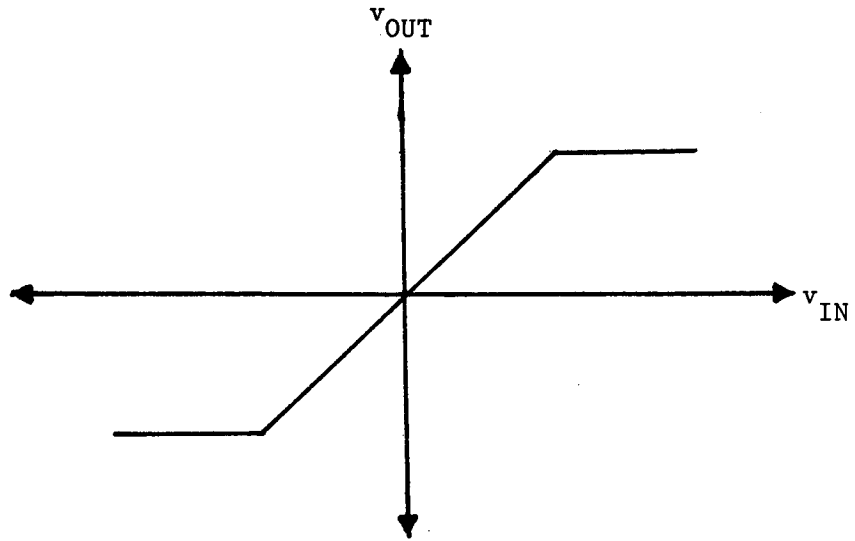


Figure 1.1a. Piecewise Linear Limiter.

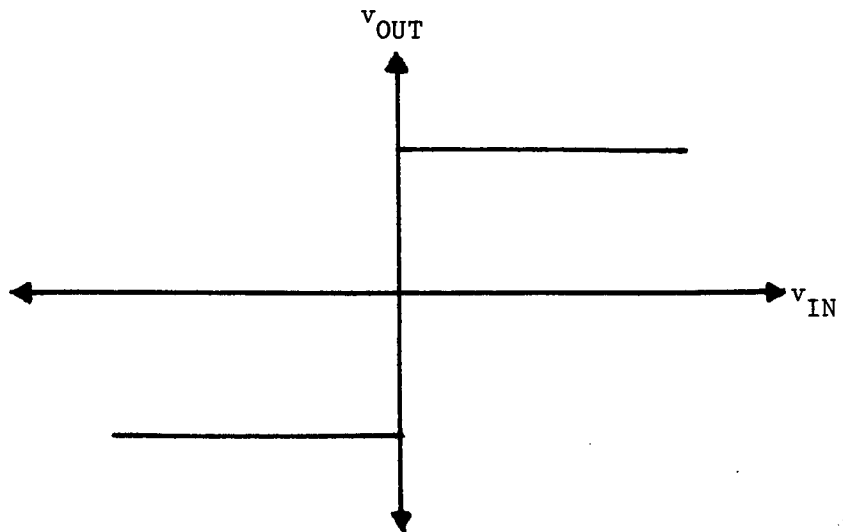


Figure 1.1b. Comparator.

1.2.2 Nonlinear systems effectively without memory

The additional requirement for membership in this category is that the nonlinear phase and amplitude transfer functions do not have a measurable frequency response due to either (or both) of the following causes:

- (a) The input signals are restricted to a narrow band over which no significant frequency response is observed.
- (b) The nonlinear transfer functions simply do not depend on frequency.

An important implication of this system requirement is that phase nonlinearities can be present, but no frequency response is allowed. Such a system therefore represents a cross between the memoryless system, and a full-memory nonlinear system.

Members of this category have the following mathematical description.

If

$$v_{IN} = A \cos (\omega t + \theta) \quad (3)$$

then the bandpass component of the output would be

$$v_{OUT_{BP}} = G(A) \cos (\omega t + \theta + F(A)) \quad (4)$$

where $G(A)$ represents the AM-to-AM coefficient and $F(A)$ represents the envelope-dependent phase or AM-to-PM coefficient. It must be emphasized that $G(A)$ and $F(A)$ are respectively due to the amplitude and phase voltage nonlinearities. These systems can therefore only be used for narrowband inputs/outputs centered around the input passband.

The "effectively without memory" type of nonlinearity is popular for the analysis of microwave HPAs because of the inclusion of a description for AM-to-PM conversion. Modelling of these systems is more complex than for memoryless systems, Volterra series representations often being used. Conventional power series analysis may be employed if the complex amplitude and phase nonlinearities are represented by the "in-phase/quadrature" method [2], [3]. For example, an output voltage

$$v_{\text{OUT}_{\text{BP}}} = G(A) \cos (\omega t + \theta + F(A)) \quad (5)$$

can be resolved into quadrature components $P(A)$, $Q(A)$ where

$$P(A) = G(A) \cos (F(A)) \quad (6)$$

$$Q(A) = G(A) \sin (F(A)) \quad (7)$$

see Figure 1.2. Therefore

$$v_{\text{OUT}_{\text{BP}}} = P(A) \cos (\omega t + \theta) - Q(A) \sin (\omega t + \theta), \quad (8)$$

see Figure 1.3. The resultant output power spectrum is found by addition of the individual spectra for each of the two signal paths, since they are linearly independent for narrow band systems (see Appendix 1 for a definition of "linear independence", and its relevance to this situation).

This type of nonlinearity is frequently used for modelling TWT amplifiers because they are normally operated over a bandwidth small compared with their inherent broadband capabilities.

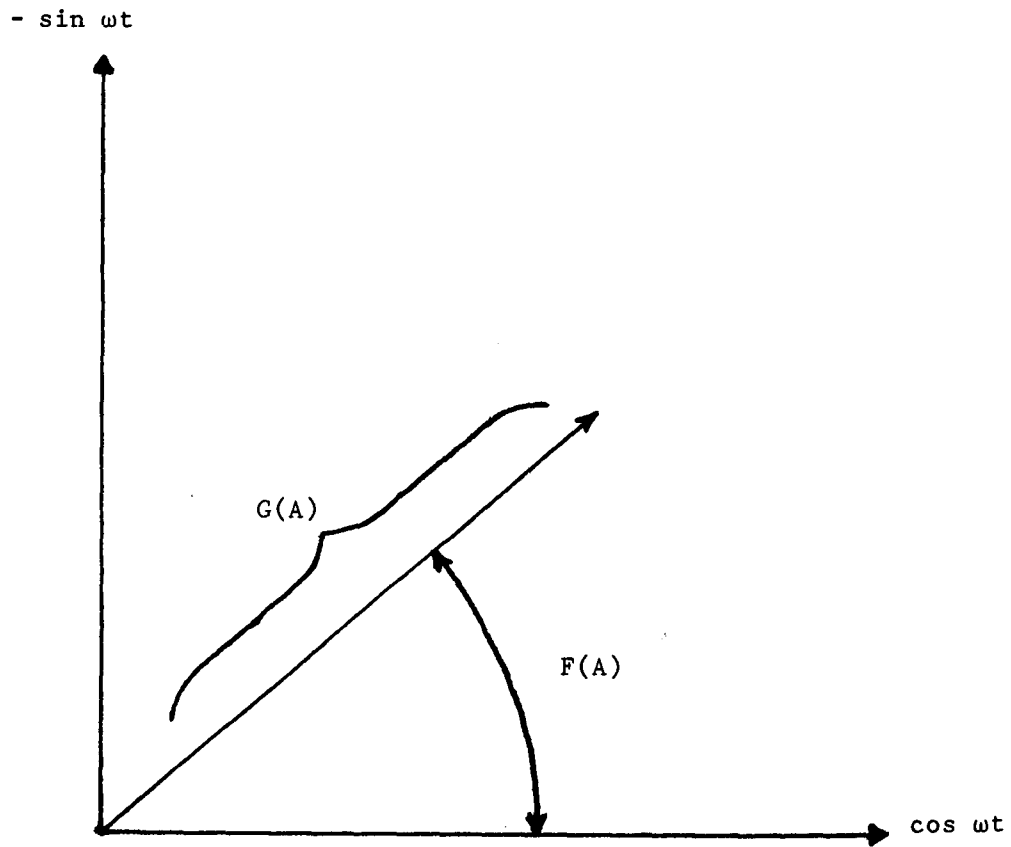


Figure 1.2. "In-phase/quadrature" representation.

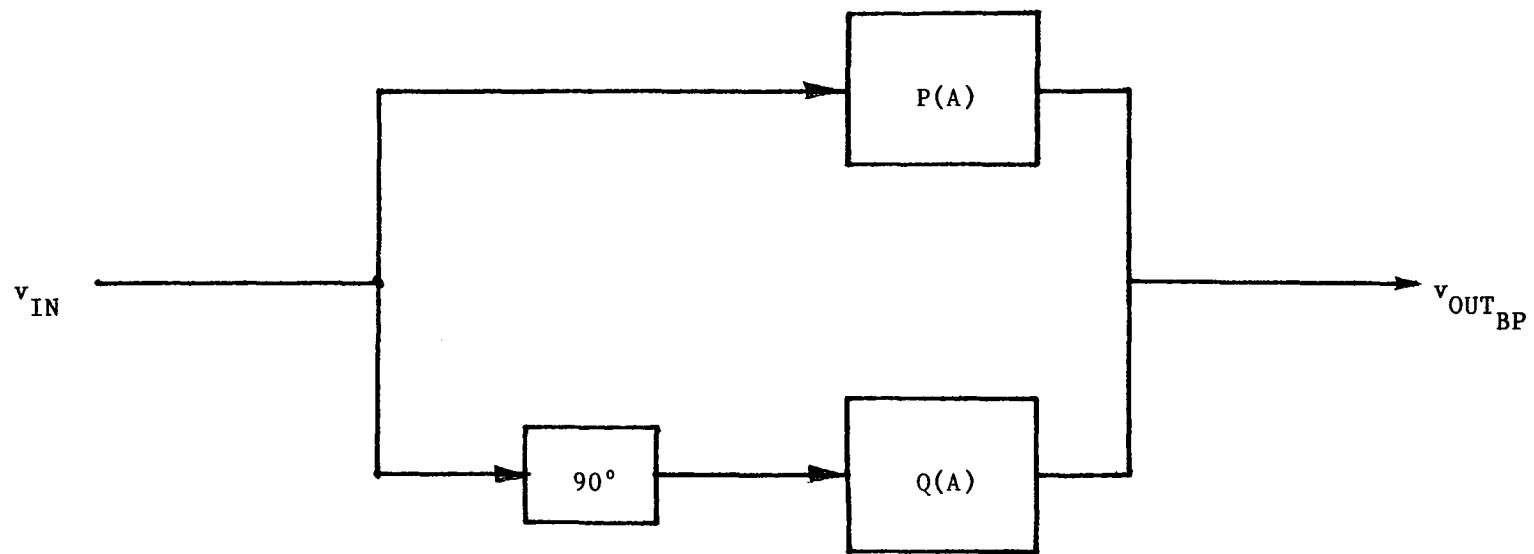


Figure 1.3. "In-phase/quadrature" representation.

1.2.3 Nonlinear systems with memory

This last category is the most general. It includes the previous two categories as special cases. All of the nonlinear effects of the previous two categories are still present, but the additional property of a frequency dependence in the AM-to-AM and AM-to-PM coefficients may be observed.

Mathematically, members of this category can be defined in the following way. If

$$v_{IN} = A \cos (\omega t + \theta) \quad (9)$$

then the bandpass component at the output would be

$$v_{OUT_{BP}} = G(A, \omega) \cos (\omega t + \theta + F(A, \omega)) \quad (10)$$

Proper modelling requires that attention be paid to the frequency characteristics of the nonlinearities. The Volterra series is an appropriate representation [4], although frequency dependent "in-phase/quadrature" models have been proposed [5].

Potential applications for nonlinear models incorporating memory include broadband amplifiers, where the input signal is spread over a wide frequency range, and narrowband amplifiers. This would include all present TWT and solid-state amplifiers.

1.3 Analysis Methods for Nonlinearities

1.3.1 Introduction

Mathematical analyses of nonlinear systems tend to be complicated, mainly because of the infinite number of possible frequency combinations produced at the output. Certain analysis methods tend to dominate the majority of modelling efforts; some of them will be presented here.

1.3.2 Classical power series

The power series representation of nonlinear functions involves the determination of the Taylor series coefficients expanded about the point of operation, for example

$$v_0 = \sum_{n=0}^{\infty} a_n v_{IN}^n \quad . \quad (11)$$

The power series approach is useful for modelling of weak, memoryless nonlinearities. Convergence problems may prevail for more severe types of nonlinearities.

An important characteristic of the power series representation is that a given term of the series produces frequency products of order no higher than the power of that term. Thus for a sinusoidal input of frequency f_{IN} , a model including terms up to the seventh order would produce harmonic frequencies no greater than $7 f_{IN}$. This most easily demonstrated with the help of the Chebyshev transform [6]. Modelling of high-order intermodulation or harmonic components, therefore requires

one to increase the number of terms present in the series representation. This represents a serious limitation to the modelling of general nonlinearities.

1.3.3 Fourier methods

Fourier methods involve fitting a Fourier series to the transfer characteristic. For example, for

$$v_o = f(v_{IN}) \quad (12)$$

the Fourier approximation might be synthesized as shown in Figure 1.4.

It is important to clarify the proper use of the Fourier series. One must not think in terms of harmonic analysis of time domain waveforms, rather the concept is similar to the power series approach where the goal is an analytic description of the input-output relationship.

George, Kaye and Eric [3] proposed a periodic extension to the transfer curve to aid in convergence of the fitted series:

$$v_o = \sum_{\ell=1}^{\infty} b_{\ell} \sin \left[\frac{(2\ell-1)\pi v_{IN}}{R} \right]; \quad -\frac{R}{2} \leq v_{IN} \leq \frac{R}{2} \quad (13)$$

This is shown in Figure 1.5. The b_{ℓ} coefficients are usually determined numerically, using either a discrete Fourier series algorithm or a least-squares curve-fitting procedure.

Assuming that the Fourier series converges, then since the sine functions can be expressed as powers of their arguments, (here the input

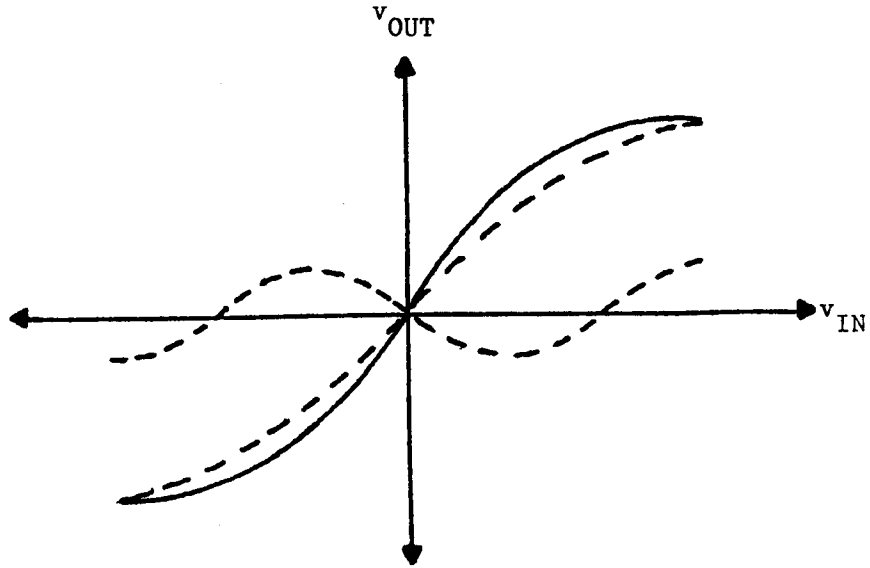


Figure 1.4. Fourier series representation.

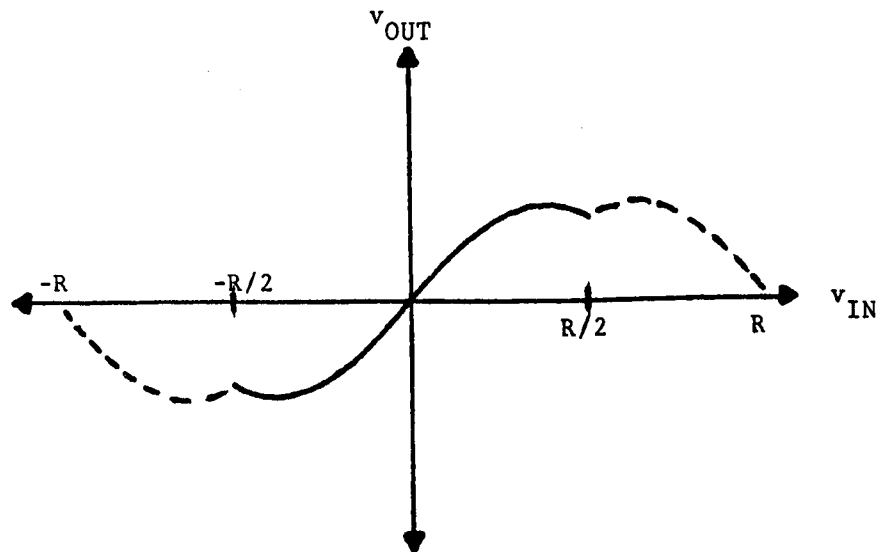


Figure 1.5. Periodic extension of Fourier representation.

voltage), then the Taylor expansion can be deduced from the Fourier series. Thus since

$$v_o = \sum_{\ell=1}^{\infty} b_{\ell} \sin \left[\frac{(2\ell-1)\pi v_{IN}}{R} \right]; \quad -\frac{R}{2} \leq v_{IN} \leq \frac{R}{2} \quad (14)$$

and

$$\sin x = \sum_{K=0}^{\infty} (-1)^K \frac{x^{2K+1}}{(2K+1)!} \quad (15)$$

then

$$v_o = \sum_{\ell=1}^{\infty} b_{\ell} \sum_{K=0}^{\infty} (-1)^K \frac{\left[\frac{(2\ell-1)\pi v_{IN}}{R} \right]^{2K+1}}{(2K+1)!} \quad (16)$$

Note that the resultant power series involves an infinite number of terms. It does not terminate at a given order; this fact is independent of the number of sinusoids involved in the Fourier series. (A practical Fourier series representation requires truncation after a finite number of terms). Hence Fourier methods appear to be more useful for the prediction of high-order products than are the conventional power series approaches.

1.3.4 Chebyshev transform methods

The Chebyshev transform is a mathematical operation used to predict fundamental and harmonic components generated by an arbitrary nonlinear, memoryless amplitude characteristic. Mathematically, it is equivalent to the determination of the time-domain output waveform for a single sinusoidal input. The output waveform is then harmonically analysed by a Fourier series, and the envelope level of each fundamental and harmonic

component tabulated. The Fourier series employed for this operation is one which relates the time domain to the frequency domain, as opposed to the series described in the previous section which relates input levels to output levels. An analytic description of the transfer characteristic and the use of the Chebyshev transform is sufficient for modelling memoryless amplitude-dependent nonlinearities with a single input sinusoid.

Thus for a transfer function described by a power series

$$v_o = \sum_{n=1}^{\infty} a_n v_{IN}^n, \quad n \text{ odd}, \quad (17)$$

where

$$v_{IN} = A \cos(\omega t + \theta) \quad (18)$$

one obtains using Transform T5 of Blachman [6] (see Appendix 2)

$$v_o(A)_{\text{FUNDAMENTAL}} = \sum_{\substack{n=1 \\ m=1}}^{\infty} 2a_n \left(\frac{1}{2}\right)^{n-m} \left(\frac{A}{2}\right)^n \cos(\omega t + \theta) \quad (19)$$

Note that only odd powers are employed for the Taylor series, since only odd power coefficients contribute to the fundamental output. This follows directly from the indicated Chebyshev transform. Any desired harmonic output could just as easily have been obtained from the series representation simply by substituting for m the required harmonic number; $m \leq n$, m odd. The Chebyshev transform approach also emphasizes the fact an n^{th} -order power cannot produce harmonic terms of frequency greater than n times the input, although it will produce lower-order harmonics.

For the Fourier method representation, T7 of Blachman can be used [6], see Appendix 2. Thus, for the Fourier representation as per equation (13)

$$v_o(A) = \sum_{\ell=1}^{\infty} \sum_{m=1}^{\infty} (-1)^{\ell} \frac{1/(2(M-1))}{b_{\ell}} 2J_m \left[\frac{(2\ell-1)\pi v_{IN}}{R} \right] \cos m(\omega t + \theta) \quad (20)$$

where $J_m(u)$ is the Bessel function of the first kind of order m .

Selecting $m=1$ yields the fundamental output

$$v_o(A)_{\text{FUNDAMENTAL}} = \sum_{\ell=1}^{\infty} 2b_{\ell} J_1 \left[\frac{(2\ell-1)\pi v_{IN}}{R} \right] \cos(\omega t + \theta) \quad (21)$$

An interesting application of the Chebyshev transform method is the analysis of the effect of amplitude nonlinearities on phase modulated signals. One can readily see from either equations (19) or (21) that for a simple amplitude nonlinearity, the bandpass output phase-modulated signal is undistorted, the amplitude level conveying no information. This is the basis of the commonly accepted notion that class C (highly nonlinear) amplifiers can be employed for successful power amplification of angle-modulated signals with no resultant distortion. Unfortunately, this concept is not entirely realistic for two reasons. First, if a multi-carrier FM system is to be employed over an octave bandwidth (or greater), second harmonics will fall in band. This effect would not be troublesome at microwave frequencies, on account of the usually small fractional bandwidths, but could be a problem in lower frequency applications. Second, and more important, no real nonlinear system is memoryless and

consequently phase distortion will occur, resulting in potentially severe distortion of the angle modulation and a corresponding loss of information. For a single carrier input, the net effect to the FM user would be a distorted demodulated output (i.e. the effects of AM-to-PM conversion would be present in the output signal). For multi-carrier systems, however, severe in-band intermodulation may result, filling the passband with noise and obviating the usefulness of the communication channel.

1.3.5 A mathematical description of phase nonlinearities and resultant AM-to-PM conversion: nonlinear envelope modelling

Having introduced a discussion of phase nonlinearities, a more detailed analysis is now in order. This exercise will show the effect of phase nonlinearities and the degree of complexity involved in their analysis.

Consider a system which is nonlinear only in phase. Thus for

$$v_{IN} = A \cos \omega_o t \quad (22)$$

we describe the output as

$$v_o = A(\cos [\omega_o t + \phi(v_{IN})]) \quad (23)$$

where the phase nonlinearity of the input voltage is described by the Taylor series

$$\phi(v_{IN}) = \sum_{n=0}^{\infty} a_n v_{IN}^n \quad (24)$$

The mathematical analysis is complicated for the general case.

However, insight may be obtained by truncating the phase nonlinearity after a single quadratic term, thus

$$\phi(v_{IN}) = a_2 v_{IN}^2, \quad (25)$$

so that

$$v_o = A \cos(\omega_o t + a_2 (A \cos \omega_o t)^2). \quad (26)$$

The trigonometric identity

$$\cos(A+B) = \cos A \cos B - \sin A \sin B \quad (27)$$

then gives

$$v_o = A(\cos \omega_o t \cos (a_2 A^2 \cos^2 \omega_o t) - \sin \omega_o t \sin (a_2 A^2 \cos^2 \omega_o t)). \quad (28)$$

Using the trigonometric relationships

$$\cos^2 \theta = \frac{1 + \cos 2\theta}{2}, \quad (29)$$

$$\sin(A+B) = \sin A \cos B + \cos A \sin B \quad (30)$$

and equation (28), one obtains

$$\begin{aligned} v_o = & A(\cos \omega_o t [\cos(\frac{a_2 A^2}{2}) \cos((\frac{a_2 A^2}{2}) \cos 2 \omega_o t) \\ & - \sin(\frac{a_2 A^2}{2}) \sin((\frac{a_2 A^2}{2}) \cos 2 \omega_o t)] \\ & - \sin \omega_o t [\sin(\frac{a_2 A^2}{2}) \cos((\frac{a_2 A^2}{2}) \cos 2 \omega_o t) \\ & + \cos(\frac{a_2 A^2}{2}) \sin((\frac{a_2 A^2}{2}) \cos 2 \omega_o t)]). \end{aligned} \quad (31)$$

Finally, use of the sine-Bessel relationships

$$\cos (u \cos x) = J_0(u) + 2 \sum_{n=1}^{\infty} (-1)^n J_{2n}(u) \cos [2nx] \quad (32)$$

$$\sin (u \cos x) = 2 \sum_{n=1}^{\infty} (-1)^{n+1} J_{2n-1}(u) \cos [(2n-1)x] \quad (33)$$

yields the result

$$\begin{aligned} v_o = A(\cos \omega_o t \{ \cos \left(\frac{a_2 A^2}{2}\right) [J_0\left(\frac{a_2 A^2}{2}\right) + 2 \sum_{n=1}^{\infty} (-1)^n J_{2n}\left(\frac{a_2 A^2}{2}\right) \cos \{4n \omega_o t\}] \\ - \sin \left(\frac{a_2 A^2}{2}\right) [2 \sum_{n=1}^{\infty} (-1)^{n+1} J_{2n-1}\left(\frac{a_2 A^2}{2}\right) \cos \{(2n-1) 2 \omega_o t\}] \\ - \sin \omega_o t \{ \sin \left(\frac{a_2 A^2}{2}\right) [J_0\left(\frac{a_2 A^2}{2}\right) + 2 \sum_{n=1}^{\infty} (-1)^n J_{2n}\left(\frac{a_2 A^2}{2}\right) \cos \{4n \omega_o t\}] \\ - \cos \left(\frac{a_2 A^2}{2}\right) [2 \sum_{n=1}^{\infty} (-1)^{n+1} J_{2n-1}\left(\frac{a_2 A^2}{2}\right) \cos \{(2n-1) 2 \omega_o t\}] \} \} . \end{aligned} \quad (34)$$

Note that the single quadratic phase-voltage relationship has produced every order harmonic of the input. The same quadratic relationship for multiple FM signals would result in severe intermodulation distortion.

Continuing the derivation by extracting the bandpass components centered about the input frequency yields

$$\begin{aligned} v_{o_{BP}} = A\{ \cos \omega_o t \{ \cos \left(\frac{a_2 A^2}{2}\right) J_0\left(\frac{a_2 A^2}{2}\right) - \sin \left(\frac{a_2 A^2}{2}\right) J_1\left(\frac{a_2 A^2}{2}\right) \} \\ - \sin \omega_o t \{ \sin \left(\frac{a_2 A^2}{2}\right) J_0\left(\frac{a_2 A^2}{2}\right) - \cos \left(\frac{a_2 A^2}{2}\right) J_1\left(\frac{a_2 A^2}{2}\right) \} \} \quad (35) \end{aligned}$$

hence the bandpass output phase is given by

$$\phi_{\text{OUT}_{\text{BP}}} = \arctan \frac{\sin\left(\frac{a_2 A^2}{2}\right) J_0\left(\frac{a_2 A^2}{2}\right) - \cos\left(\frac{a_2 A^2}{2}\right) J_1\left(\frac{a_2 A^2}{2}\right)}{\cos\left(\frac{a_2 A^2}{2}\right) J_0\left(\frac{a_2 A^2}{2}\right) - \sin\left(\frac{a_2 A^2}{2}\right) J_1\left(\frac{a_2 A^2}{2}\right)} \quad (36)$$

where $\phi_{\text{OUT}_{\text{BP}}}$ refers to the resultant phase shift obtained from the bandpass output of equation (23). This is commonly referred to as the AM-to-PM coefficient. Note that the coefficient is envelope-dependent, although the original quadratic phase nonlinearity responds to instantaneous input voltages. It is analogous to the Chebyshev transform relationship for memoryless nonlinearities where the bandpass resultant amplitude varies with input envelope level, although caused by instantaneous voltage nonlinearities.

To summarize, nonlinear results presented to the system user may appear to be envelope-dependent, and one may choose to model the nonlinearity according to the AM-to-AM and AM-to-PM coefficients. However, this is not in general correct, except for the case of single-carrier (or at the most narrowband) inputs restricted to the frequency range within which the AM-to-AM and AM-to-PM coefficients apply. The effect of memory is to enable the nonlinear envelope coefficients to change with frequency, as well as with envelope level. This places a more fundamental limitation on the applicability of the "in-phase /quadrature" modelling method. Not only is the bandwidth restricted

according to the "linearly independent" restriction previously discussed, but the AM-to-AM and AM-to-PM coefficients can be expected to vary considerably over a wide bandwidth.

A demonstration of the error incurred by modelling nonlinearities in terms of their envelope coefficients will now be presented. Consider a memoryless cubic nonlinearity

$$v_o = v_{IN}^3 \quad (37)$$

where

$$v_{IN} = A \sin \omega t \quad (38)$$

Using simple trigonometry or the Chebyshev transform, the output is found to be

$$v_o = \frac{A^3}{4} (3 \sin \omega t + \sin 3 \omega t) \quad (39)$$

The bandpass result seen by the system user is therefore

$$v_{o_{BP}} = \frac{3}{4} A^3 \quad (40)$$

and an attempt might be made to use this model for prediction of the third harmonic level, giving the output

$$v_o = \frac{3}{4} (A \sin \omega t)^3 \quad (41)$$

or

$$v_o = \frac{3}{16} A^3 (3 \sin \omega t + \sin 3 \omega t) \quad (42)$$

which is an incorrect result. The correct approach is to apply the inverse Chebyshev transform, [6], to the observed $\frac{3}{4} A^3$ relationship for the fundamental, obtaining the correct nonlinear characteristic of equation (37), as required for further modelling.

A similar result for an observed AM-to-PM coefficient could be obtained by adjusting the a_2 coefficient in equation (36) for best fit for the predicted AM-to-PM relationship.

To summarize, nonlinearities are caused by instantaneous voltage relationships, not envelope levels. Prediction of narrowband nonlinearities can be obtained by simply using the measured nonlinear coefficients. Wideband prediction requires one to obtain the voltage relationships by a mathematical inversion process.

1.3.6 Power series with frequency response

This representation includes the effect of a system frequency response, while maintaining memoryless conditions through isolation of the nonlinearity from the input and output filters [4]. That is, the three cascaded networks of Figure 1.6 are assumed to be non-interacting. It is assumed that $x(t)$ consists of Q different cosine signals:

$$x(t) = \sum_{q=1}^Q |E_q| \cos(\omega_q t + \theta_q) . \quad (43)$$

Analysis is simplified by the use of complex representation, thus:

$$E_q = |E_q| \exp(j\theta_q) ; E_{-q} = E_q^* ; \omega_{-q} = -\omega_q \quad (44)$$

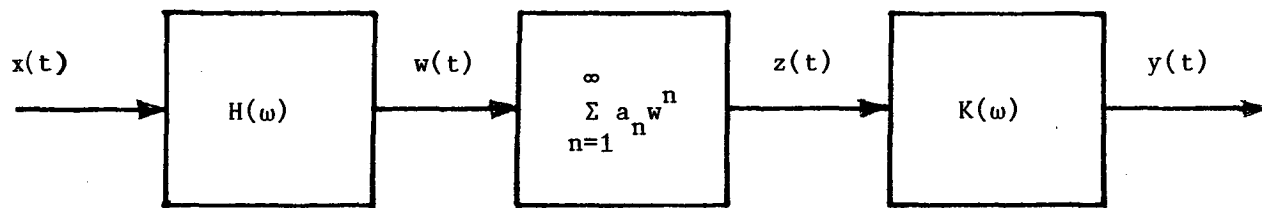


Figure 1.6. Power series with frequency response system block.

so that (43) becomes

$$x(t) = \frac{1}{2} \sum_{q=1}^Q [E_q \exp(j\omega_q t) + E_q^* \exp(-j\omega_q t)] \quad (45)$$

or

$$x(t) = \frac{1}{2} \sum_{q=-Q}^Q E_q \exp(j\omega_q t) \quad (46)$$

which represents a real input signal. If the response of the first filter is represented by

$$H(\omega) = |H(\omega)| \exp[j\psi(\omega)] \quad (47)$$

then

$$w(t) = \frac{1}{2} \sum_{q=-Q}^Q E_q H(\omega_q) \exp[j\omega_q t] \quad (48)$$

where $w(t)$ is taken to be real so that

$$H(-\omega) = H^*(\omega) \quad . \quad (49)$$

This prefiltered waveform, $w(t)$, can now be input to the memoryless nonlinearity:

$$z(t) = \sum_{n=1}^N a_n w^n(t) \quad (50)$$

where

$$w^n(t) = \left[\frac{1}{2} \sum_{q=-Q}^Q E_q H(\omega_q) \exp(j\omega_q t) \right]^n \quad (51)$$

A useful concept for nonlinear analysis is to change an n^{th} -power relationship into an n -fold product, indexing each term in the multiplication to distinguish individual terms. In this way we can write

$$w^n(t) = \left[\frac{1}{2} \sum_{q_1=-Q}^Q E_{q_1} H(\omega_{q_1}) \exp(j\omega_{q_1}t) \right] \dots \\ \cdot \left[\frac{1}{2} \sum_{q_n=-Q}^Q E_{q_n} H(\omega_{q_n}) \exp(j\omega_{q_n}t) \right] . \quad (52)$$

Interchanging the order of summation and multiplication yields

$$w^n(t) = \frac{1}{2^n} \sum_{q_1=-Q}^Q \dots \sum_{q_n=-Q}^Q E_{q_1} \dots E_{q_n} H(\omega_{q_1}) \dots H(\omega_{q_n}) \\ \cdot \exp \{j(\omega_{q_1} + \dots + \omega_{q_n}) t\} . \quad (53)$$

Therefore

$$z(t) = \sum_{n=1}^N \frac{1}{2^n} a_n \sum_{q_1=-Q}^Q \sum_{q_n=-Q}^Q E_{q_1} \dots E_{q_n} H(\omega_{q_1}) \dots H(\omega_{q_n}) \\ \cdot \exp \{j(\omega_{q_1} + \dots + \omega_{q_n}) t\} . \quad (54)$$

The final output, $y(t)$, is simply the response of the post-filter to $z(t)$.

Since

$$K(\omega) = |K(\omega)| \exp(j[\phi(\omega)]) \quad (55)$$

then

$$y(t) = \sum_{n=1}^N \sum_{q_1=-Q}^Q \dots \sum_{q_n=-Q}^Q \frac{a_n}{2^n} E_{q_1} \dots E_{q_n} H(\omega_{q_1}) \dots H(\omega_{q_n}) \\ K(\omega_{q_1} + \dots + \omega_{q_n}) \cdot \exp [j(\omega_{q_1} + \dots + \omega_{q_n}) t] . \quad (56)$$

The filtered memoryless system described is ideal for band-limited representation of nonlinearities, e.g. using the "in-phase/quadrature" method. The concept of frequency mixing is useful for the prediction of the total output at any given frequency [4]. Denote the frequency mix vector

$$M = (m_{-Q}, \dots, m_{-1}, \dots, m_Q) \quad (57)$$

where m_{-Q} denotes the number of times that frequency ω_{-Q} appears in the frequency mix. For example, for a third-order intermodulation mix of $2\omega_2 - \omega_1$, the frequency mix vector $(m_{-2}, m_{-1}, m_1, m_2)$ would be given as $(0, 1, 0, 2)$ since $m_{-1} = 1$, $m_2 = 2$. The frequency is then given by

$$0 \cdot \omega_{-2} + 1 \cdot \omega_{-1} + 0 \cdot \omega_1 + 2 \cdot \omega_2 = 2\omega_2 - \omega_1 . \quad (58)$$

In general, the resultant frequency mix is given by

$$\omega_M = \sum_{\substack{k=-Q \\ k \neq 0}}^Q m_k \omega_k . \quad (59)$$

Also, the number of components in the mix is limited by the order of the nonlinearity. For example, a third-order product involves three frequency elements mixed together. Thus in general

$$\sum_{\substack{k=-Q \\ k \neq 0}}^Q m_k = n \quad (60)$$

where n is the order of the nonlinearity.

Note that the third order intermodulation product $2\omega_2 - \omega_1$ can also be produced by permuting the frequency indices:

$$(-\omega_1, \omega_2, \omega_2); (\omega_2, \omega_2, -\omega_1); (\omega_2, \omega_1, \omega_2) \quad (61)$$

In fact, the number of possible permutations such that ω_{-Q} appears m_{-Q} times, ω_{-1} appears m_{-1} times etc., is given by the multinomial coefficient

$$(n; M) = \frac{n!}{(m_{-Q})! \dots (m_{-1})! (m_1)! \dots (m_Q)!} \quad (62)$$

where n is the order of the nonlinearity and M denotes the frequency mix vector. For the $2\omega_2 - \omega_1$ product given in (58), there are therefore

$$\frac{3!}{2! 1!} = 3 \quad (63)$$

permutations in question. The total output for the intermodulation product $2\omega_2 - \omega_1$ is therefore given by (56) in conjunction with (62):

$$\frac{(n; M)}{2^n} a_n E_{q_1} E_{q_2} E_{q_3} H(\omega_{q_1}) H(\omega_{q_2}) H(\omega_{q_3}) K(\omega_{q_1} + \omega_{q_2} + \omega_{q_3}) \exp [j (\omega_{q_1} + \omega_{q_2} + \omega_{q_3}) t] \quad (64)$$

We denote the total output of any order frequency mix as $y_n(t; M)$.

Then

$$y_3(t; -f_1, f_2, f_2) = \frac{3}{8} a_3 E_1^* E_2^2 H^*(\omega_1) H^2(\omega_2) K(2\omega_2 - \omega_1) \cdot \exp [j (2\omega_2 - \omega_1) t] \quad (65)$$

Since the output is real-valued, there exists a corresponding negative frequency output at $\omega_1 - 2\omega_2$:

$$y_3(t; f_1, f_2, f_2) = \frac{3}{8} a_3 E_1 (E_2^*)^2 H(\omega_1) (H^*(\omega_2))^2 K^*(2\omega_2 - \omega_1) \cdot \exp [j (-2\omega_2 + \omega_1) t] \quad (66)$$

which is in fact equal to $y_3^*(t; -f_1, f_2, f_2)$. Therefore

$$\begin{aligned} y_3(t; -f_1, f_2, f_2) + y_3^*(t; -f_1, f_2, f_2) &= 2\text{Re} \{y_3(t; -f_1, f_2, f_2)\} \\ &= \frac{3}{4} a_3 E_1^* E_2^2 H^*(\omega_1) H^2(\omega_2) K(2\omega_2 - \omega_1) \cos (2\omega_2 - \omega_1) t. \end{aligned} \quad (67)$$

The above example demonstrates the relative ease of analysis of any particular frequency component produced by any order of nonlinearity.

Note that the net frequency component of $2\omega_2 - \omega_1$ could be formed from a fifth-order mix, $(-\omega_1, -\omega_2, \omega_2, \omega_2, \omega_2)$ or from any higher-order odd-power nonlinearity. Therefore the total output at any given frequency is likely to involve a summation of all contributing powers. The products

produced by individual powers will either be in phase or out of phase, with products produced by other orders of nonlinearity, depending on the sign of the power series coefficient. For example, if a_3 is positive and a_5 negative, then the products generated by the third- and fifth-order nonlinearities will add out of phase. The resultant phase outputs from the pre- and post-filters are identical for all powers, as they produce identical net frequency components. This fact eliminates any phase dependence on input amplitude level other than 0° or 180° .

Finally, it is instructive to show the result for the total output at any frequency mix, ω_M , for any power:

$$y_n(t;M) = \frac{(n;M)}{2^n} a_n (E_Q^*)^{m-Q} \dots (E_1^*)^{m-1} (E_1)^{m-1} \dots (E_Q)^{m_Q} [H^*(\omega_Q)]^{m-Q} \dots [H^*(\omega_1)]^{m-1} [H(\omega_1)]^{m_1} \dots [H(\omega_Q)]^{m_Q} \exp [j \omega_M t]. \quad (68)$$

This will be useful for comparison with the results generated by the Volterra series, as derived in the next section.

1.3.7 Volterra series:

The Volterra series [4] allows modelling for the full effects of memory, although the resultant mathematical expression may be difficult to work with.

The series involves calculating impulse responses due to an n^{th} -order nonlinearity, where the driving signal consists of an n -fold product of

the input signals in convolutional form. The n^{th} -order output therefore depends on the current input, as well as all previous inputs. In this manner, the system models memory; it is similar to an impulse response of a linear system as calculated by a convolution integral, where the output at any time depends on all previous inputs. Separate n^{th} -order impulse responses are then added together, forming the composite time-domain output. A mathematical description follows. If the input at any time t is $x(t)$, then the n^{th} -order output is given by

$$y_n(t) = \int_{-\infty}^{\infty} \int_{-\infty}^{\infty} \dots \int_{-\infty}^{\infty} h_n(\tau_1, \tau_2, \dots, \tau_n) x(t-\tau_1) x(t-\tau_2) \dots x(t-\tau_n) d\tau_1 d\tau_2 \dots d\tau_n \quad (69)$$

where the integration limits for the convolution integrals have been extended to $-\infty$, as the input is assumed to be zero for $t < 0$ and the impulse response, $h_n(\tau_1, \tau_2, \dots, \tau_n)$ is assumed to be zero for negative arguments. The output is therefore

$$y(t) = \sum_{n=1}^N y_n(t) \quad (70)$$

assuming that the system is truncated after the N^{th} -order response.

Since $x(t)$ has not been specified, the nonlinear system response can be calculated for any input signal.

1.3.7.1 Volterra response for multiple sinusoidal inputs

For this derivation, it is illuminating to use the complex exponential form to represent sinusoids, as was done in Section 1.3.6.

That is,

$$x(t) = \frac{1}{2} \sum_{q=-Q}^Q E_q \exp j \omega_q t \quad (71)$$

so that

$$\begin{aligned} y_n(t) = & \int_{-\infty}^{\infty} \dots \int_{-\infty}^{\infty} h_n(\tau_1, \dots, \tau_n) \left[\sum_{q_1=-Q}^Q \frac{1}{2} E_{q_1} \exp j \omega_{q_1} (t-\tau_1) \right] \\ & \dots \left[\sum_{q_n=-Q}^Q \frac{1}{2} E_{q_n} \exp j \omega_{q_n} (t-\tau_n) \right] \\ & d\tau_1 \dots d\tau_n . \end{aligned} \quad (72)$$

Interchanging the order of summation and integration yields

$$\begin{aligned} y_n(t) = & \frac{1}{2^n} \sum_{q_1=-Q}^Q \sum_{q_n=-Q}^Q E_{q_1} \dots E_{q_n} \exp j (\omega_{q_1} + \dots + \omega_{q_n}) t \\ & \int_{-\infty}^{\infty} \dots \int_{-\infty}^{\infty} h_n(\tau_1, \dots, \tau_n) \exp -j (\omega_{q_1} \tau_1 + \dots + \omega_{q_n} \tau_n) \\ & d\tau_1 \dots d\tau_n . \end{aligned} \quad (73)$$

Defining the n^{th} -order Fourier transform of the n^{th} -order impulse response to be

$$\begin{aligned} H_n(\omega_{q_1}, \dots, \omega_{q_n}) = & \int_{-\infty}^{\infty} \dots \int_{-\infty}^{\infty} h_n(\tau_1, \dots, \tau_n) \\ & \exp [-j (\omega_{q_1} \tau_1 + \dots + \omega_{q_n} \tau_n)] d\tau_1 \dots d\tau_n \end{aligned} \quad (74)$$

$y_n(t)$ is given by

$$y_n(t) = \frac{1}{2^n} \sum_{q_1=-Q}^Q \dots \sum_{q_n=-Q}^Q E_{q_1} \dots E_{q_n} H_n(\omega_{q_1}, \dots, \omega_{q_n}) \exp [j (\omega_{q_1} + \dots + \omega_{q_n}) t] . \quad (75)$$

The quantity $H_n(\omega_1, \omega_2, \dots, \omega_n)$ is sometimes called the n^{th} -order nonlinear transfer function. Note that the restriction to a real output signal implies that

$$H_n(-\omega_1, \dots, -\omega_n) = H_n^*(\omega_1, \dots, \omega_n) . \quad (76)$$

Again, the frequency mix concept is employed to calculate the total n^{th} -order response for any given frequency; so that

$$\omega_M = \sum_{\substack{k=-Q \\ k \neq 0}}^Q m_k \omega_k \quad (77)$$

and

$$\sum_{\substack{k=-Q \\ k \neq 0}}^Q m_k = n . \quad (78)$$

Also, permuting the indices will produce the same frequency result, hence the multinomial coefficient

$$(n; M) = \frac{n!}{(m_{-Q})! \dots (m_{-1})! (m_1)! \dots (m_Q)!} . \quad (79)$$

Therefore the total third-order response for any given frequency mix would be

$$y_3(t;M) = \frac{(n;M)}{8} E_{q_1} E_{q_2} E_{q_3} H_3(\omega_{q_1}, \omega_{q_2}, \omega_{q_3}) \exp [j (\omega_{q_1} + \omega_{q_2} + \omega_{q_3}) t] . \quad (80)$$

For example, for a total output of $2\omega_2 - \omega_1$, one obtains

$$y_3(t;M) = \frac{3}{8} E_1^* E_2^2 H_3(-\omega_1, \omega_2, \omega_2) \exp [j (-\omega_1 + 2\omega_2) t] . \quad (81)$$

Again

$$y_3^*(t;-M) = y_3(t;M) \quad (82)$$

so the total real response is

$$2\text{Re} \{y_3(t;M)\} = \frac{3}{4} E_1^* E_2^2 H_3(-\omega_1, \omega_2, \omega_2) \cos [(2\omega_2 - \omega_1) t] , \quad (83)$$

a result similar to the result generated by the power-series-with-frequency-response approach. In fact, it is not immediately obvious how this result differs from those of the previous section. Examination of which fifth-order transfer function would generate the frequency $2\omega_2 - \omega_1$ yields

$$H_5(-\omega_1, -\omega_2, \omega_2, \omega_2, \omega_2) . \quad (84)$$

Note that in general, $H_n(\omega_1, \omega_2, \dots, \omega_n)$ is a complex-valued function with amplitude and phase components. Hence the $2\omega_2 - \omega_1$ components produced by $H_3(-\omega_1, \omega_2, \omega_2)$ and $H_5(-\omega_1, -\omega_2, \omega_2, \omega_2, \omega_2)$ could add in any

arbitrary phase, not just in phase or out of phase as for the memoryless case. This allows for the output phase to be a nonlinear function of the input, and is the end result of allowing the n^{th} -order output to depend on values input previously in time.

The general result for any particular frequency mix produced by an n^{th} -order transfer function is:

$$\begin{aligned}
 y_n(t;M) = & \frac{(n;M)}{2^n} (E_Q^*)^{m-Q} \dots (E_1^*)^{m-1} (E_1)^{m_1} \dots (E_Q)^{m_Q} \cdot \\
 & \cdot H_n(\underbrace{\omega_{-Q}, \dots, \omega_{-Q}}_{m-Q}, \dots, \underbrace{\omega_{-1}, \dots, \omega_{-1}}_{m-1}, \dots, \underbrace{\omega_1, \dots, \omega_1}_{m_1}) \\
 & \dots \underbrace{\omega_Q, \dots, \omega_Q}_{m_Q} \exp(j \omega_M t) \cdot \quad (85)
 \end{aligned}$$

The total real result is simply twice the above value.

It is useful to compare the power-series-with-frequency response with the special Volterra case without memory. Both systems will then provide identical results. Thus

$$\begin{aligned}
 \frac{(m;M)}{2^n} a_n (E_Q^*)^{m-Q} \dots (E_1^*)^{m-1} (E_1)^{m_1} \dots (E_Q)^{m_Q} [H^*(\omega_Q)]^{m-Q} \\
 \dots [H^*(\omega_1)]^{m-1} [H(\omega_1)]^{m-1} [H(\omega_Q)]^{m_Q} K(\omega_M) \exp(j \omega_M t)
 \end{aligned}$$

$$\begin{aligned}
&= \frac{(n;M)}{2^n} (E_Q^*)^{m-Q} \dots (E_1^*)^{m-1} (E_1)^{m_1} \dots (E_Q)^{m_Q} \\
&\quad H_n(\omega_{-Q}, \dots, \omega_{-Q}, \dots, \omega_{-1}, \dots, \omega_{-1}, \dots, \omega_1, \dots, \omega_1, \\
&\quad \omega_Q, \dots, \omega_Q) \exp(j \omega_M t) .
\end{aligned} \tag{86}$$

Hence

$$\begin{aligned}
&a_n [H^*(\omega_Q)]^{m-Q} \dots [H^*(\omega_1)]^{m-1} [H(\omega_1)]^{m_1} \dots [H(\omega_Q)]^{m_Q} K(\omega_M) \\
&= H_n(\underbrace{\omega_{-Q}, \dots, \omega_{-Q}}_{m-Q}, \dots, \underbrace{\omega_{-1}, \dots, \omega_{-1}}_{m-1}, \dots, \underbrace{\omega_1, \dots, \omega_1}_{m_1}, \\
&\quad \underbrace{\omega_Q, \dots, \omega_Q}_{m_Q})
\end{aligned} \tag{87}$$

This exercise demonstrates that an n^{th} -order Volterra transfer function consists of an n^{th} -order power coefficient and a frequency response transfer function. This result will aid in the analysis of cascade relationships for nonlinear systems.

CHAPTER 2

CORRECTION METHODS FOR MICROWAVE AMPLIFIER NONLINEARITIES

2.1 Introduction

A wide variety of nonlinear distortion correction systems have been proposed and implemented. An excellent overview of some of these systems has been presented by Green [7], while King [8] has related amplifier linearity to the concerns of efficiency in a spacecraft environment. Feedforward linearization has been utilized by Seidel [9], Bennet [10], and Prochazka and Neumann [11], the latter having attempted a wideband linearization scheme. Predistortion systems are popular, with analysis and implementation of such linearizers having been undertaken by George, Kaye, and Eric [3] and Hetrakul and Taylor [12] among others. Envelope elimination and restoration systems were pioneered by Kahn [13] and later developed by Cox [14]. However, some of these systems have limitations affecting their usefulness at higher frequencies or require a great deal of complexity for practical realization. An examination of some of these methods follows.

2.1.1 Power back-off

The linearization method of power back-off [15], [16] consists of keeping the magnitude of the input envelope sufficiently small so as to ensure operation over a region of linear amplification. In this approach, there is no true linearization of the amplifier, rather one submits to the limitations imposed by the system. An extension to this method is to use power dividers with multiple amplifiers, each amplifier therefore being backed off to a region of linear operation.

Given a memoryless voltage nonlinearity with a (v_{IN}, v_o) - relationship given by

$$v_o = \sum_{n=1}^{\infty} a_n v_{IN}^n \quad (88)$$

use of two identical system amplifiers in parallel, with their outputs recombined will yield, see Figure 2.1,

$$v_o = \sqrt{2} \sum_{n=1}^{\infty} a_n \left(\frac{v_{IN}}{\sqrt{2}} \right)^n \quad (89)$$

or

$$v_o = \sum_{n=1}^{\infty} a_n \frac{v_{IN}^n}{(\sqrt{2})^{n-1}} \quad (90)$$

Hence each term in the nonlinear series has been reduced by a factor of $\sqrt{2}^{n-1}$ compared with that of a single amplifier system.

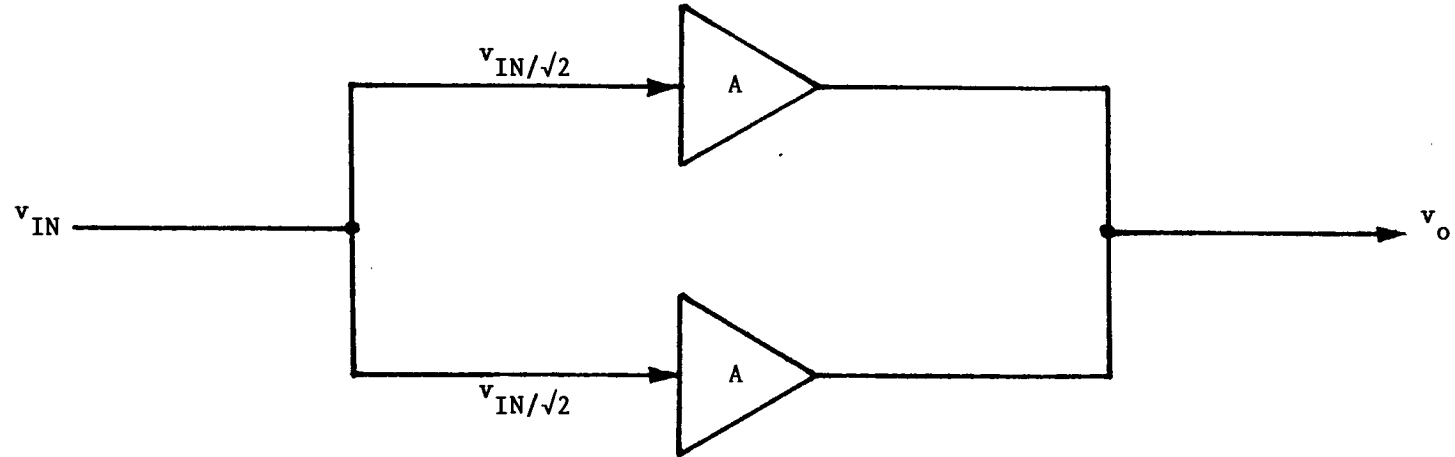


Figure 2.1. Dual amplifier topology.

The advantage of this system is the ease of implementation of the "linearizer". The drawbacks are obvious, and include the increased weight and power consumption for the additional amplifier(s).

2.1.2 Negative feedback

Negative feedback [17] is a familiar concept and is a popular method of minimizing nonlinear distortion at low frequencies. At microwave frequencies, however, transit-time delays preclude the use of feedback on a modular^o level. Some success can be obtained by applying feedback at the device (e.g., transistor) level, although careful design is required to ensure stability over all frequencies and source/load impedances [18].

Feedback also results in a loss of HPA gain, a somewhat costly drawback.

2.1.3 Feedforward

Feedforward [19] is a less familiar concept than feedback, although similar in function. Both systems are based on the comparison of the input signal with the distorted output signal, generating an error signal. Feedforward, however, does not encounter the transit time difficulties associated with the feedback system, and consequently does not degrade amplifier stability. The feedforward system does require two amplifiers (the main and an error amplifier) which have substantially the same performance. In addition, the overall system is very sensitive to errors

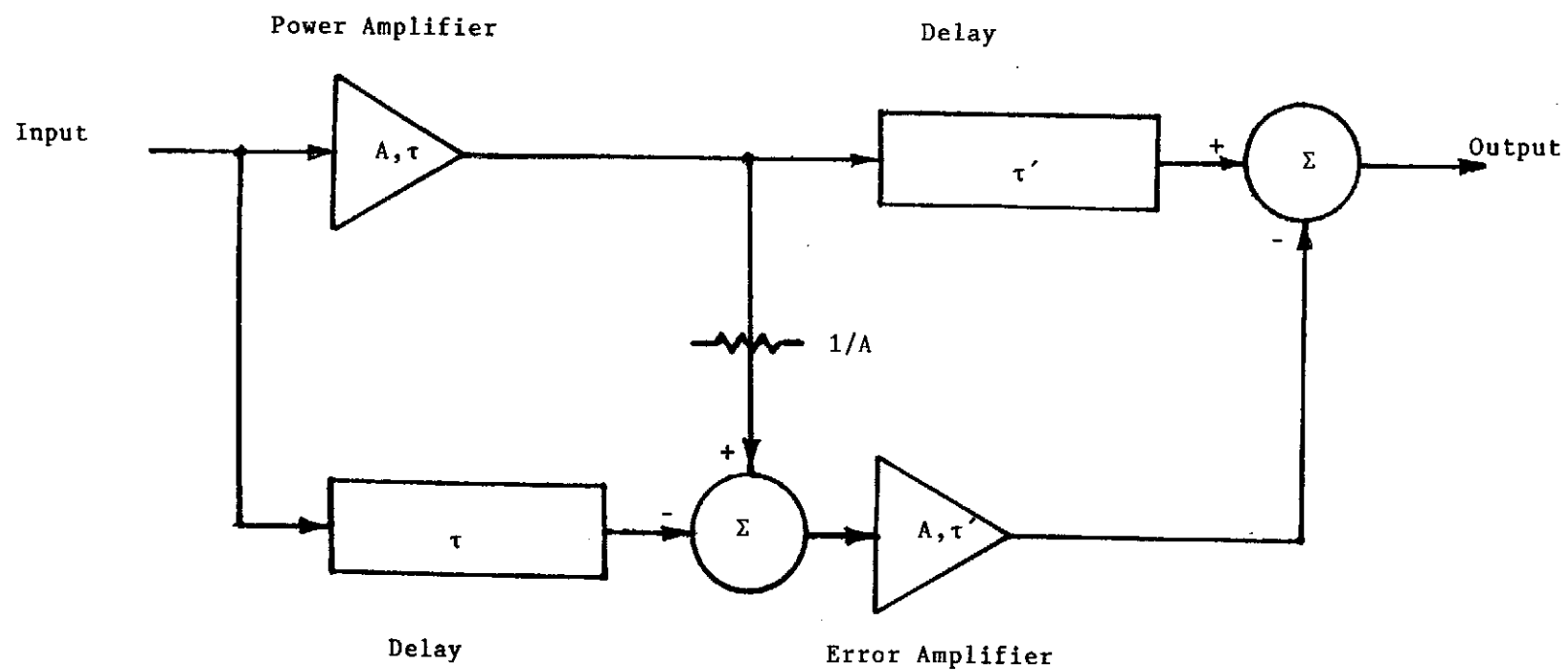


Figure 2.2. Feedforward distortion reduction topology.

in coupling factors and delay lines, therefore a high level of precision is required for these components [20]. Adaptive control is almost essential [9] in order to compensate for drifting and aging incurred by the system components. See Figure 2.2.

Feedforward does have the capability of distortion correction regardless of the type of amplifier frequency response (i.e., including nonlinearities with memory) and should be a topic for future research.

2.1.4 Predistortion/postdistortion techniques

Pre- and postdistortion [3], [12], [21] - [30] are functionally the same concept, differing only in the order in which the signal encounters the nonlinear amplification and correction devices. The following discussion applies specifically to predistortion, postdistortion being less in favour due to the inherently larger power losses involved in distorting a higher signal level.

Predistortion systems involve the introduction of a nonlinearity complementary to that of the amplifier, the result being an essentially linear amplifier up to the point of amplifier compression. This predistortion can occur at baseband, intermediate frequency, or directly at RF, the only limitation being the generation of in-band harmonics for up-converted systems (see Chapter 3.2.6).

By implementation of an "in-phase/quadrature" system [3], both

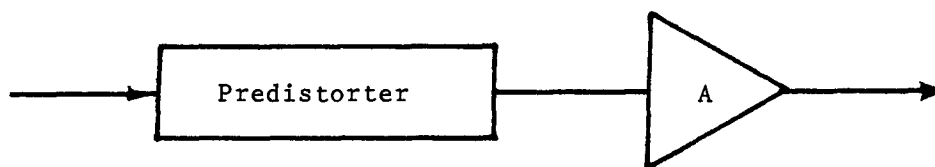


Figure 2.3a. Predistortion system.

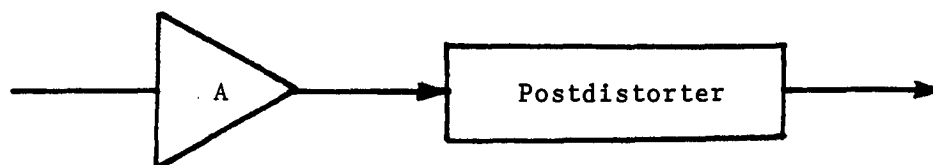


Figure 2.3b. Postdistortion system.

amplitude and phase nonlinearities can be corrected using two nonlinear amplitude predistorters, as shown in Figure 2.4. Drawbacks to this system include the difficulties in predistorter design, particularly for nonlinearities with memory, and potential system performance degradation with temperature changes or ageing. An adaptive system may be required.

2.1.5 Linear amplification with nonlinear components (LINC)

LINC involves the separation of the complex AM signal input into two angle-modulated components [13], [14], [31], [32]. Amplification is then achieved by high-efficiency Class C amplification, and the signals recombined to regenerate an amplified, undistorted AM signal, as shown in Figure 2.5.

The system has a very serious flaw, even with perfect component separation, if phase nonlinearities are present in the Class C HPA's.

Here

$$S_{1a}(t) = \left(\frac{E_M}{2}\right) \sin(\omega_o t + \phi(t)); \quad S_{2a}(t) = \left(\frac{E_M}{2}\right) \sin(\omega_o t - \phi(t)) \quad (91)$$

where E_M represents the maximum input amplitude.

If the amplifiers only possess memoryless nonlinearities, then the output is given by

$$GS_{1a}(t) - GS_{2a}(t) = GE_M \sin \phi(t) \cos \omega_o t \quad , \quad (92)$$

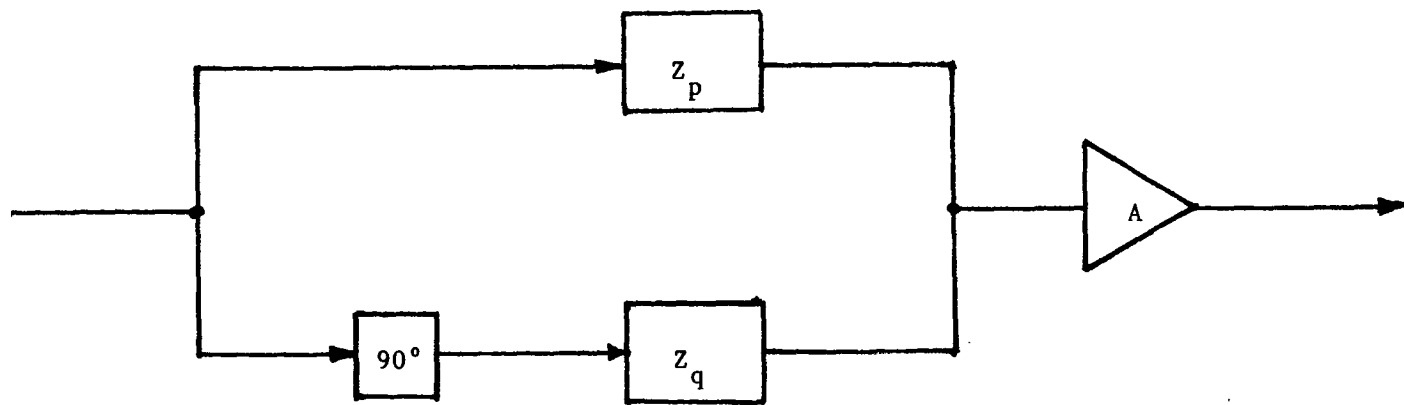


Figure 2.4. "In-phase/quadrature" predistortion topology.

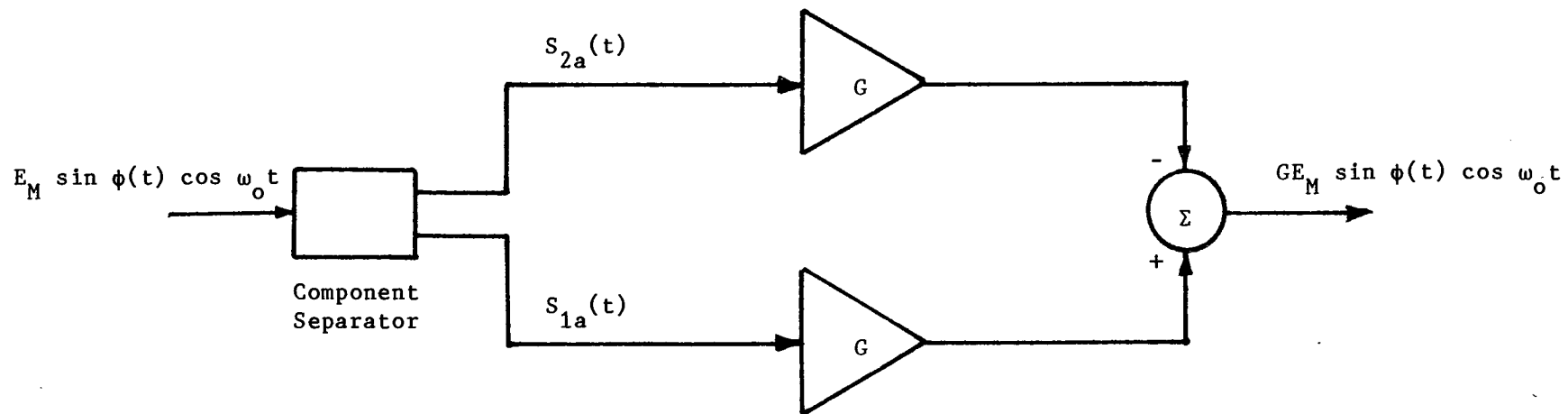


Figure 2.5. LINC topology.

an undistorted replica of the input. If, however, a phase nonlinearity is present, then

$$GS'_{1a}(t) = G\left(\frac{E_M}{2}\right) \sin(\omega_0 t + \phi(t) + \Theta(E)) \quad (93a)$$

and

$$GS'_{2a}(t) = G\left(\frac{E_M}{2}\right) \sin(\omega_0 t - \phi(t) + \Theta(E)) \quad (93b)$$

where $\Theta(E)$ represents an AM-to-PM term present in the HPA's.

Now

$$GS'_{1a}(t) - GS'_{2a}(t) = GE_M \sin \phi(t) \cos(\omega_0 t + \Theta(E)) \quad (94)$$

Thus the original AM-to-PM term for the amplifier is still present. Recalling that AM-to-PM conversion represents not only a change in the instantaneous frequency of the signal, but is symptomatic of harmonic and intermodulation distortion (Section 1.3.5), one sees that LINC has a major flaw, precluding its use as a stand-alone linearization technique.

CHAPTER 3

PREDISTORTION: CONCEPT AND THEORY

After a survey of known linearization techniques, it was decided to attempt to realize a predistortion system. This technique was chosen on account of its relative ease of implementation while utilizing only one HPA. It was also decided, in advance, to employ an adaptive system, that is the predistorter would be required to realize a wide variety of nonlinear transfer functions.

Before attempting a design, all mechanisms of predistortion correction should be thoroughly understood. A detailed theory of predistortion follows.

3.1 A Heuristic View of Predistortion

Superficially, a predistortion system appears to be readily analyzed. For example, if an amplifier exhibits a convex type nonlinearity, correction requires predistortion with a concave nonlinearity.

Understanding of predistortion requires a thorough examination of correction requirements over a wide range of system conditions. These requirements are considered in detail below.

3.1.1 Cascading of transfer functions

This operation yields little insight into predistortion, but serves the purpose of solidifying general concepts.

Given two memoryless amplitude nonlinearities represented by $f(x)$, $g(y)$, (see Figure 3.1), the output is given by

$$y = f(x) \tag{95}$$

$$z = g(y) = g(f(x)) \tag{96}$$

The functions $f(x)$ and $g(y)$ can be representative of the instantaneous voltage transfer functions, or of the envelope transfer functions (Chebyshev transforms). The instantaneous voltage transfer function representation is useful for wideband applications, while the envelope transfer function approach is useful for narrowband systems. In either case, the desired end result is

$$z = Ax \tag{97}$$

or

$$Ax = g(f(x)) \tag{98}$$

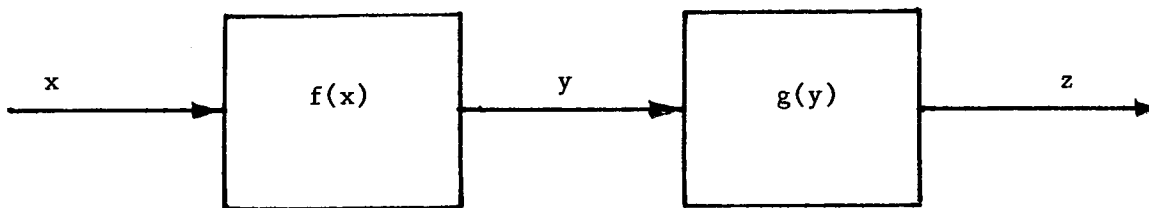


Figure 3.1. Cascaded amplitude transfer functions.

where A represents the overall system gain. Thus one requires

$$f(x) = g^{-1}(Ax) \quad . \quad (99)$$

Hence the correct predistorter transfer function is given by a scaled reflection of the amplifier transfer function in the line $f(x) = x$.

Thus if

$$g(y) = y^2 \quad (100)$$

and the desired over-all linear gain is 1/4, then

$$g^{-1}(x) = \sqrt{x} \quad (101)$$

$$g^{-1}\left(\frac{x}{4}\right) = \sqrt{\frac{x}{4}} \quad . \quad (102)$$

A similar discussion can be given for the compensation of phase nonlinearities, see Figure 3.2. Here the phase functions $\phi(x)$, $\theta(y)$ represent either AM-to-PM coefficients (narrowband case), or the phase transfer function (wideband case). From Figure 3.2

$$\psi_1 = \phi(x) \quad (103)$$

$$\psi_2 = \psi_1 + \theta(y) \quad . \quad (104)$$

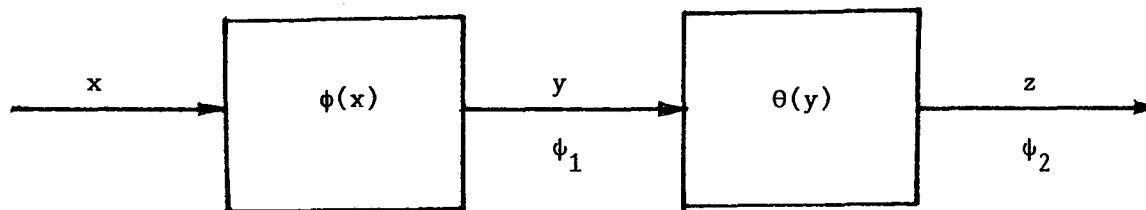


Figure 3.2. Cascaded phase transfer functions.

We now assume that $y = Ax$, that is, a linearly scaled variable. Then

$$\psi_2 = \phi(x) + \theta(Ax) = \text{Constant} = K \quad (105)$$

so that

$$\phi(x) = K - \theta(Ax) \quad (106)$$

Hence one must introduce an opposite sense of AM-to-PM conversion (narrowband nonlinearity) or an opposite sense of phase nonlinearity for a wideband system.

Analysis by these methods is practical for two extreme cases; a wideband system where one can assume that all nonlinear products are passed unaltered on to the next stage, or a narrowband single-carrier system where only the fundamental appears at the output. These two extremes are examined in greater detail in the next two sections, for memoryless nonlinearities.

3.1.2 Cascading of power series

Given two wideband nonlinearities represented by their instantaneous voltage Taylor series transfer functions, the output is given by:

$$v_o = \sum_{m=1}^{\infty} b_m \left[\sum_{n=1}^{\infty} a_n v_{IN}^n \right]^m, \quad (107)$$

see Figure 3.3.

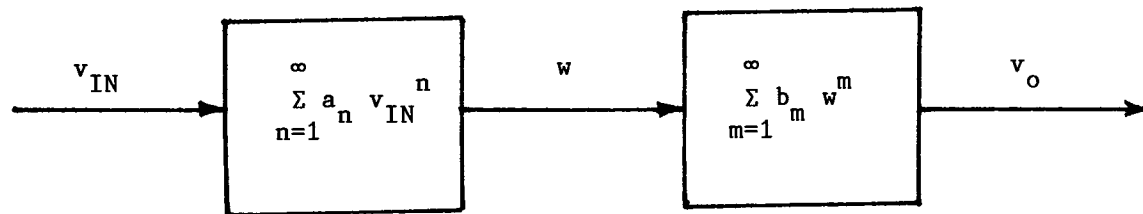


Figure 3.3. Cascaded power series.

This result is best handled by changing the m^{th} power into an m -fold indexed product:

$$v_o = \sum_{m=1}^{\infty} b_m \sum_{n_1=1}^{\infty} \sum_{n_2=1}^{\infty} \dots \sum_{n_m=1}^{\infty} a_{n_1} a_{n_2} \dots a_{n_m} v_{IN}^{(n_1+n_2+\dots+n_m)} \quad (108)$$

Gathering coefficients of powers of v_{IN} , up to the fifth order, yields:

$$\begin{aligned} v_o = & a_1 b_1 v_{IN} + v_{IN}^2 [b_1 a_2 + b_2 a_1^2] + v_{IN}^3 [b_1 a_3 + 2a_2 a_1 b_2 + b_3 a_1^3] \\ & + v_{IN}^4 [b_1 a_4 + b_2 [a_2^2 + 2a_3 a_1] + 3b_3 a_1^2 a_2 + b_4 a_1^4] \\ & + v_{IN}^5 [b_1 a_5 + 2b_2 a_1 a_4 + 2b_2 a_3 a_2 + b_3 [3a_1^2 a_3 + 3a_2^2 a_1] \\ & + 4b_4 a_1^3 a_2 + b_5 a_1^5] \quad (109) \end{aligned}$$

Elimination of all coefficients other than those of v_{IN} effectively linearizes the system. Thus the 2nd order linearization condition is

$$b_1 a_2 = -b_2 a_1^2 \quad (110)$$

and the 3rd order linearization condition is

$$b_1 a_3 + 2a_2 a_1 b_2 + b_3 a_1^3 = 0 \quad (111)$$

This procedure can be continued for any order desired, defining the exact power series relationships required for the predistorter.

This analysis approach appears to have limited usefulness for narrowband systems. In general, the system will have a frequency response. Correspondingly, some frequency products produced by a given order of nonlinearity will be eliminated. This will reduce the total signal attributable to that order of nonlinearity. The extreme case of this condition occurs for even-order nonlinearities which do not produce any bandpass products whatsoever. It thus appears doubtful whether the power series approach is of great utility for RF amplifiers, which in general operate over less than an octave bandwidth under current frequency plans and band allotments.

3.1.3 Envelope transfer function linearization: Cascading of the Chebyshev transform

A more useful predistorter linearization result can be obtained by extracting the bandpass components at the output of each nonlinear element. These linearization results are derived initially for a single carrier input, but will be shown later to hold for narrowband multi-carrier inputs. Mathematically, the derivation is identical to that for the cascade relationship for the power series, but in this case a unity-gain, ideal bandpass filter follows each element. This filtering action is performed by taking the first order Chebyshev transform [6] of the power series transfer functions, see Figure 3.4.

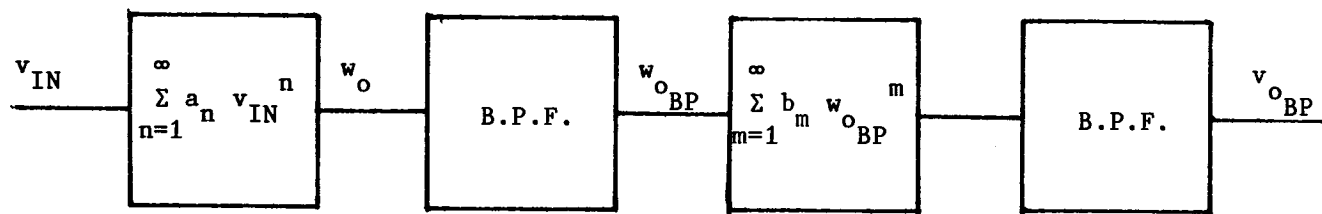


Figure 3.4. Cascading of the Chebyshev transform.

For any given order of nonlinearity, n , the fundamental output is given by transform T5 of Blackman [6] (see Appendix 2) namely

$$w_{oBP} = \sum_{n=1}^{\infty} 2a_n \binom{n}{\frac{1}{2}(n-1)} \left(\frac{v_{IN}}{2}\right)^n \quad (112)$$

therefore

$$v_{oBP} = \sum_{m=1}^{\infty} 2b_m \binom{m}{\frac{1}{2}(m-1)} \left[\sum_{n=1}^{\infty} a_n \binom{n}{\frac{1}{2}(n-1)} \left(\frac{v_{IN}}{2}\right)^n \right]^m \quad (113)$$

Again it is useful to change the m -exponent into an m -fold indexed multiplication:

$$v_{oBP} = \sum_{m=1}^{\infty} 2b_m \binom{m}{\frac{1}{2}(m-1)} \sum_{n_1=1}^{\infty} \sum_{n_2=1}^{\infty} \dots \sum_{n_m=1}^{\infty} a_{n_1} a_{n_2} \dots a_{n_m} \binom{n_1}{\frac{1}{2}(n_1-1)} \binom{n_2}{\frac{1}{2}(n_2-1)} \dots \binom{n_m}{\frac{1}{2}(n_m-1)} \left(\frac{v_{IN}}{2}\right)^{(n_1+n_2+\dots+n_m)} \quad (114)$$

Noting that even-order nonlinearities do not contribute to a bandpass component, and gathering coefficients of odd powers of v_{IN} , up to the fifth order yields

$$\begin{aligned}
v_{o_{BP}} = & a_1 b_1 v_{IN} + \frac{v_{IN}^3}{4} [b_1 a_3 \binom{3}{1} + 2a_2 b_2 a_1 \binom{2}{1/2}^2 + b_3 a_1^3 \binom{3}{1}] \\
& + \frac{v_{IN}^5}{16} [b_1 a_5 \binom{5}{2} + 2b_2 a_1 a_4 \binom{2}{1/2} \binom{4}{3/2} + 2b_2 a_3 a_2 \binom{2}{1/2}^2 \\
& + b_3 \binom{3}{1} [3a_1^2 a_3 \binom{3}{1} + 3a_2^2 a_1 \binom{2}{1/2}^2] \\
& + 4b_4 a_1^3 a_2 \binom{4}{3/2} \binom{2}{1/2} + b_5 a_1^5 \binom{5}{2}] \quad . \quad (115)
\end{aligned}$$

It is not obvious, but some of these odd-order terms can be eliminated as they are caused by out-of-band interactions between the two nonlinearities. It will be shown later, in Section 3.1.4, that any terms containing even-order Taylor coefficients can be eliminated. The end result therefore is:

$$v_o = a_1 b_1 v_{IN} + \frac{v_{IN}^3}{4} [3b_1 a_3 + 3b_3 a_1^3] + \frac{v_{IN}^5}{16} [10b_1 a_5 + 27b_3 a_1^2 a_3 + 10b_5 a_1^5] \quad . \quad (116)$$

Elimination of all coefficients other than those of v_{IN} effectively linearizes the system. That is, the 3rd order linearization condition is:

$$b_1 a_3 = -b_3 a_1^3 \quad (117)$$

and the 5th order linearization condition is:

$$10b_1a_5 + 27b_3a_1^2a_3 + 10b_5a_1^5 = 0 . \quad (118)$$

An important point is the discrepancy that exists between linearization of the instantaneous voltage transfer function and linearization of the envelope transfer function (compare (111) to (118)). Obviously, the predistorter power series coefficients differ for these two cases, indicating that for cascaded nonlinearities, one can obtain either a linearized voltage transfer function, or linearized envelope transfer function but these two conditions do not occur simultaneously. Consequently, one cannot apply the Chebyshev transform for cascaded nonlinear systems. This is contrary to existing ideas, see for example George, Kaye and Eric [3]. This result can be emphasized by proposing linearization on the basis of the envelope transfer function. Not only are the odd-order predistorter coefficients different from those specified by voltage linearization (excepting those of the third-order), but even-order curvatures, which have no effect on the bandpass envelope, cannot be corrected for in a narrowband system. These coefficients will remain unchanged for envelope linearization. Hence for narrowband systems, one should approach linearization on the basis of envelope transfer functions, and not on the misconception of an overall linearized voltage response [23], [30].

The final concept to be presented in this subsection deals with amplitude and phase compensation by the "in-phase/quadrature" method. If the amplifier has been modelled by the narrowband "in-phase/quadrature" approach, it is reasonable to assume that amplitude envelope linearization

of both signal paths would result in an amplitude and phase compensated amplifier [3], [12], [25], [26] (see Figure 3.5).

The two signal paths for the predistorter simultaneously supply a complementary sense of AM-to-AM, and AM-to-PM conversion to that of the amplifier, the net result being an amplitude and phase compensated amplifier.

3.1.4 Cascaded Volterra series

The cascaded Volterra series results yield by far the most information on the performance of predistortion systems, this being due to the inherent ease of handling nonlinear systems with memory. The cascade derivation proceeds as follows.

As in the case of the derivation of the Volterra series relationship, we start by defining the input. In this case, the desired input is governed by the n^{th} -order nonlinear transfer function G_n of the first nonlinear system, see Figure 3.6. Here

$$x(t) = \sum_{n=1}^N \frac{(n; M_{ni})}{2^n} G_n(\omega_1, \dots, \omega_n) \exp j\omega_{M_{ni}} t \quad (119)$$

where $\omega_{M_{ni}}$ represents the frequency mix governed by the n^{th} -order nonlinear transfer function. Here n is indexed over all values and i is indexed over all mixes governed by the n^{th} power. Hence all possible outputs of the first system are included.

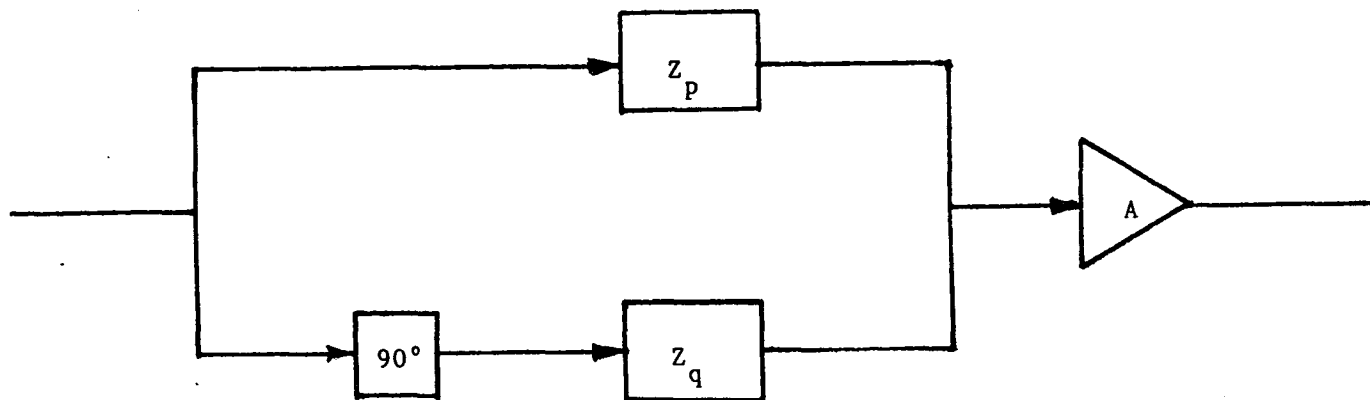


Figure 3.5. "In-phase/quadrature" predistortion system.

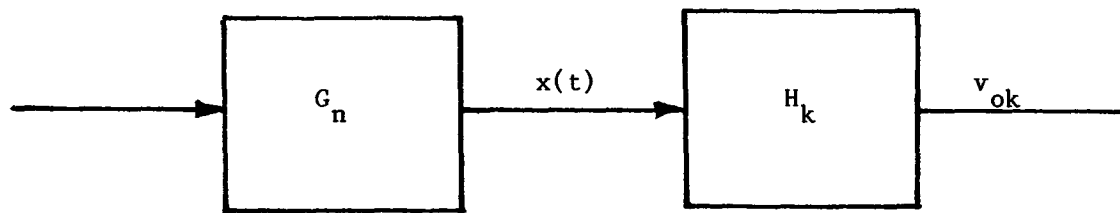


Figure 3.6. Cascaded Volterra system.

The output of the second system is given by the k^{th} -order nonlinear transfer function, as directed by the k^{th} -order impulse response:

$$v_{ok} = \int_{-\infty}^{\infty} \int_{-\infty}^{\infty} \dots \int_{-\infty}^{\infty} h_k(\tau_1, \tau_2, \dots, \tau_k) x(t-\tau_1) x(t-\tau_2) \dots x(t-\tau_k) d\tau_1 d\tau_2 \dots d\tau_k, \quad (120)$$

thus

$$v_{ok} = \int_{-\infty}^{\infty} \int_{-\infty}^{\infty} \dots \int_{-\infty}^{\infty} h_k(\tau_1, \tau_2, \dots, \tau_k) \sum_{n_1=1}^N \frac{(n_1; M_{n_1})}{2^{n_1}} G_{n_1}(\omega_{11}, \dots, \omega_{n_1}) \exp(j\omega_{M_{n_1}}(t-\tau_1)) \dots \sum_{n_k=1}^N \frac{(n_k; M_{n_k})}{2^{n_k}} G_{n_k}(\omega_{1k}, \dots, \omega_{n_k}) \exp(j\omega_{M_{n_k}}(t-\tau_k)) d\tau_1 \dots d\tau_k. \quad (121)$$

Re-arranging the integral gives

$$v_{ok} = \sum_{n_1=1}^N \dots \sum_{n_k=1}^N \frac{(n_1; M_{n_1})}{2^{n_1}} G_{n_1}(\omega_{11}, \dots, \omega_{n_1}) \dots \frac{(n_k; M_{n_k})}{2^{n_k}} G_{n_k}(\omega_{1k}, \dots, \omega_{n_k}) \exp(j(\omega_{M_{n_1}} + \dots + \omega_{M_{n_k}})t) \int_{-\infty}^{\infty} \dots \int_{-\infty}^{\infty} h_k(\tau_1, \dots, \tau_k) \exp(-j(\omega_{M_{n_1}}\tau_1 + \dots + \omega_{M_{n_k}}\tau_k)) d\tau_1 \dots d\tau_k \quad (122)$$

The total exponential response requires the addition of all permutations producing the same frequency, a factor of $(k; M_{OUT})$, where M_{OUT} represents the frequency mix vector of the total system output. The total real response is twice the exponential response. Thus

$$v_{ok} = 2 \sum_{n_1=1}^N \dots \sum_{n_k=1}^N \frac{(n_1; M_{n1})}{2^{n_1}} G_{n_1}(\omega_{11}, \dots, \omega_{n_1}) \dots \frac{(n_k; M_{nik})}{2^{n_k}} G_{n_k}(\omega_{1k}, \dots, \omega_{nk}) H_k(\omega_{M_{n1}}, \dots, \omega_{M_{nik}}) (k; M_{OUT}) \cos(\omega_{M_{n1}} + \dots + \omega_{M_{nik}}) t \quad (123)$$

where

$$H_k(\omega_{M_{n1}}, \dots, \omega_{M_{nik}}) \quad (124)$$

is the k^{th} -order nonlinear transfer function with inputs governed by the frequency mix of the first nonlinear system. Also

$$\omega_{M_{OUT}} = \omega_{M_{n1}} + \omega_{M_{n2}} + \dots + \omega_{M_{nik}} \quad (125)$$

Others [4], [21], have analyzed cascaded Volterra systems, but their results differ from those presented here for the following reason. At the output of the first nonlinear system, one is required to sum all components produced by a given power, at the frequency mix of interest. Hence the origin of the $(n; M)$ terms for the cascaded result. The cascade results derived in this thesis will be shown to agree with the cascaded envelope transfer function results (derived in Section 3.1.3), verifying the analysis.

Weiner and Spina [4], have demonstrated a close relationship between cascade results for the power series and the Volterra series, see Table 1.

TABLE 1

Coefficient of	Power Series	Volterra Series
v_{IN}	$a_1 b_1$	$G_1(\omega_1) H_1(\omega_1)$
v_{IN}^3	$b_1 a_3 + 2a_2 a_1 b_2 + b_3 a_1^3$	$\frac{(3;M)}{2} G_3(\omega_1, \omega_2, \omega_3) H_1(\omega_1 + \omega_2 + \omega_3)$ $+ 2G_2(\omega_1, \omega_2) G_1(\omega_3) H_2(\omega_1 + \omega_2, \omega_3)$ $\frac{(2;M)}{2} (2;M_{OUT})$ $+ G_1(\omega_1) G_1(\omega_2) G_1(\omega_3) H_3(\omega_1, \omega_2, \omega_3)$ $\frac{(3;M_{OUT})}{2}$

Note that the frequency dependence of the Volterra transfer functions allows the elimination of certain terms which can be filtered out of band. For example, by examining the middle term in the third-order Volterra relationship of Table 1:

$$2G_2(\omega_1, \omega_2) G_1(\omega_3) H_2(\omega_1 + \omega_2, \omega_3) \frac{(2;M)}{2} (2;M_{OUT}) \quad (126)$$

one sees that the $G_2(\omega_1, \omega_2)$ term will mix the frequency products at ω_1 and ω_2 , providing an output at $\omega_1 + \omega_2$. In general, ω_1 and ω_2 can represent any frequency, positive or negative. Thus if ω_1 is positive and ω_2 is negative, then the output is a second-order intermodulation product at $\omega_1 - \omega_2$. If $\omega_1 = \omega_2$ (both either positive or negative), the output is then a second harmonic at $2\omega_1$. Note that neither of these products are bandpass components and they will therefore have no effect on the cascaded system performance. In general, any even-order transfer functions involved in a cascade relationship can be ignored for narrowband linearization, as these products will be filtered out. The remaining third-order cascade result is therefore

$$\frac{(3;M)}{2} G_3(\omega_1, \omega_2, \omega_3) H_1(\omega_1 + \omega_2 + \omega_3) + G_1(\omega_1) G_1(\omega_2) G_1(\omega_3) H_3(\omega_1, \omega_2, \omega_3) \frac{(3;M)}{2} . \quad (127)$$

If we let $\omega_2 = \omega_3$, $\omega_1 = -\omega_1$, producing a third-order intermodulation product at $2\omega_2 - \omega_1$, the linearization condition requires

$$G_3(-\omega_1, \omega_2, \omega_2) H_1(2\omega_2 - \omega_1) = -G_1(\omega_1) G_1(\omega_2) G_1(\omega_2) H_3(-\omega_1, \omega_2, \omega_2) . \quad (128)$$

In terms of real signals, linearization of the third-order term involves generation of a third-order intermodulation product by the predistorter, followed by amplification by the linear component of the HPA. This product must have equal amplitude to but opposite phase from the same frequency intermodulation product produced by the third-order component

of the amplifier, preceded by the linear component of the predistorter. In simpler terms, the predistorter must generate nonlinear and linear products which combine with the nonlinear and linear products generated by the amplifier, so as to eliminate all undesired frequency terms and odd-order curvatures of the transfer function.

One can also obtain the cascaded Chebyshev transform results directly from the cascaded Volterra series results. For example, by examination of the fifth-order results, and generating a fundamental output for a single carrier input at ω_1 , one finds that the coefficients of v_{IN}^5 are from (123)

$$\begin{aligned}
 & \frac{(5; -\omega_1, -\omega_1, \omega_1, \omega_1, \omega_1)}{16} G_5(-\omega_1, -\omega_1, \omega_1, \omega_1, \omega_1) H_1(\omega_1) \\
 & + 3G_1(\omega_1)G_1(\omega_1)G_3(-\omega_1, -\omega_1, -\omega_1)H_3(\omega_1, \omega_1, -\omega_1) \frac{(3; -\omega_1, -\omega_1, \omega_1)}{16} (3; \omega_1, \omega_1, -\omega_1) \\
 & + G_1(\omega_1)G_1(\omega_1)G_1(\omega_1)G_1(-\omega_1)G_1(-\omega_1)H_5(-\omega_1, -\omega_1, \omega_1, \omega_1, \omega_1) \\
 & \cdot \frac{(5; -\omega_1, -\omega_1, \omega_1, \omega_1, \omega_1)}{16} \tag{129}
 \end{aligned}$$

which is equal to

$$\frac{10}{16} G_5(-\omega_1, -\omega_1, \omega_1, \omega_1, \omega_1) H_1(\omega_1) + \frac{27}{16} G_1(\omega_1) G_1(\omega_1) G_3(-\omega_1, -\omega_1, \omega_1)$$

$$\cdot H_3(\omega_1, \omega_1, -\omega_1) + \frac{10}{16} G_1(\omega_1)G_1(\omega_1)G_1(\omega_1)G_1(-\omega_1)G_1(-\omega_1)H_5(-\omega_1, -\omega_1, \omega_1, \omega_1, \omega_1) .$$

(130)

These coefficients are seen to agree exactly with the linearization conditions as set for the Chebyshev transform, assuming memoryless conditions (see equation (116) for comparison). Note that the above derivation could just as easily have been done for the frequency mix for a fifth-order intermodulation product at $2\omega_2 - \omega_1$, i.e., for the first term

$$\frac{(5; -\omega_1, \omega_1, -\omega_1, \omega_2, \omega_2)}{16} G_5(-\omega_1, \omega_1, -\omega_1, \omega_2, \omega_2) H_1(2\omega_2 - \omega_1) + \dots \quad (131)$$

The coefficients are identical to those for the cascade relationship for the Chebyshev transform. It would appear, therefore, that linearization of the envelope transfer function is optimal for narrowband predistortion systems.

The cascade results for the Volterra series can be transformed into cascade results for the power-series-with-frequency response by substitution of (87) into (123) (substitution for the n^{th} -order nonlinear transfer function by the similar memoryless transfer function in the cascaded Volterra result). Thus the linear response $G_1(\omega_1)H_1(\omega_1)$ is readily transformed into

$$\begin{aligned}
G_1(\omega_1)H_1(\omega_1) &= g_1 h_1 G(\omega_1)G'(\omega_1)H(\omega_1)H'(\omega_1) \\
&= g_1 h_1 G(\omega_1)K(\omega_1)H'(\omega_1)
\end{aligned} \tag{132}$$

where

$$K(\omega_1) = G'(\omega_1)H(\omega_1) , \tag{133}$$

see Figure 3.7.

3.1.5 The creation of new nonlinear products for cascaded systems

A point of interest for cascaded nonlinear systems concerns the creation of nonlinear products not associated with either nonlinear system. Let us assume that the predistorter and HPA can be completely represented by a linear and a third-order component, as shown in Figure 3.8. The output will now contain products up to the ninth order (i.e., a cubic power cubed). Examining the fifth-order result, retaining only the relevant bandpass components, one obtains

$$v_o = a_1 b_1 v_{IN} + \dots + v_{IN}^5 [b_1 a_5 + 3b_3 a_1^2 a_3 + b_5 a_1^5] . \tag{134}$$

Cancellation of the fifth-order coefficient requires that

$$b_1 a_5 + b_5 a_1^5 + 3b_3 a_1^2 a_3 = 0 . \tag{135}$$

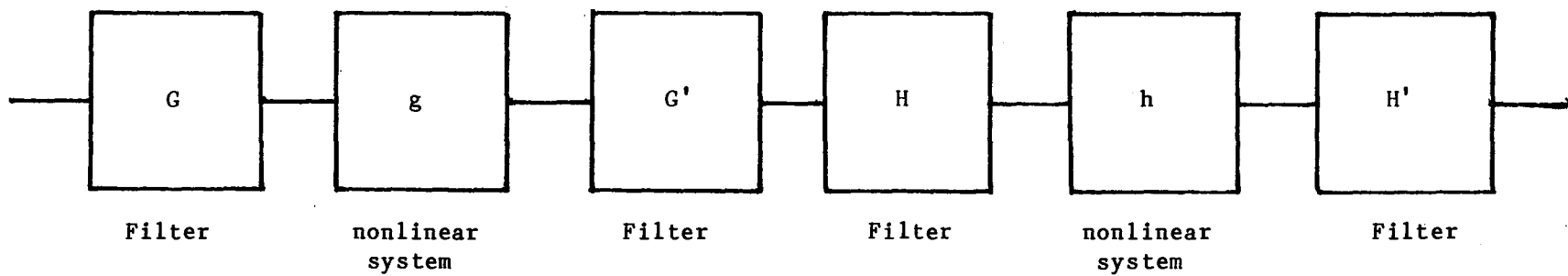


Figure 3.7. Power series with frequency response cascade.

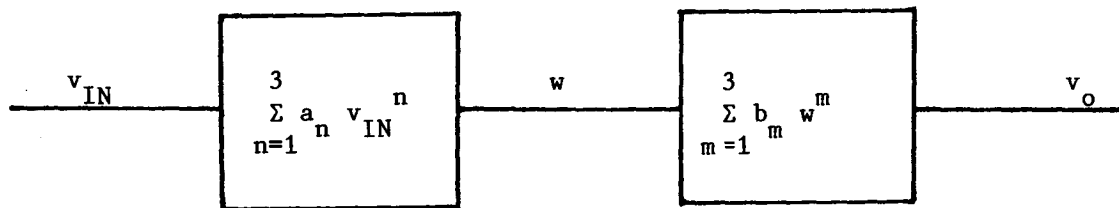


Figure 3.8. Cascaded third-order systems.

However, since a_5 and b_5 are zero, the resultant $3b_3a_1^2a_3$ term cannot be eliminated. In a practical predistortion system, one would therefore expect to possibly see an increase in fifth-order products, if the system objective was absolute minimization of third-order products. This argument holds for all higher-order products and this effect is evident in most predistortion systems. A perfectly complementary predistorter would, of course, provide absolute linearization, but is a practical impossibility. Note that the third-order nonlinear products are usually the largest, and a substantial decrease in these products, while slightly increasing the much lower amplitude higher-order products, is a desirable result.

3.1.6 Predistortion system performance for upconverted systems

The question arises, at what frequency band should the predistorter be introduced, at the baseband, some IF, or directly at RF? In terms of complexity, certainly the baseband predistortion system is the easiest to realize with the multitude of low-frequency compression and expansion function modules available. In general, IF predistortion is the next easiest system to implement, while direct RF predistortion is the most difficult, since circuit difficulties increase with increasing frequency.

This question can be partially answered analytically. We start with a general predistortion system which incorporates an upconversion between the predistorter and the amplifier, see Figure 3.9. Examination of the overall second-order transfer function gives

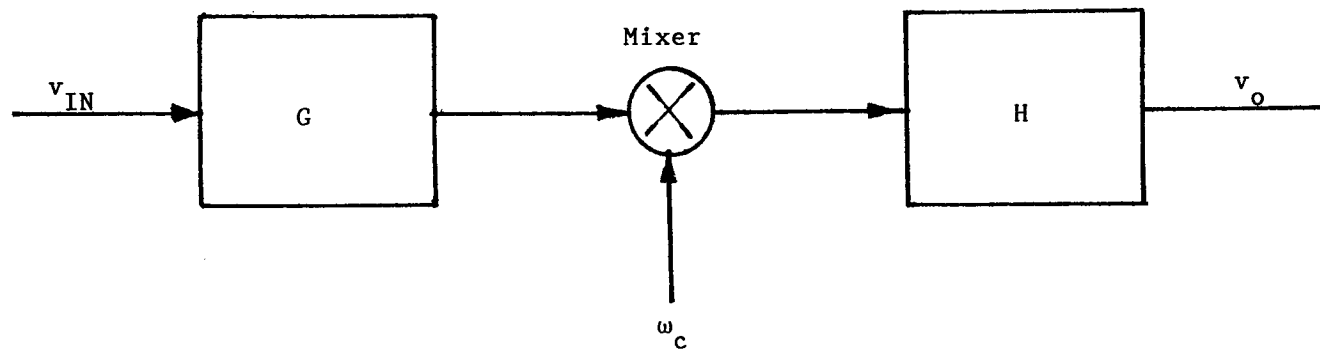


Figure 3.9. Predistortion system with upconversion.

$$K_2(\omega_1, \omega_2) = G_2(\omega_1, \omega_2)H_1(\omega_c + \omega_1 + \omega_2) + G_1(\omega_1)G_1(\omega_2)H_2(\omega_c + \omega_1, \omega_c + \omega_2), \quad (36)$$

where $K_2(\omega_1, \omega_2)$ is the cascaded, second-order Volterra transfer function and where coefficients of the transfer functions have been omitted, as we are only concerned with the frequencies involved in the Volterra transfer functions. Cancellation requires the amplitude of the first term in (136) to be of equal amplitude, but of opposite phase to the second term. However, the first term produces an output of frequency $\omega_c + \omega_1 + \omega_2$, while the second term produces a frequency $2\omega_c + \omega_1 + \omega_2$. Therefore, cancellation cannot occur, and the bandpass $\omega_c + \omega_1 + \omega_2$ term will remain due to the frequency translation by upconversion. This is in general true for all harmonic terms in an upconverted predistortion system. Note that cancellation can only occur if

$$\omega_c + \omega_1 + \omega_2 = 2\omega_c + \omega_1 + \omega_2 \quad (37)$$

or

$$\omega_c = 0. \quad (38)$$

An examination of predistorter performance for intermodulation products yields

$$\begin{aligned}
K_3(-\omega_1, \omega_2, \omega_2) &= G_3(-\omega_1, \omega_2, \omega_2) H_1(\omega_c - \omega_1 + 2\omega_2) \\
&+ G_1(-\omega_1) G_1(\omega_2) G_1(\omega_2) H_3(-\omega_c - \omega_1, \omega_c + \omega_2, \omega_c + \omega_2) \\
&+ 2G_1(-\omega_1) G_2(\omega_2, \omega_2) H_2(\omega_c + 2\omega_2, \omega_c - \omega_1) \quad . \quad (139)
\end{aligned}$$

The first and second terms have outputs at $\omega_c + 2\omega_2 - \omega_1$, the third term at $2\omega_c + 2\omega_2 - \omega_1$ and this last term can be filtered out. Hence the two bandpass terms represent intermodulation products at the same frequency and cancellation can occur.

The mathematical results can be summarized as follows. If predistortion is to be employed in a linearization system, one must ensure that harmonics produced by the predistorter do not degrade performance of the system. Good performance can be achieved either by refraining from converting frequencies after predistortion, or by filtering out the predistorter harmonics prior to amplification by the HPA. Note that baseband predistortion systems will not satisfy the above conditions. For example, in a multicarrier voice system, predistorting at baseband will produce harmonics that cannot be removed by filtering. After upconverting and passing through the HPA, these baseband-originated harmonic terms will not be cancelled.

IF predistortion systems require selection of an intermediate frequency such that harmonics lie out of band, that is

$$2f_c \geq f_c + BW \quad (140)$$

or

$$f_c \geq BW \quad (141)$$

where f_c is the local oscillator frequency for the upconverter and BW is the system bandwidth.

RF predistortion avoids any frequency translation and may also be useful in the elimination of in-band harmonic terms. In addition, RF predistortion allows for wider band systems than does IF predistortion, IF bandwidth being limited by the upconversion frequency, as dictated by (141). Indeed, as the IF is increased to accommodate a wider bandwidth, the circuitry required to achieve the predistortion becomes comparable in complexity to that required for RF predistortion.

For the above reasons, it was decided to attempt a direct RF predistortion system. Interest in the MSAT program directed the choice of frequency to the 900 MHz UHF range.

3.1.7 Effect of predistortion on amplifier efficiency

Predistortion possesses the added benefit of increasing amplifier efficiency. This effect is the result of the linearization of the NPA, allowing higher RF output powers. For example, an increase in the 1 dB

compression point by 3 dB would double the efficiency of a linearly biased (class AB) HPA. This effect is of great significance for satellite transponders where power considerations are of paramount importance.

3.2 Summary of Theoretical Advancements

Several advancements to nonlinear theory have been developed in this report. First, the cascading of two nonlinear systems and the derivation of the resultant envelope transfer function was presented in Section 3.1.3. It was demonstrated that linearization of the envelope transfer function was not equivalent to linearization of the instantaneous voltage transfer function. Hence the Chebyshev transform (or its mathematical inverse) is not applicable for cascaded nonlinear systems.

Section 3.1.4 illustrated the cascading of two nonlinearities modelled by their Volterra representations. This result was shown to be equivalent to the result of Section 3.1.3, for the single-carrier, memoryless case. In addition, linearization of the envelope transfer function was shown to simultaneously minimize bandpass intermodulation products. Thus the optimum compensating function for narrowband predistortion was proven to be the nonlinear characteristic that would linearize the single-carrier, envelope transfer function.

Finally, Section 3.1.6 demonstrated the effect of a frequency conversion for a predistortion system. Baseband predistortion was found to have

limited usefulness in the linearization of RF amplifiers due to the generation of in-band harmonic products. Hence IF or RF predistortion would have to be employed for any microwave system.

CHAPTER 4

RF PREDISTORTER DESIGN

4.1 Introduction

The design and realization of nonlinear circuits is in general a difficult task. These difficulties become compounded at RF, where even linear circuits can become complicated on account of packaging parasitics and other residual reactances.

A unique RF predistorter that overcomes the problems of parasitics, but remains flexible enough to realize a wide variety of transfer functions for adaptive systems is presented.

4.2 Proposed RF Predistortion System

For RF predistortion systems, two topologies are the most prevalent; the "in-phase/quadrature" system and the "phase modulator" system [3], see Figure 4.1. The "in-phase/quadrature" method requires two nonlinear amplitude predistorters, while the alternative system requires a single

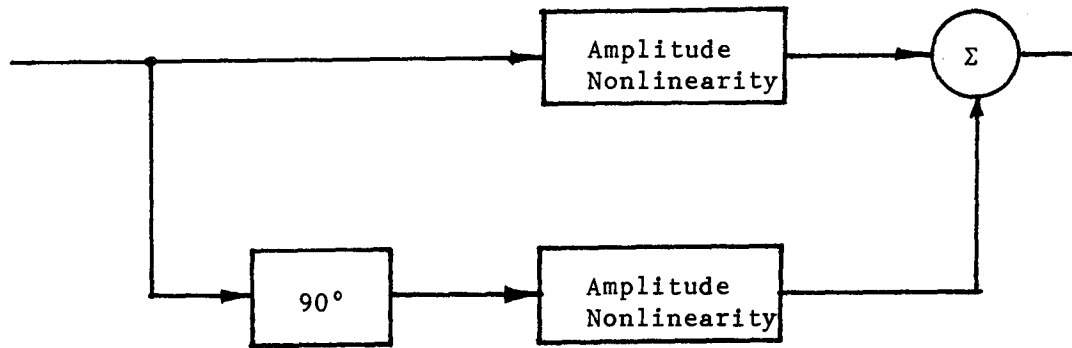


Figure 4.1a. "In-phase/quadrature" predistorter.

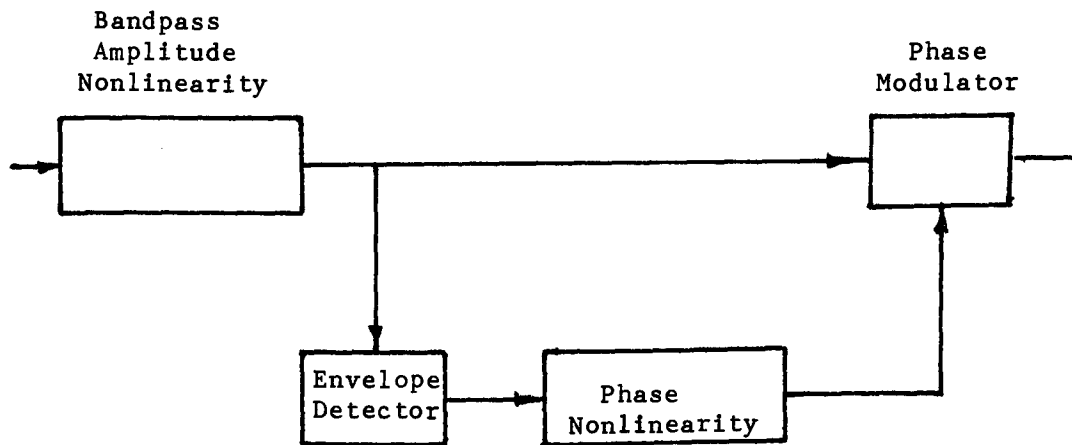


Figure 4.1b. Phase modulator predistorter.

amplitude predistorter and a phase modulator. This phase modulator responds to the detected RF envelope, modulating with an opposite sense of AM-to-PM conversion. Hence the "phase modulator" topology requires one to develop both an amplitude nonlinearity and a phase nonlinearity (two circuits), while the "in-phase/quadrature" method only requires two amplitude nonlinearities (one circuit). For this reason, the "in-phase/quadrature" method was selected for the predistortion scheme.

4.3 Development of An RF Predistorter

Having selected the "in-phase/quadrature" system, nonlinear circuit design was reduced to the development of an RF circuit that would realize a wide variety of nonlinear amplitude characteristics. Note that since the opposite sense of AM-to-PM conversion is generated by amplitude modulation of the two quadrature components, the amplitude predistorters should be designed so as to minimize any AM-to-PM conversion generated by these circuits. The circuit objectives can therefore be summarized as follows:

- (1) The circuit must respond in a nonlinear manner to the RF cycle, producing a specific nonlinear transfer characteristic.
- (2) The circuit should not generate a large amount of AM-to-PM conversion, that is, the nonlinearity should be "memoryless". Note that the predistorter will possess a frequency response as this is inevitable in RF design.

A survey of predistorter papers [22], [24], [25] revealed little on approaches to the design of an amplitude predistorter. All that was evident was that Schottky diodes could be employed in an anode-to-cathode ("head-to-tail") fashion, see Figure 4.2. Holbrook and Rockwell [22] have demonstrated a high frequency (7 MHz) predistorter circuit, employing semi-conductor diodes as nonlinear resistors in a divider arrangement, see Figure 4.3. These authors voiced some concerns about linear phase distortion generated by the circuit, but ignored any nonlinear phase distortion. Presumably if the predistortion circuit exhibited a significant enough frequency response to generate linear phase distortion over a narrow bandwidth, the effects of memory would be prevalent and AM-to-PM would be observed. Of course, the circuit could be tuned to resonance at a center frequency, and if the Q was low, the predistorter might appear to be memoryless close to the center frequency. Since the circuit is nonlinear, however, circuit resonance could not occur over the full range of operation of the signal. The reactance of the diodes would exhibit a significant change, depending on the junction voltage. For a microwave predistorter, these effects are more severe as the parasitic and junction reactances are usually of such a value that tuning of the circuit can be attained over only a moderate range of the input signal. As such, resonance represents an inadequate solution for the effective tuning of microwave nonlinearities. Another mechanism would need to be employed that minimized amplitude-dependent phase shifts over the full range of the amplitude characteristic.

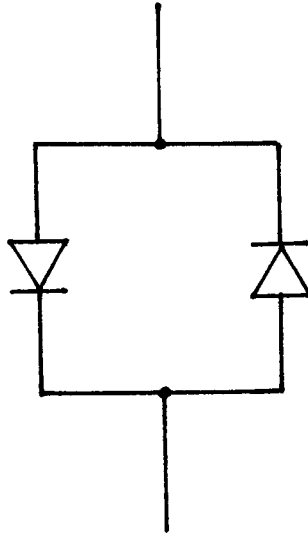


Figure 4.2. Anode to cathode nonlinear element.

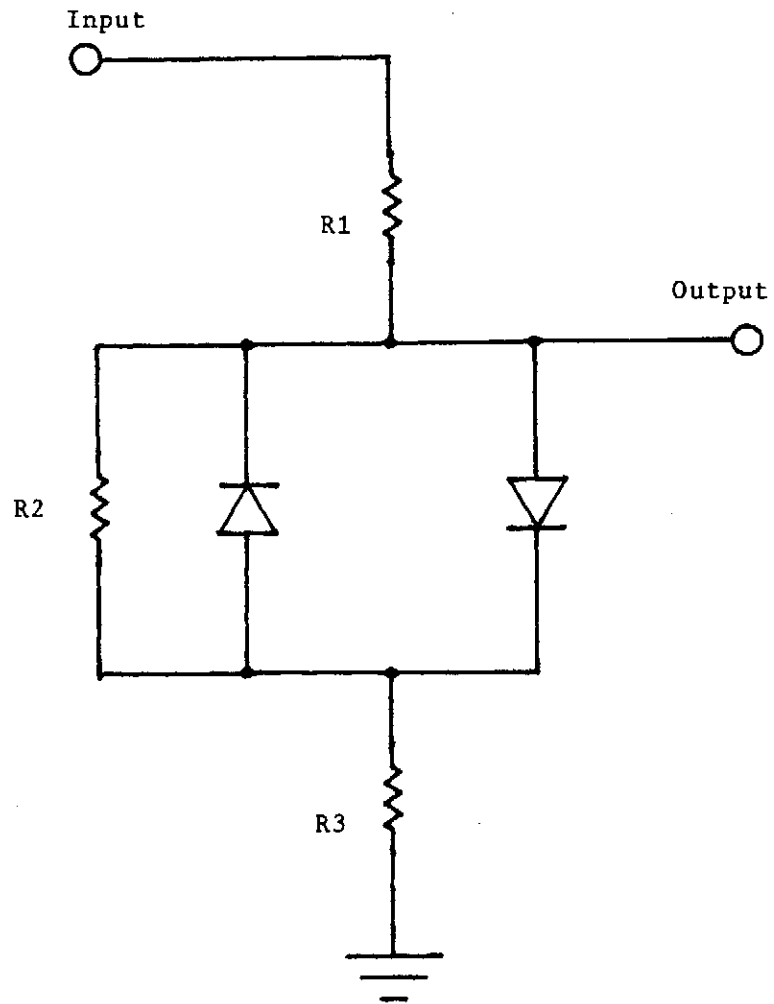


Figure 4.3. High frequency predistorter.

The solution to this phase shift problem begins with an examination of a suitable model for a Schottky diode to be employed in the predistorter, see Figure 4.4. Here C_p represents parasitic packaging capacitance, L is the packaging lead inductance, R is the junction resistance and C_I is the junction capacitance. This model was found to be totally adequate for the modelling of all diodes employed in the predistorter. The impedance of the model is given by

$$Z_{IN} = \frac{R(1-\omega^2 LC_I) + j\omega L}{(1-\omega^2 LC_p) + j(\omega C_p R(1-\omega^2 LC_I) + \omega RC_I)} \quad (142)$$

and a contour of impedance with varying voltage is presented in Figure 4.5. Here the junction capacitance is assumed to be invariant; the junction resistance is taken to be the variable element. In fact, both elements would vary but the results generated by (141) with a variable junction resistance were found to agree closely to impedance measurements made with a network analyzer on actual devices. This approximation is also justified by the fact that junction resistance varies exponentially with voltage, while junction capacitance increases according to a power-law relationship (diffusion capacitance assumed to be negligible for Schottky diodes). Hence junction resistance is the dominant effect on the junction impedance.

For the "diode off" state (infinite resistance), the junction capacitance is the dominant reactive effect. For the "diode on" state (zero resistance), the lead inductance is the dominant reactive effect.

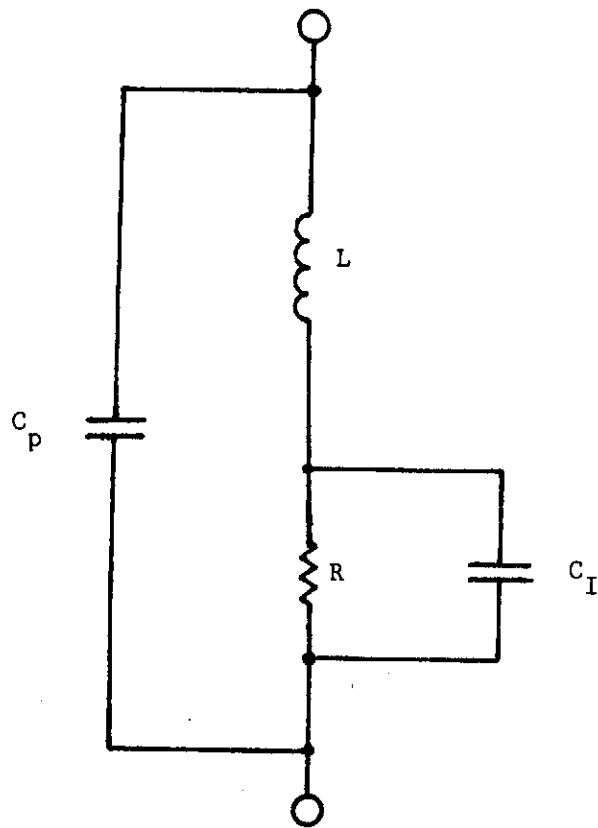


Figure 4.4. Schottky diode model.

$C_I = 2.2 \text{ pF}$

$C_P = .2 \text{ pF}$

$L = 2.5 \text{ nH}$

IMPEDANCE OR ADMITTANCE COORDINATES

$Z_0 = 50 \Omega$

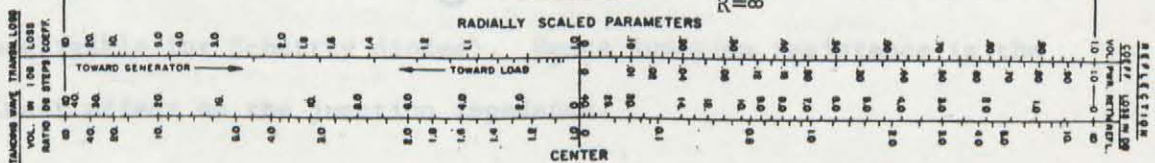
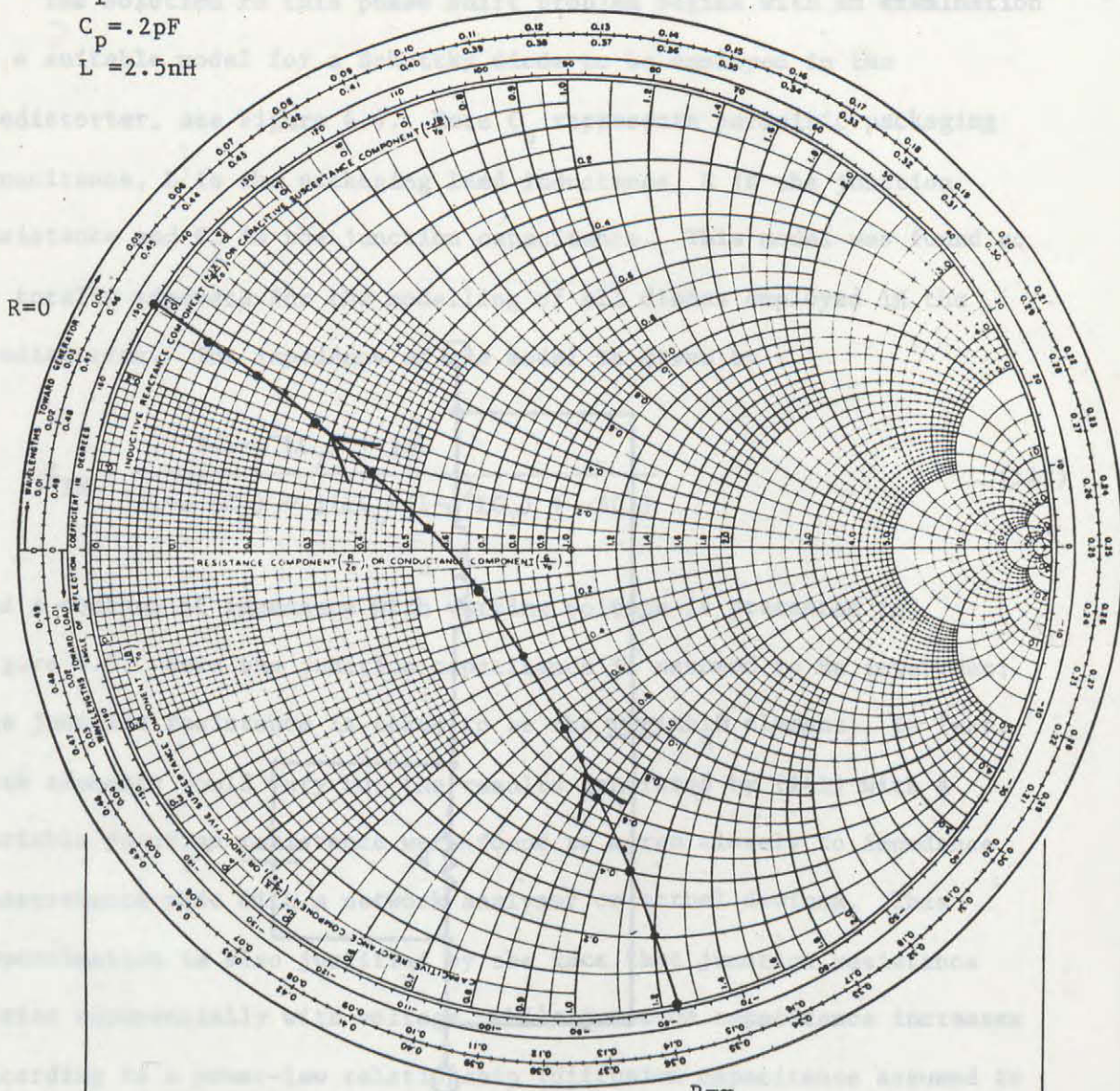


Figure 4.5. Impedance contour of diode model with varying resistance.

In general, the inductive reactance is lower in magnitude than the junction capacitance in the off state. Therefore any attempt at tuning the diode would probably involve the addition of an inductive shunt stub, to resonate the diode in the off state. This procedure would produce the impedance contour of Figure 4.6. The diode is now presenting a more ideal impedance contour, following the real axis over a wide range. The inductive reactance problem remains, however. Evidently another mechanism other than tuning to resonance would be required to produce a "memoryless" predistorter.

The solution to the problem is to base the design of the predistorter on nonlinear reflection as opposed to nonlinear transmission. The concept of the reflection-based circuit is as follows, see Figure 4.7. Given a Schottky diode that has been tuned, the impedance contour follows the real axis, with the reflection coefficient varying from ideally $1\angle 0^\circ$ to $1\angle 180^\circ$. Note that the reflection coefficient approaches 0 in magnitude, and the reflection angle changes from 0° to 180° as the contour sweeps by the center of the Smith Chart. Hence this point is to be avoided because of the erratic phase and amplitude characteristics in this vicinity. In addition, the predistorter should possess the lowest insertion loss possible. This requirement restricts operation to the outside regions of the Smith Chart where reflection coefficient is largest in magnitude. Now two areas of operation are possible, the extreme right-hand portion of the Smith Chart on the real axis, and the extreme left-hand portion of the Smith Chart. The right-hand portion provides a

IMPEDANCE OR ADMITTANCE COORDINATES

$C_1 = 2.2 \text{ pF}$
 $C_p = .2 \text{ pF}$
 $L = 2.5 \text{ nH}$

$Z_0 = 50 \Omega$

$L_{\text{shunt}} = 10.8 \text{ nH}$

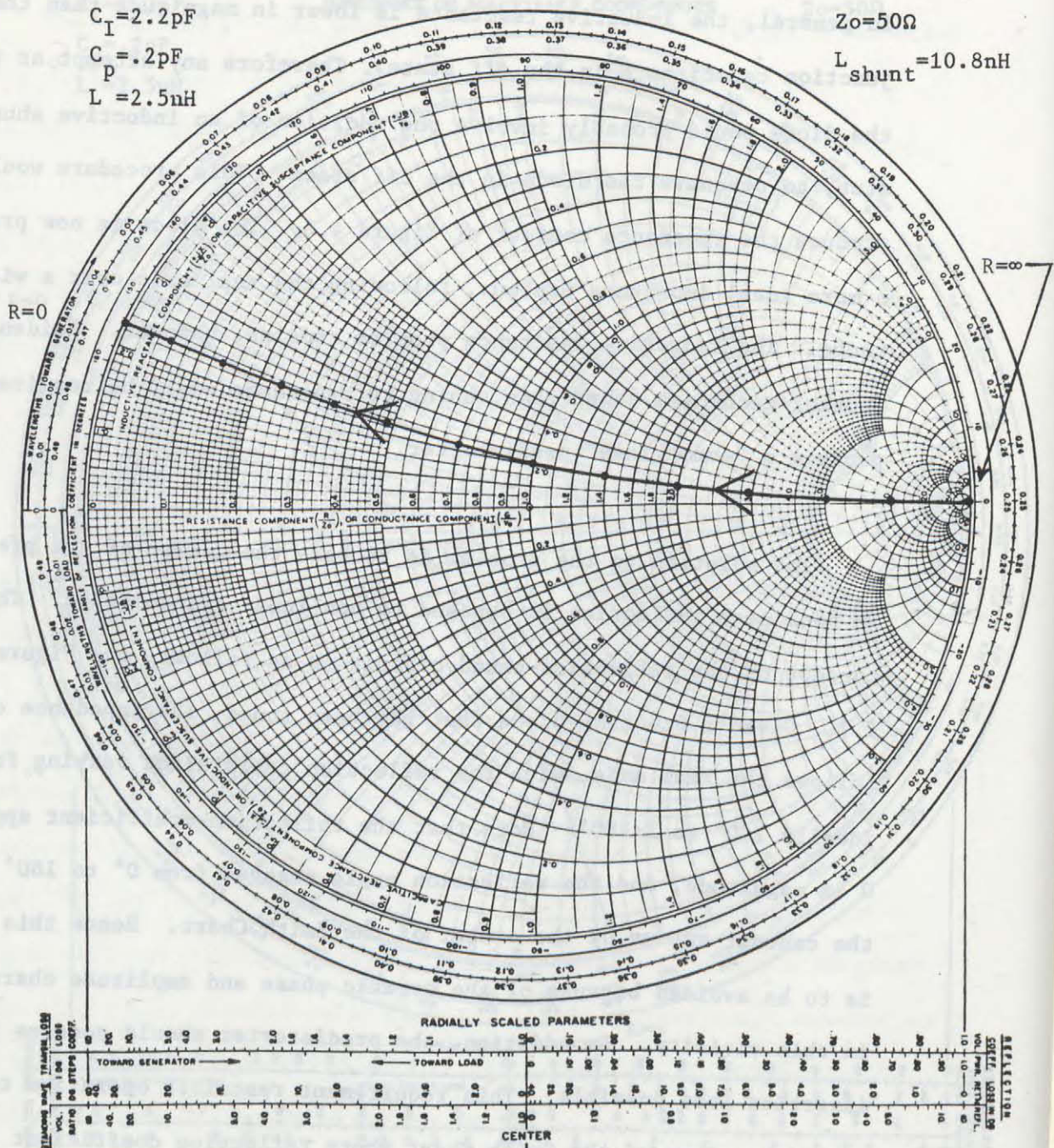


Figure 4.6. Resonated impedance contour.

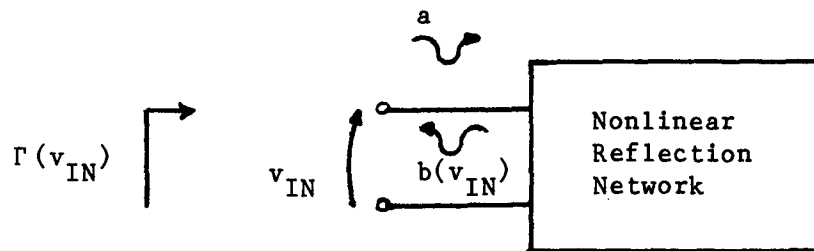


Figure 4.7. General nonlinear reflection network.

decreasing reflection coefficient with increasing input amplitude and therefore produces a concave type of nonlinearity. The left region, on the other hand, provides an increasing reflection coefficient with increasing input amplitude and therefore produces a convex type of nonlinearity. The true advantage of the reflection-based predistorter, however, is in the minimization of amplitude-dependant phase shifts due to any residual reactances. Referring to any Smith Chart, it is obvious that a change in reactance will affect the reflection angle on the left-hand region of the chart much more severely than the right-hand portion. For example, a residual reactance of $\pm j 1$ (normalized reactance) would provide a phase shift of $\pm 90^\circ$ on the $0 \pm jX$ contour. The same reactance, however, would provide a negligible change in reflection angle as one approaches the $\infty \pm jX$ contour. Hence the obvious approach is to map the diode impedance into the right-hand region of the Smith Chart, on the real axis. This mapping process is achieved by using a high characteristic impedance, quarter-wave series transformer. The contour of Figure 4.6, used in conjunction with a 100-Ohm impedance quarter-wave section, as shown in Figure 4.8, produces the impedance contour of Figure 4.9. Note that the reflection angle varies far less than the original impedance contour reflection angle. The direction of the impedance contour, however, has been reversed, varying from left to right. This is a consequence of the quarter-wave section, which compresses the impedance contour into the high impedance region through an admittance-to-impedance conversion. In general, the diode would be tuned to resonance and the impedance contour would sweep from $1 \angle 180^\circ$ to $1 \angle 0^\circ$.

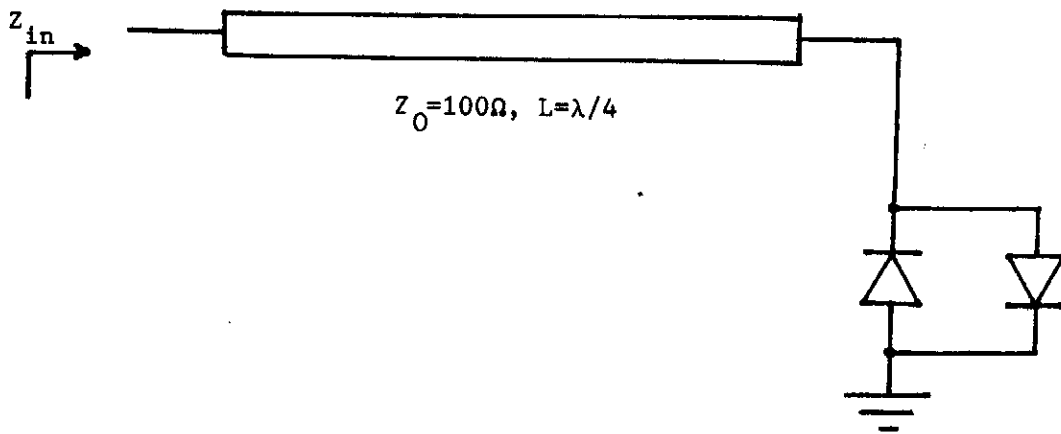


Figure 4.8. Transformed Schottky diode pair.

IMPEDANCE OR ADMITTANCE COORDINATES

$C_I = 2.2 \text{ pF}$
 $C_P = .2 \text{ pF}$
 $L = 2.5 \text{ nH}$

$Z_o = 50 \Omega$
 $L_{\text{shunt}} = 10.8 \text{ nH}$

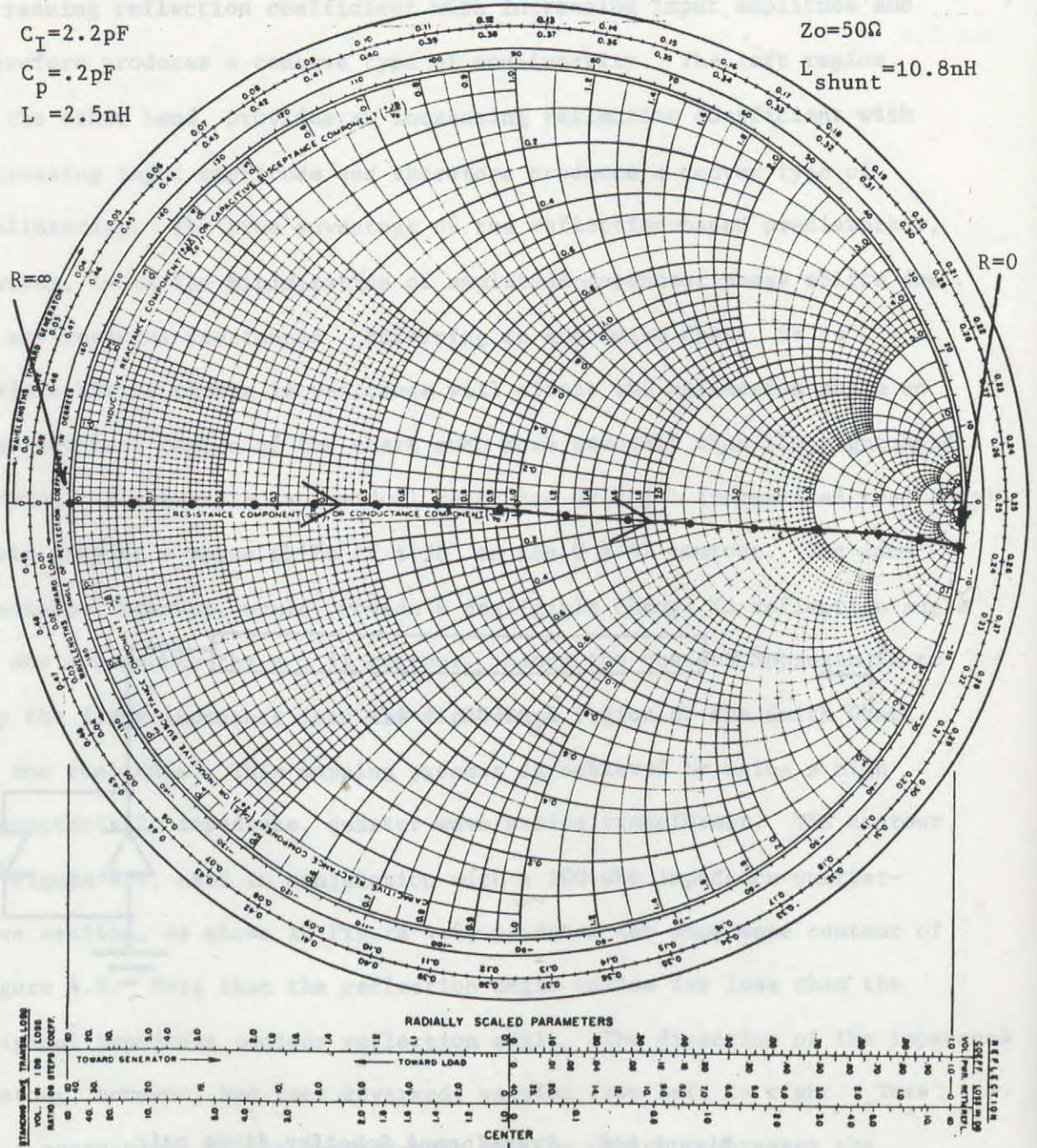


Figure 4.9. Transformed impedance contour.

with increasing input voltage. Therefore operation in the left region produces a concave nonlinearity; operation in the right region produces a convex nonlinearity. Normal predistortion compensation of an HPA requires a convex nonlinearity, as all amplifiers will invariably be found to saturate.

The next phase in predistortion design involves the search for a mechanism which would allow for some control over the transfer function that the predistorter would produce. A voltage divider arrangement, as shown in Figure 4.10, would appear to be a good starting point, although such a circuit becomes unrealizable for most microwave circuits due to the physical length of the resistors. The solution, in fact, was to employ a single resistor in shunt with the Schottky diodes, see Figure 4.11. This resistor could be made variable by utilizing a PIN diode, that is, a diode in which the RF impedance could be varied by changing the D.C. bias current, [35].

The mechanism that allows a single resistor to affect the transfer function can heuristically be explained as follows. Since the predistorter is based on reflection, the effects of reflection coefficient on the Schottky diode must be examined. For any network with a given incident wave amplitude, the voltage across the network depends not only on the wave amplitude, but also on the reflection coefficient. For example, examination of a general two port by S parameters gives, see Figure 4.12,

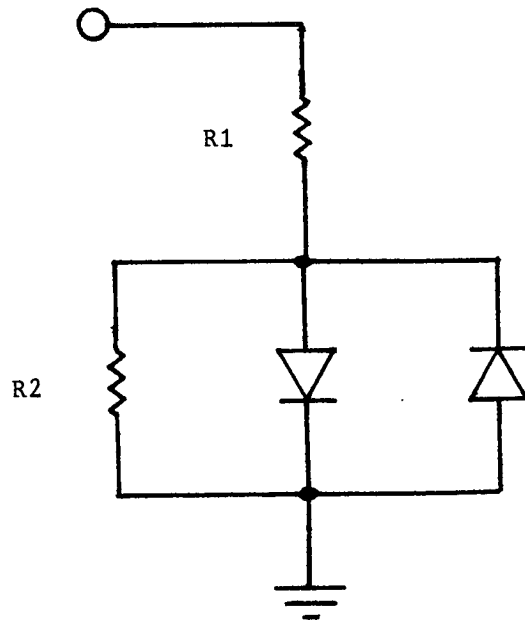


Figure 4.10. Voltage divider topology.

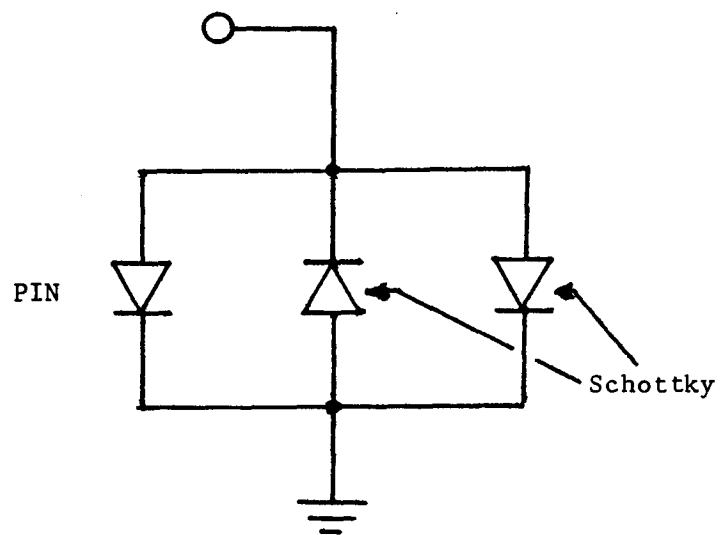


Figure 4.11. Shunt PIN diode topology.

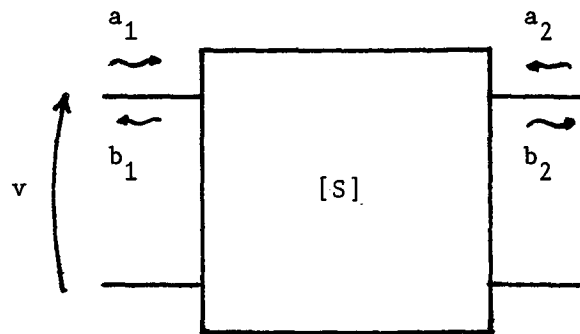


Figure 4.12. General two-port network.

$$b_1 = S_{11} a_1 + S_{12} a_2 \quad (143)$$

$$b_2 = S_{21} a_1 + S_{22} a_2 \quad (144)$$

where a_1 , a_2 represent incident waves, and b_1 , b_2 represent reflected waves in accordance with normal S parameter concepts, [33]. Examining the voltage of the input port, v gives

$$v = a_1 + b_1 = a_1 (1 + S_{11}) \quad (145)$$

where

$$S_{11} = \left. \frac{b_1}{a_1} \right|_{a_2=0} \quad (146)$$

Hence for any given a_1 , the input port voltage could vary from 0, ($S_{11} = -1 =$ short circuit), to $2a_1$, ($S_{11} = 1 =$ open circuit). One can readily visualize how this effect could be utilized in a Schottky predistorter. Referring to Figure 4.13, one can see that the impedance of the Schottky diode/resistor network is a function of the magnitude of the incident input wave, as well as the reflection coefficient. If the shunt resistor is omitted, it would be anticipated that the Schottky diodes could readily conduct at a sufficient wave amplitude. If, however, the resistor is low in value, approaching a short circuit, then the Schottky diodes may not realize a conduction state for any practical wave amplitude, as the diode voltage would be kept low by the resistor.

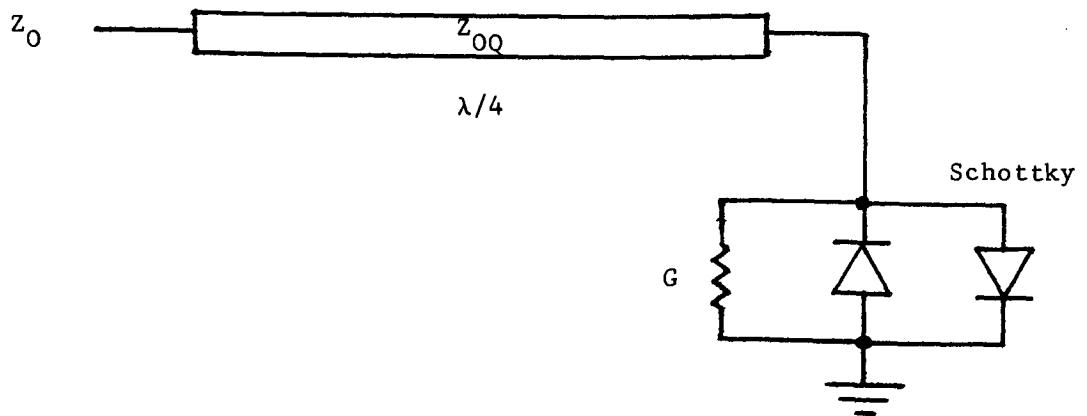


Figure 4.13. RF predistorter topology.

An additional mechanism for adaptive control would be to reverse bias the Schottky diodes, effectively increasing the input wave amplitude required for conduction.

Combining all of the mechanisms described yields the final convex predistorter configuration of Figure 4.14. Important points to note are the following:

- (1) The quarter-wave section characteristic impedance is sufficiently high so as to transform the semi-conductor device impedance to a real value approaching an open circuit. This will aid in minimizing amplitude-dependant phase shifts and provide a low insertion loss.
- (2) The Schottky diodes are the nonlinear elements, responding to the RF cycle.
- (3) The PIN diode presents a shunt resistance to the Schottky diodes. It is a linear element with its RF impedance controlled by a DC bias through a suitable choke structure.
- (4) The Schottky diodes can be reverse biased through a suitable choke.
- (5) The diode network is tuned with a single shunt element.
- (6) In order to ensure operation of the predistorter in the high impedance region of the Smith Chart, a fixed resistor shunts the PIN diode. This resistor sets the minimum reflection coefficient attainable by the predistorter and prevents operation near the center of the Smith Chart (matched conditions). The net linear resistance is therefore the fixed resistance in parallel with the PIN resistance.

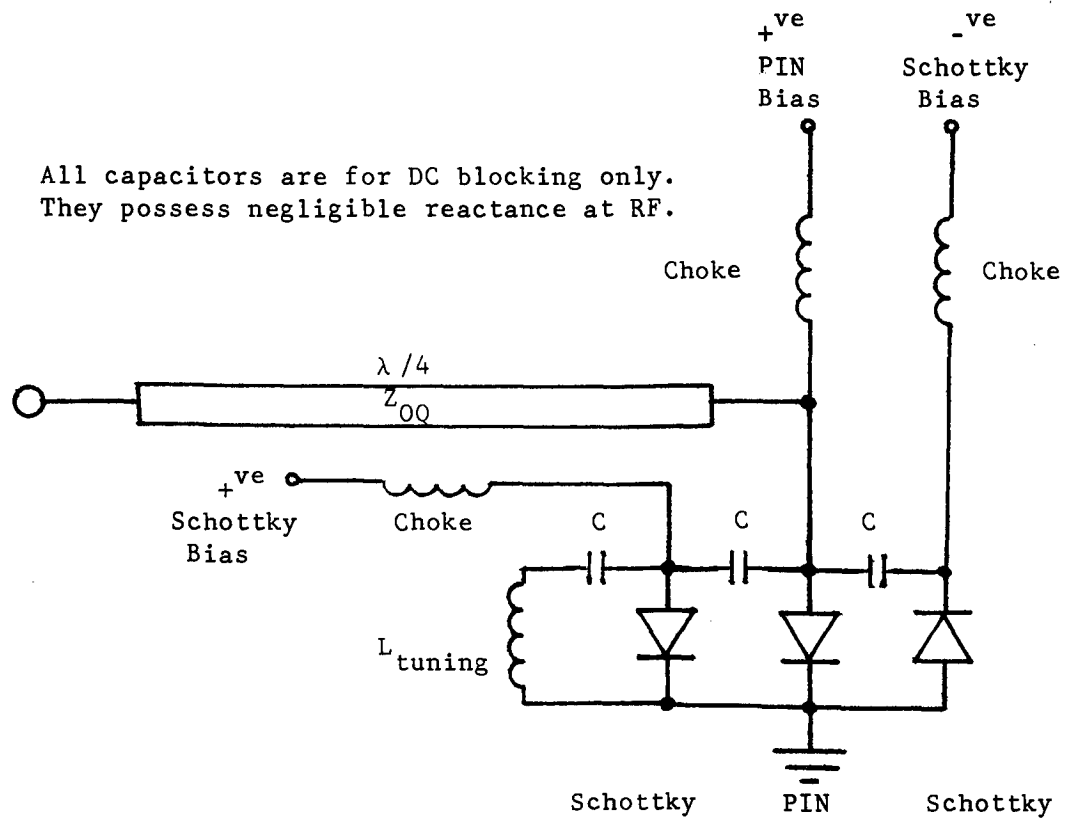


Figure 4.14. RF predistorter implementation.

A detailed analysis of the predistorter, and the transfer functions it produces is now presented with the aid of Figure 4.15. Here Z_0 is the characteristic impedance of the system (nominally 50 Ω); Z_{0Q} is the characteristic impedance of the quarter-wave section; Z_L is the total impedance presented by the network before transformation by the quarter-wave section; v_{PK} is the peak voltage across the diode network; P_{IN} is the input power; and Γ is the reflection coefficient of the total predistorter.

Analysis begins by noting that in a lossless medium, if a wave is not transmitted it must be reflected. Therefore

$$P_{DISS} = P_{IN} - P_{REF} \quad (147)$$

where P_{DISS} is the power dissipated in the network, and P_{REF} is the power reflected from the network, thus

$$P_{REF} = P_{IN} \Gamma^2 \quad (148)$$

so

$$P_{DISS} = P_{IN} (1 - \Gamma^2) \quad (149)$$

Since P_{DISS} must be dissipated in the network, the voltage across the network can be obtained. Hence

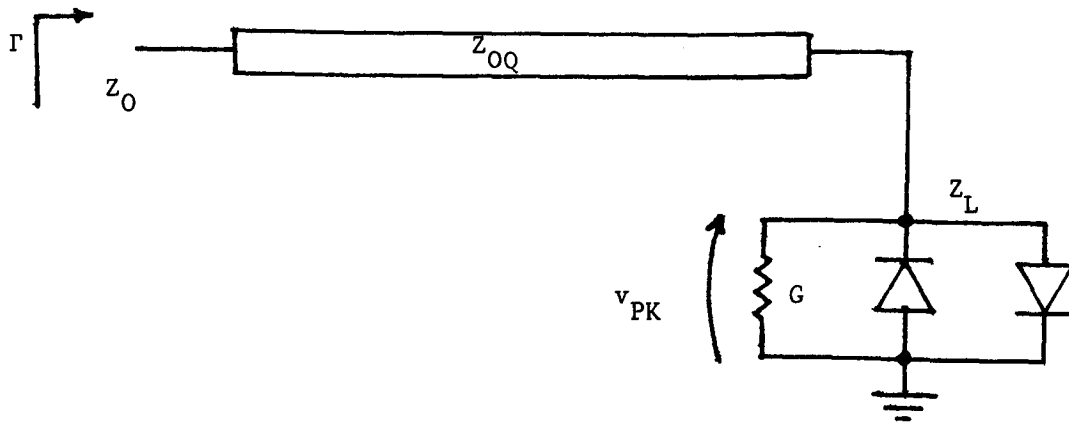


Figure 4.15. Analysis of the RF predistorter.

$$P_{\text{DISS}} = \frac{v_{\text{PK}}^2}{2Z_L} = P_{\text{IN}} (1-\Gamma^2) \quad (150)$$

where Z_L is assumed to be real. Therefore,

$$v_{\text{PK}} = \sqrt{2Z_L P_{\text{IN}} (1-\Gamma^2)} \quad (151)$$

All that is now required is to substitute for Γ and Z_L in terms of the voltage-dependant impedance. We model the Schottky diodes by the ideal equation

$$i_0 = K_s (e^{\lambda v} - 1) \quad (152)$$

Here i_0 is the diode current, K_s represents the saturation current, and λ is the temperature dependant constant $\frac{q}{nKT}$ (q is the electron charge, K is Boltzman's constant, T is the temperature and n is the ideality factor). Since the diodes are utilized in a "head-to-tail" topology, the net diode current is

$$i_D = K_s (e^{\lambda v} - 1) - K_s (e^{-\lambda v} - 1) = 2K_s \sinh(\lambda v) \quad (153)$$

We define impedance to be the single-frequency ratio of voltage to current. Admittance is the reciprocal of this value. Hence one must obtain the fundamental component of current in (153). For an input of $v_{\text{PK}} \cos \omega_0 t$, the current of (153) can be expressed with the aid of transform T10 of Blachman [6], (see Appendix 2), as

$$i_D = 2K_S \left[\sum_{m=1}^{\infty} 2I_m(\lambda v_{PK}) \cos m \omega_0 t \right]; \quad m \text{ odd}; \quad (154)$$

where $I_m(\lambda v_{PK})$ is the modified Bessel function of the first kind of order m . Thus the fundamental component of this current is

$$i_D = 4K_S I_1(\lambda v_{PK}) \quad . \quad (155)$$

The diode admittance can now be defined as

$$y_D = \frac{i_D(v_{PK})}{v_{PK}} = \frac{4K_S I_1(\lambda v_{PK})}{v_{PK}} \quad (156)$$

and the total network admittance is the Schottky admittance, plus the admittance of the linear shunt resistance G .

$$y_{TOTAL} = y_D + G = G + \frac{4K_S I_1(\lambda v_{PK})}{v_{PK}} \quad . \quad (157)$$

Now

$$\Gamma = \frac{\frac{Z_{OQ}^2}{Z_L} - Z_0}{\frac{Z_{OQ}^2}{Z_L} + Z_0} = \frac{Z_{OQ}^2 - Z_0 Z_L}{Z_{OQ}^2 + Z_0 Z_L} \quad (158)$$

and substitution of (158) into (151) gives

$$v_{PK} = \frac{Z_{OQ} Z_L}{(Z_{OQ}^2 + Z_0 Z_L)} \sqrt{8 P_{IN} Z_0} \quad (159)$$

where Z_L is the reciprocal of (157), that is

$$Z_L = \frac{v_{PK}}{Gv_{PK} + 4K_s I_1(\lambda v_{PK})} \quad (160)$$

Putting (159) into (160) and simplifying yields an equation that defines the transfer characteristic,

$$Z_{OQ}^2 [Gv_{PK} + 4K_s I_1(\lambda v_{PK})] + Z_O v_{PK} = Z_{OQ} \sqrt{8 P_{IN} Z_O} \quad (161)$$

Note that the output power can be obtained from (158)

$$\Gamma = \frac{Z_{OQ}^2 [Gv_{PK} + 4K_s I_1(\lambda v_{PK})] - Z_O v_{PK}}{Z_{OQ}^2 [Gv_{PK} + 4K_s I_1(\lambda v_{PK})] + Z_O v_{PK}} \quad (162)$$

and Γ^2 represents the input-power, output-power transfer characteristic.

Therefore, one would use (161) to solve for P_{IN} for any given v_{PK} and then substitute v_{PK} into (162) to obtain Γ and

$$P_{OUT} = \Gamma^2 P_{IN} \quad (163)$$

The effects of reverse bias on the Schottky diodes can now be obtained by substituting

$$\lambda v_{PK}' = \lambda(v_{PK} - V_{BIAS}) \quad (164)$$

for the Bessel function arguments in (161) and (162). Here V_{BIAS} represents the DC Schottky bias. The substitution is required to account for the lower diode current produced by the RF signal due to the lower net voltage. $I_1(\lambda v_{\text{PK}}')$ is assumed to equal zero for negative arguments.

Curves illustrating some of the transfer characteristics produced by the predistorter for various values of G and V_{BIAS} are presented in Figure 4.16 and 4.17. Note that varying the conductance G has the effect of changing the degree of curvatures of the transfer characteristic, shifting along the gain axis. Varying the Schottky bias produces the effect of delaying Schottky conduction, shifting the transfer characteristic along the P_{IN} axis. The two effects combined provide the ability to synthesize a wide variety of convex characteristics.

The predistorters were constructed using microstrip on a low-dielectric-constant duroid substrate ($\epsilon_r \approx 2.1$), see Figure 4.18 and 4.19. Diodes were of the "general application variety", with glass packages and high parasitic reactances, see Appendix 3. The resonating shunt stub has been replaced with a silver-mica capacitor with its leads cut to a specific length. The tuning process was performed on a network analyzer, with a selected center frequency of 890 MHz. Note that the capacitor, in fact, appears inductive due to the long capacitor lead-lengths. The choke structure employed for the Schottky and PIN diodes is shown in Figure 4.20. It is fairly standard and need not be further explained.

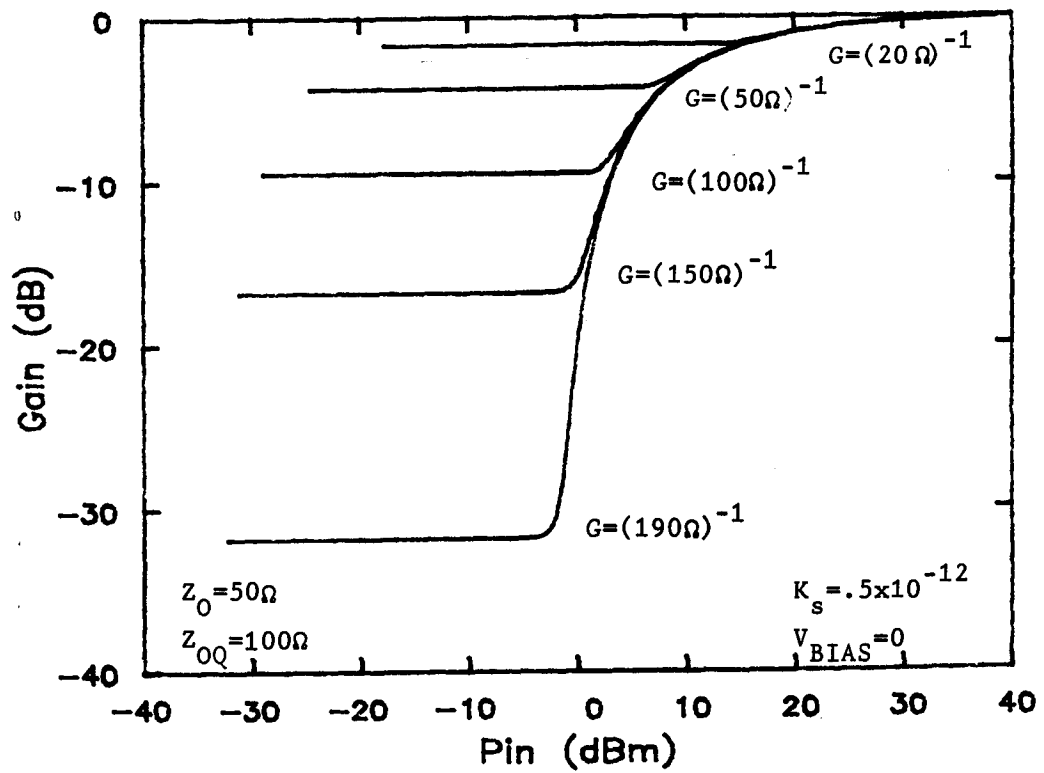


Figure 4.16. Theoretical predistorter transfer characteristic, G varying.

for the Bessel function arguments in (161) and (162). Here V_{BIAS} represents the DC Schottky bias. The substitution is required to account for the lower diode current produced by the RF signal due to the lower net voltage. $I_1(\omega_{RF})$ is assumed to equal zero for negative arguments.

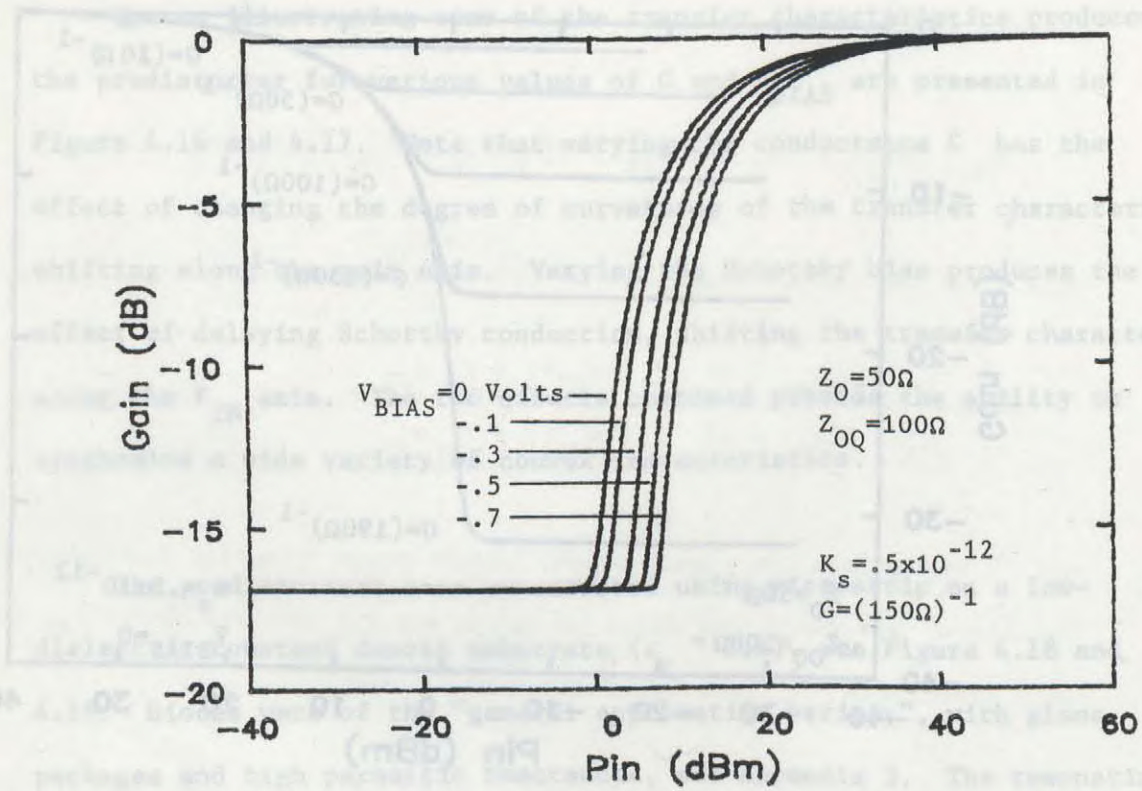


Figure 4.17. Theoretical predistorter transfer characteristic, V_{BIAS} varying.

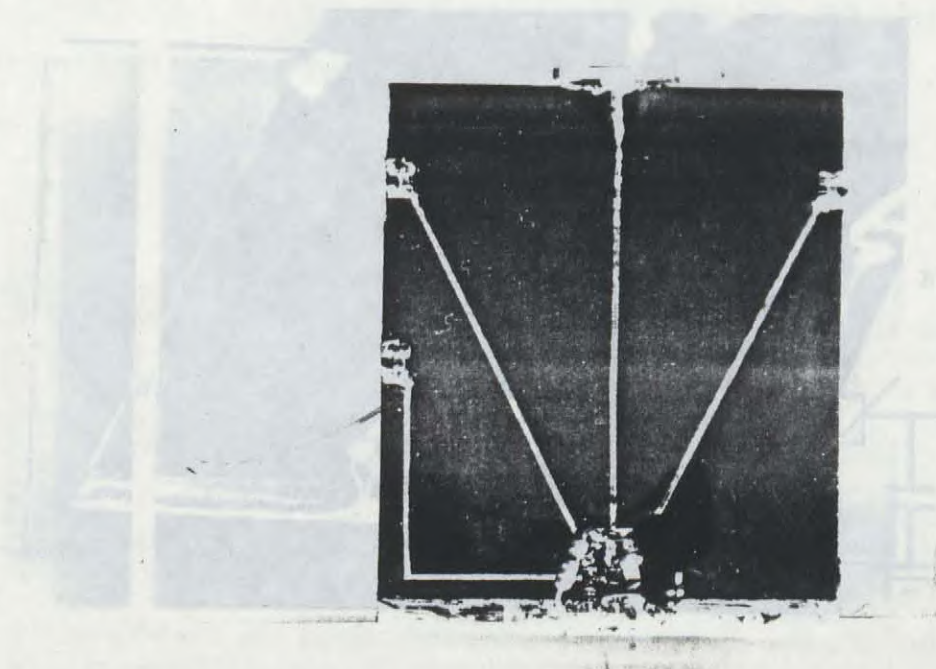


Figure 4.18. Microstrip structure for the predistorter.

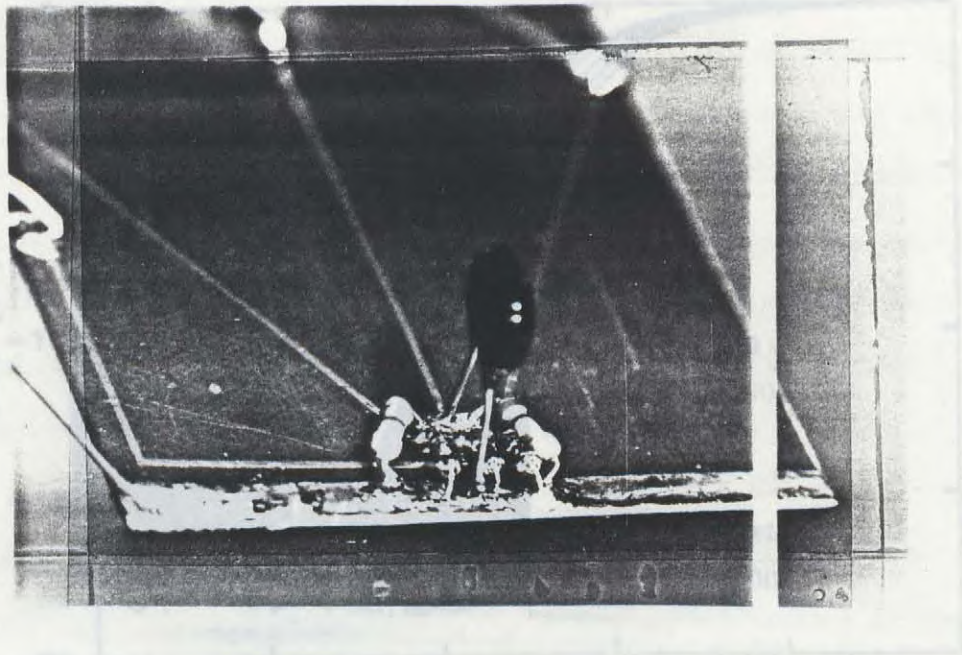


Figure 4.19. Detail of the predistorter elements.

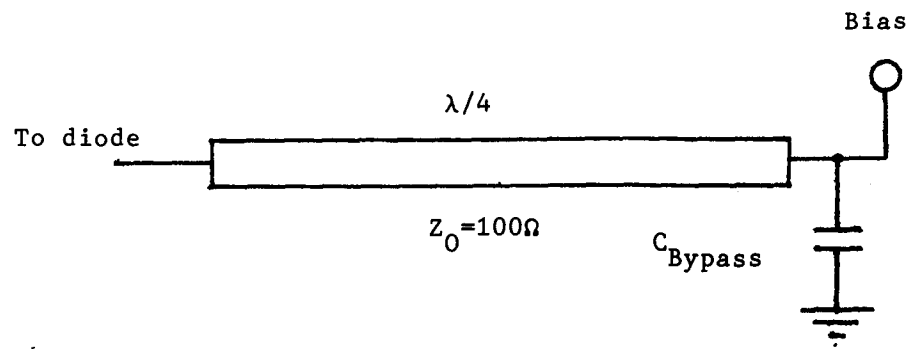


Figure 4.20. Predistorter bias structure.

Since the phase angle of the reflection coefficient must be maintained in the vicinity of 0° , the length of the coaxial-to-microstrip connector is critical. By employing a semi-rigid cable slightly less than $\lambda/2$ in length, the electrical length from the connector on the open end of the semi-rigid cable to the $\lambda/4$ transformer on the predistorter microstrip can be tuned to be $\lambda/2$. Recall that in a transmission-line medium, reflection angle is $\lambda/2$ periodic, hence the reflection angle at the quarter-wave impedance transformer (0 degrees), is also presented at the open end of the $\lambda/2$ line.

In order to provide separate input and output ports with a good degree of isolation, a circulator is employed at the open end of the $\lambda/2$ line. The circulator converts the nonlinear reflection into a nonlinear transmission.

Two 100-Ohm fixed carbon resistors shunt the diode network. The use of multiple resistors in parallel minimizes any lead inductance effects in the resistors, producing a less reactive load.

Selection of the characteristic impedance of the quarter-wave section is limited primarily by the range of impedances attainable by the diode network, and by the need for minimum insertion loss, implying a high reflection coefficient. A good compromise between these two limiting factors is the selection of a characteristic impedance in the region of 100-Ohms for a 50-Ohm system. Thus the minimum impedance after impedance

transformation is

$$Z_{IN} = \frac{Z_0^2}{R_L} = \frac{100^2}{50} = 200 \Omega, \quad (165)$$

where the 50 Ohm load is determined by the two 100 Ohm fixed carbon shunt resistors. This produces a minimum reflection coefficient of

$$\frac{200 - 50}{200 + 50} = .6 \quad (166)$$

The maximum reflection coefficient is determined by the RF input level and the impedance of the PIN device. An estimated value for the maximum reflection coefficient is greater than .9.

The final predistorter circuit is given in Figures 4.21 and 4.22.

4.3 A Proposed Concave, Convex Predistorter

Some applications might require both convex and concave curvatures. The proposed circuit of Figure 4.23 could then be employed. The cascading of two diode networks provides the ability for one section's impedance to decrease with increasing input amplitude, while the other section's impedance increases with increasing amplitude. Hence both expander and compressor functions can be realized.

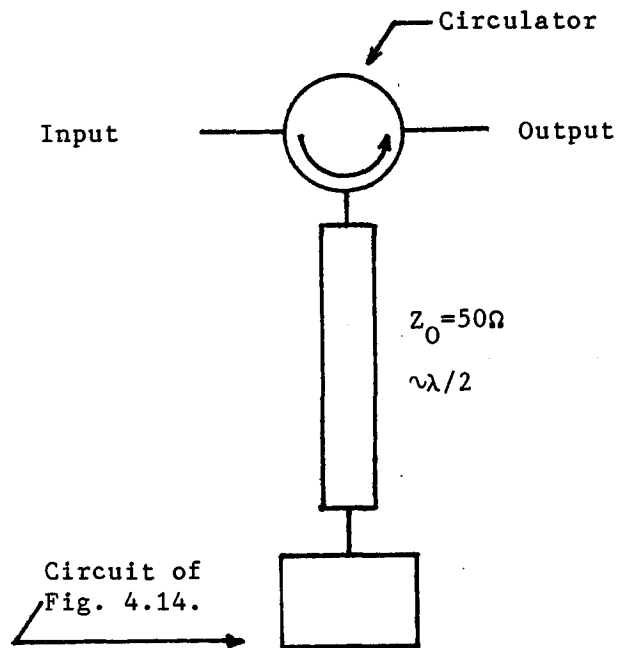


Figure 4.21. Predistortion system implementation.

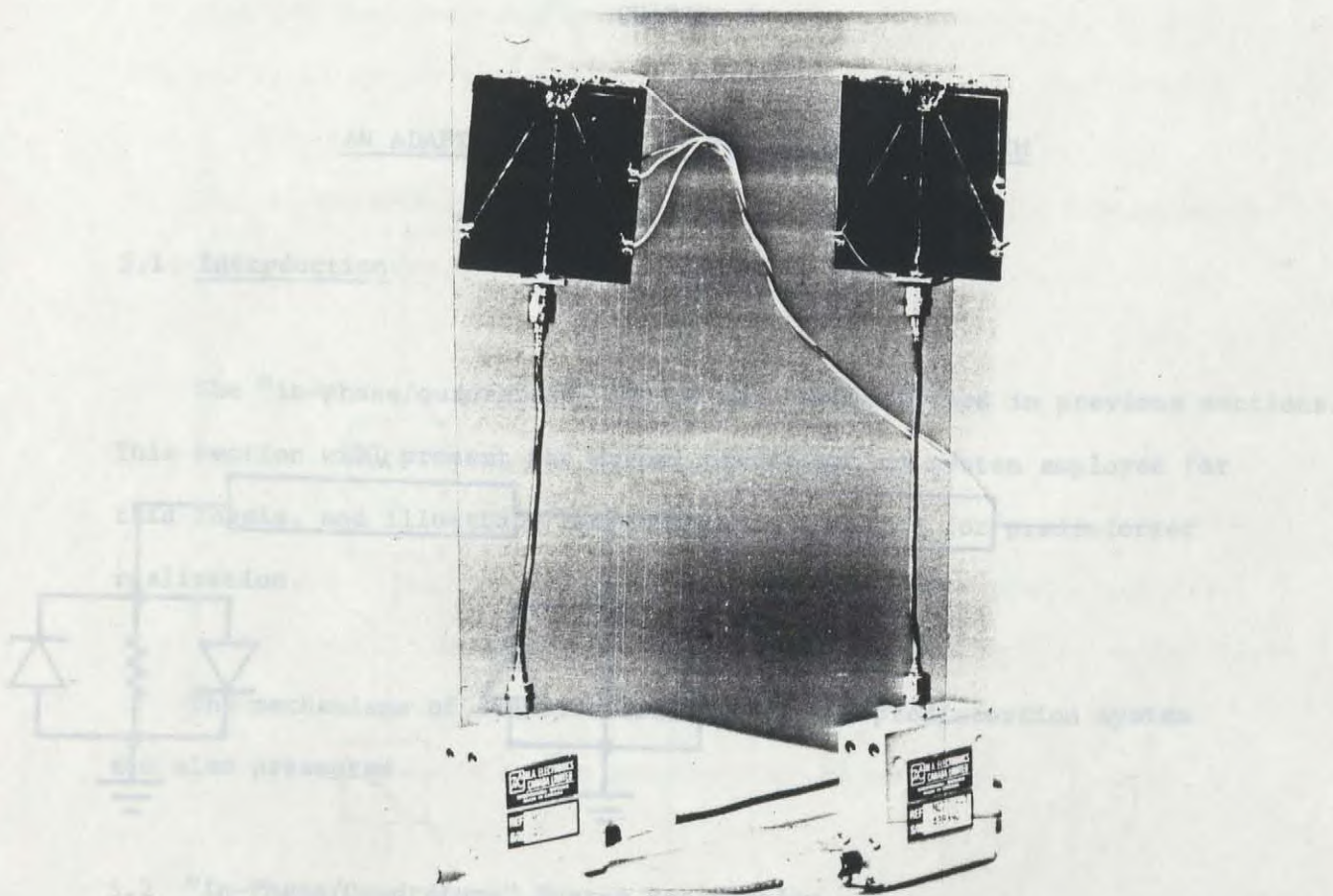


Figure 4.22. Predistorters with circulator isolators.

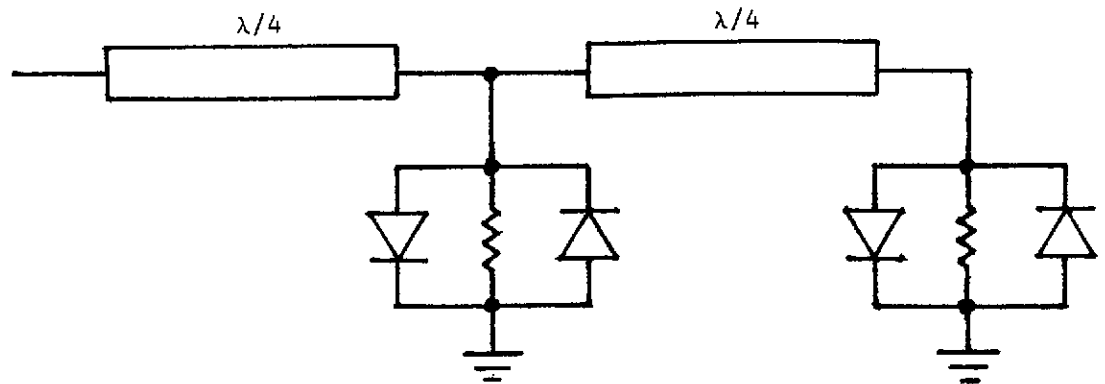


Figure 4.23. Proposed concave-convex predistorter.

CHAPTER 5

AN ADAPTIVE COMPLEX RF PREDISTORTION SYSTEM

5.1 Introduction

The "in-phase/quadrature" system has been outlined in previous sections. This section will present the actual predistortion system employed for this thesis, and illustrate the components required for predistorter realization.

The mechanisms of adaptive control for the predistortion system are also presented.

5.2 "In-Phase/Quadrature" System Realization

Realization of a practical "in-phase/quadrature" system is straight-forward; most components illustrated in the conceptual system of Figure 5.1 have a practical counterpart. For example, the input signal is readily divided into the two required quadrature components by using a 3dB, 90° hybrid. This microwave device splits the input signal

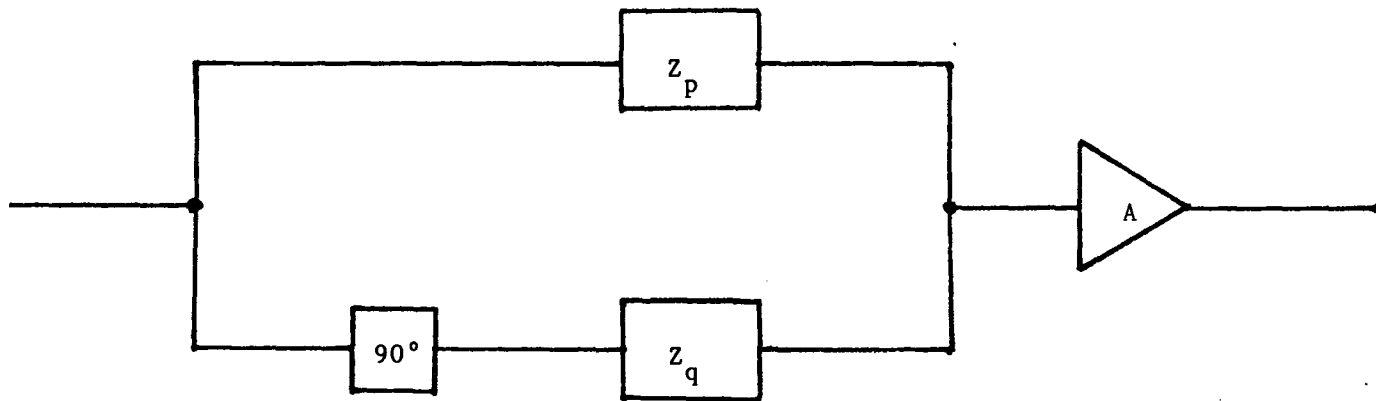


Figure 5.1. Conceptual "in-phase/quadrature" system.

into two components with equal amplitude but with the phase of one component lagging the other by 90° . Therefore such a device is ideal for realization of the quadrature component separator of the predistorter.

The two nonlinear-amplitude transfer functions, $Z_p(v_{IN})$, $Z_q(v_{IN})$, are generated by the predistorters as outlined in detail in Chapter 4.

Signal recombination is achieved through the use of a Wilkinson in-phase power combiner, [36].

The practical realization of the predistortion system is shown in Figure 5.2. Analysis of the system follows.

The predistorter must realize a certain complex transfer function, that is, a specific AM-to-AM and AM-to-PM conversion over the entire range of the input envelope. For example, let the desired complex transfer function to be realized by the predistorter be given by

$$G(A) \cos (\omega t + \theta + F(A)) \quad (167)$$

corresponding to an input of

$$v_{IN} = A \cos (\omega t + \theta) . \quad (168)$$

This representation has previously been discussed in Chapter 1.2.2. Now,

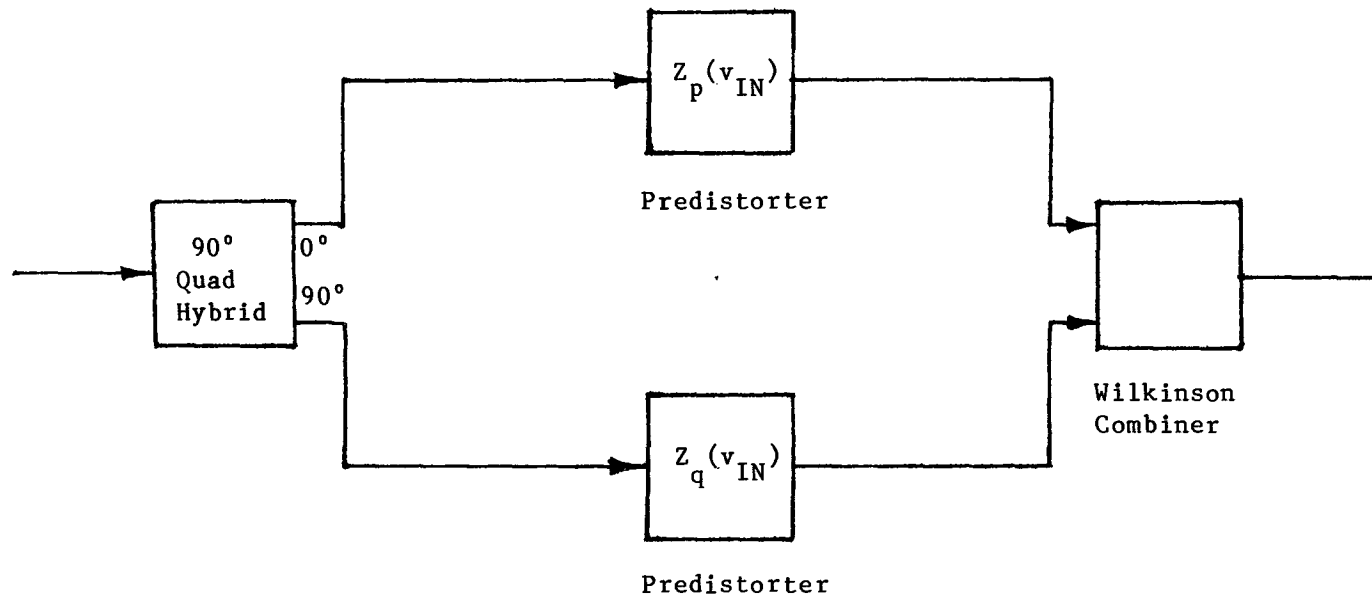


Figure 5.2. Microwave "in-phase/quadrature" topology.

normally one would resolve the amplitude and phase nonlinearities into quadrature components in accordance with equations (6), (7) and (8). The derivation of Chapter 1.2.2 assumes that if no phase nonlinearities are present, then the output signal will not possess a phase shift. The derivation also assumes that in the case of no phase nonlinearity, that the quadrature component should be absent and all of the input signal should be directed to the in-phase nonlinearity. In general, for any arbitrary phase nonlinearity, practical realization of the system in accordance with Chapter 1.2.2 would require a variable coupler to direct the power split to the two signal paths. Obviously this would be extremely difficult to implement. An easier system to realize is one based on a phase lag of 45° as opposed to the previous system's reference of 0° , see Figure 5.3. Here the output is assumed to be given by

$$v_{O_{BP}} = G(A) \cos (\omega t + \theta + F(A) - \pi/4) \quad (169)$$

and the input to be given by

$$v_{IN} = A \cos (\omega t + \theta). \quad (170)$$

Resolution of (169) into components of $\cos (\omega t + \theta)$ and $\sin (\omega t + \theta)$ yields the desired result:

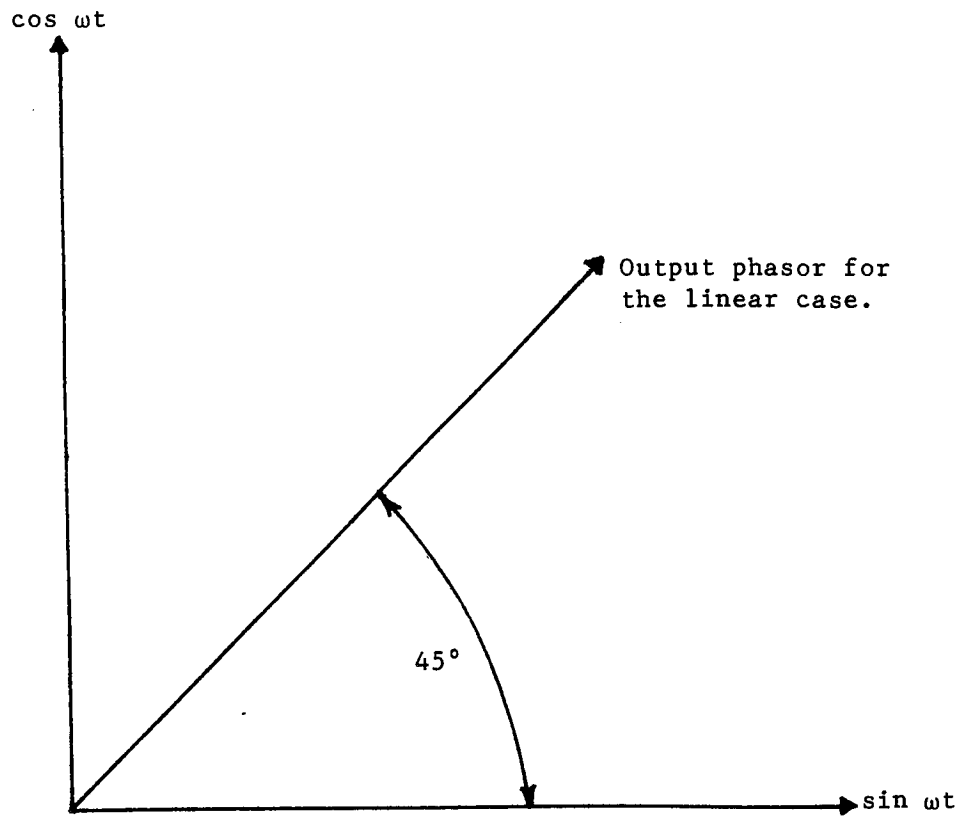


Figure 5.3. 45° reference "in-phase/quadrature" system.

$$\begin{aligned}
 v_{0_{BP}} &= \frac{G(A)}{\sqrt{2}} \cos(\omega t + \theta) [\cos F(A) + \sin F(A)] \\
 &+ \frac{G(A)}{\sqrt{2}} \sin(\omega t + \theta) [\cos F(A) - \sin F(A)] .
 \end{aligned}
 \tag{171}$$

Now, if the system requires no AM-to-AM conversion for compensation, then both the system channels will receive an equal power split and this memoryless nonlinearity will be compensated by two equal-amplitude nonlinearities. The previous "in-phase/quadrature" system based on no phase lag would require the in-phase channel to receive all the input signal, and the quadrature-signal path to be absent. Thus compensation is performed by a single amplitude nonlinearity. It must be emphasized that both systems are identical for analysis purposes, but that the 45° phase lag system more ideally suits the 3-dB 90° hybrid used to separate the signal components in a microwave system.

5.3 Adaptive Control

As outlined in Chapter 4, the predistorter developed for RF compensation lends itself readily to adaptive control. A wide variety of transfer functions can be realized simply by varying the bias for the PIN and Schottky diodes.

An adaptive system requires an "interactive figure of merit" indicating the degree of linearity of the compensated HPA. One approach to this problem is to periodically make static or dynamic measurements

of AM-to-AM and AM-to-PM conversion [34]. The goal is therefore to obtain the most linear envelope transfer function, with minimum AM-to-PM conversion. Such a process, however, is difficult to realize for any adaptive system.

The same end result of optimum linearity of the transfer functions can be attained in a far easier manner. As was demonstrated in Chapter 3.2.4, equations (128), (129) and (130), minimization of intermodulation products simultaneously provides optimum linearity of the amplitude and phase transfer functions. Thus one need only monitor intermodulation products, and attempt to minimize these products in an adaptive manner to linearize the HPA.

The final adaptive predistortion system is presented in Figure 5.4. A description of the system follows. The RF predistortion system has previously been outlined and will not be further discussed. After amplification by the HPA, a coupler samples a small component of the output signal in order to obtain a measure of the intermodulation levels present. The output spectrum is then down-converted to some IF where one can readily filter to obtain the test intermodulation products required for the figure of merit. Down-conversion is required because the filter Q would be prohibitively high for direct RF filtering. Due to filter availability, only a single third-order product was employed as a linearization parameter. Utilization of a test band of intermodulation products would be desirable, however. This test band of I.M. products would involve all contributing orders of nonlinearity involved in the

the system and provide a more complete linearization.

For any intermodulation "figure of merit", time averaging, (integration) could be employed. The adaptive control could then function even with varying envelope signal inputs.

Several stages of amplification may now be required in order to bring the signal up to a useable level. This useable level is determined by the dynamic range of the detector which converts this IF intermodulation level to a DC quantity. For example, a useful DC level would be in the range of 3 volts in order to interface to a TTL-compatible analog-to-digital converter. Now

$$P = \frac{V_{PK}^2}{2R_L} \quad (172)$$

where R_L is determined by the impedance of the operating system, nominally 50 Ohms. So for a detected 3 volt level, the required intermodulation power is

$$P = \frac{3^2}{2.50} = 90 \text{ mW} = 19.5 \text{ dBm}. \quad (173)$$

For the system of Figure 5.4, one might want to obtain a carrier-to-intermodulation (C/I) ratio of 50 dBm. Since the amplifier is limited to a useful range of approximately 30 dBm, the RF intermodulation level would correspondingly be -20 dBm. The 10-dB RF coupler would then yield

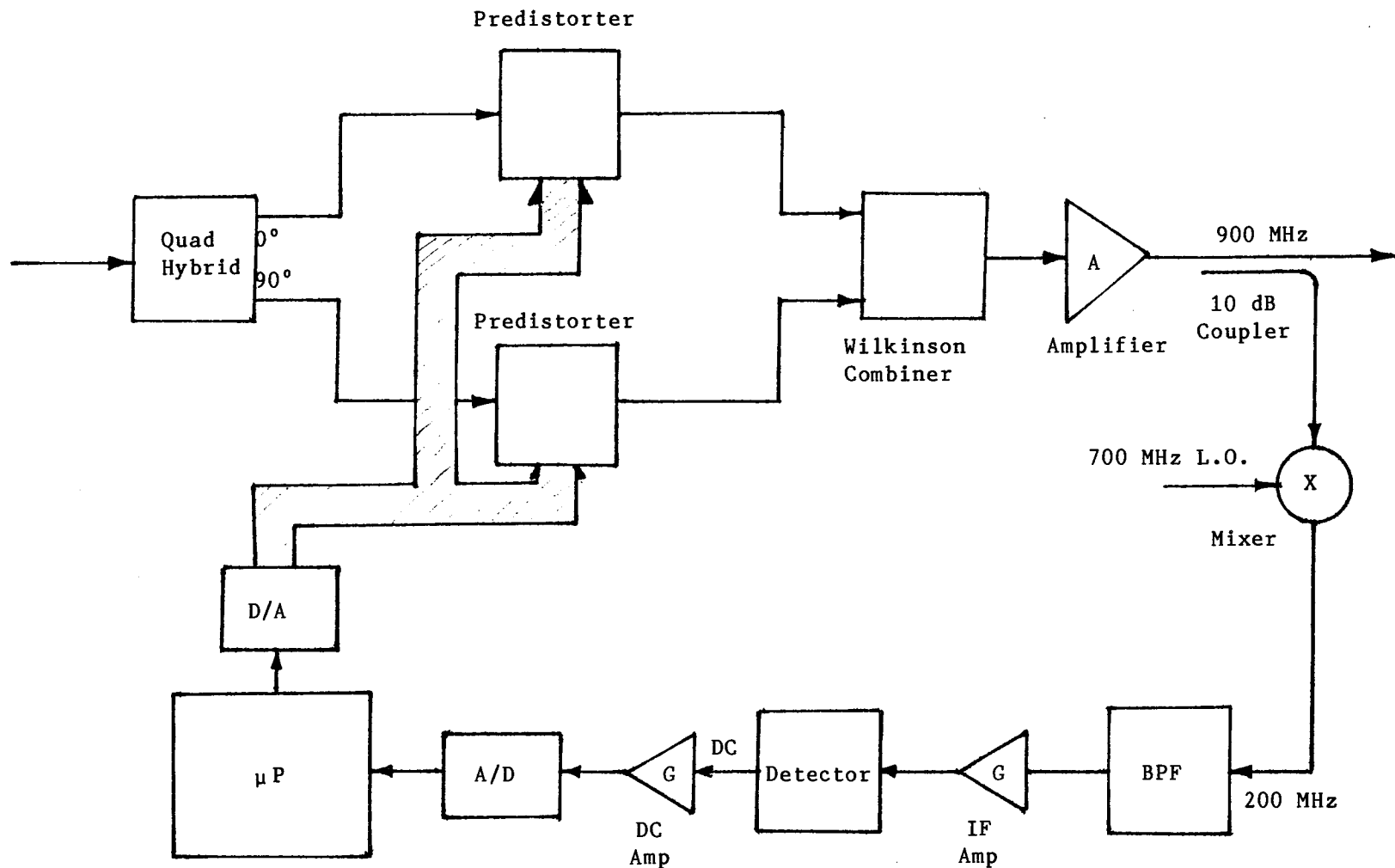


Figure 5.4a. Complex predistortion system.

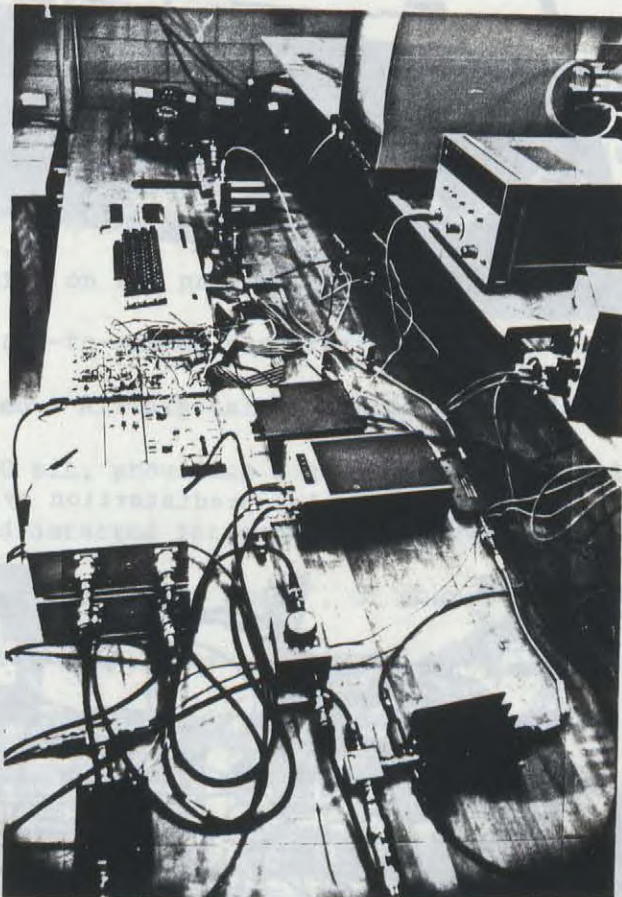


Figure 5.4b. Complex predistortion system.



Figure 5.4c. Complex predistortion system.

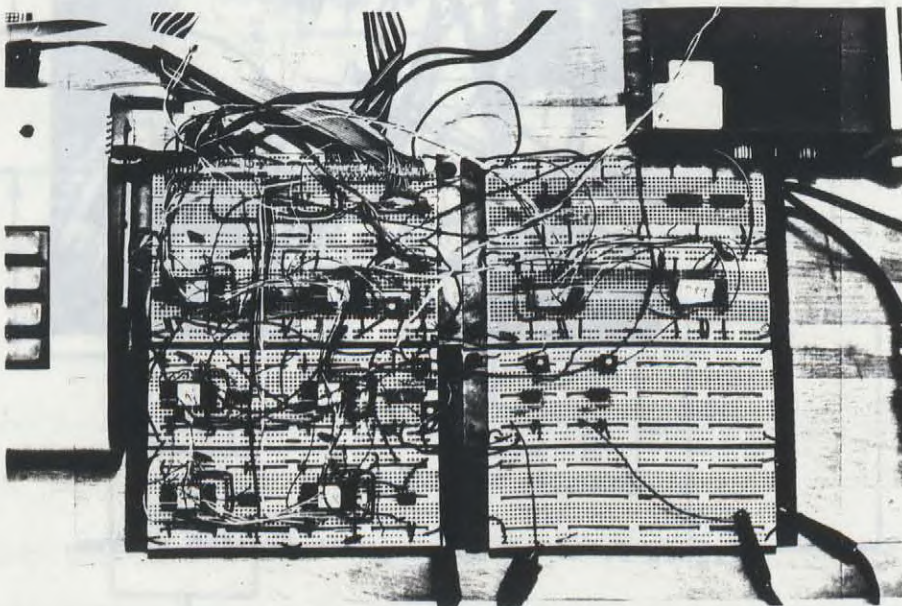


Figure 5.4d. Adaptive A/D, D/A boards.

a -30 dBm level prior to down-conversion. The mixer exhibits a conversion loss of 7 dB, so the useable IF level would approximate -37 dBm and IF gain in the vicinity of 60 dB would be required to attain the desired level as specified by (173).

The filtered and amplified intermodulation level is then detected, and input to the analog-to-digital converter. The digital output is then input to the microprocessor and software latched. A software routine then varies the bias on the predistorter diodes; the diode bias being generated by digital-to-analog converters where the digital words are software originated. All digital-to-analog and analog-to-digital converters were 10 bit, providing a good degree of resolution for both the diode bias and detected intermodulation levels. The software routine utilized was based on a "Monte Carlo", or coarse search routine. After each change in diode bias, a new intermodulation level is sampled and compared to the previous level. This process continues over the full range of the digital-to-analog converter which sets the diode bias, the optimum bias level being stored in software. The next diode bias then varies in the same manner. In all, there are six diodes to be separately biased; three diodes per predistorter. The two Schottky diodes on each predistorter are allowed to independently set their own bias; this might not be required if a set of matched diodes were to be employed.

Following this routine, the predistortion system has the ability to train itself (i.e., set the predistorter bias) from a cold start. A

suitable optimization routine could then be employed, monitoring the degree of linearity and compensating for drifting and temperature effects incurred by the amplifier and predistortion system.

CHAPTER 6

EXPERIMENTAL RESULTS

6.1 Introduction

This chapter will outline the performance of RF predistorter, which was introduced in Chapter 5 and illustrates the improvement in linearity that can be obtained through predistortion.

System performance will be presented for various linearization requirements and will demonstrate the limitation of a practical predistortion scheme.

Measurement apparatus is presented in Appendix 4.

6.2 Predistorter Results

The performance of the RF predistorter introduced in Chapter 3 will now be presented.

Recall that the predistorter should exhibit minimal AM-to-PM conversion, and generate a wide variety of convex amplitude characteristics. The curves of Figure 6.1 through Figure 6.4 present predistorter amplitude and phase characteristics for a variety of Schottky bias and PIN currents, and are the counterparts to the theoretical predistorter curves of Figure 4.16 and 4.17. Note that the effects of diode bias are as anticipated. Setting the PIN diode to a high state of conduction tends to flatten the convex curve, while Schottky bias essentially delays the effects of the nonlinearity to higher values of input powers. Phase characteristics are also reasonable, with the AM-to-PM transfer characteristics becoming more severe as the input level is decreased. This corresponds to reflection angle becoming more dependent on residual reactance as one proceeds from the right to the left regions of a Smith Chart along the real axis.

The curves of Figures 6.5 and 6.6 show the effect of memory on the predistorter frequency response. The amplitude characteristic is seen to remain consistent over a wide bandwidth, but the AM-to-PM transfer characteristic is seen to vary considerably. Hence the variation in AM-to-PM represents the major limitation for the useful bandwidth of the predistorter. In fact, a nonlinear HPA which exhibits the effects of memory will require specific predistortion coefficients for each frequency over the system bandwidth. Thus predistortion is inherently a narrowband process; system complexity increases greatly as one attempts to devise wideband predistortion systems.

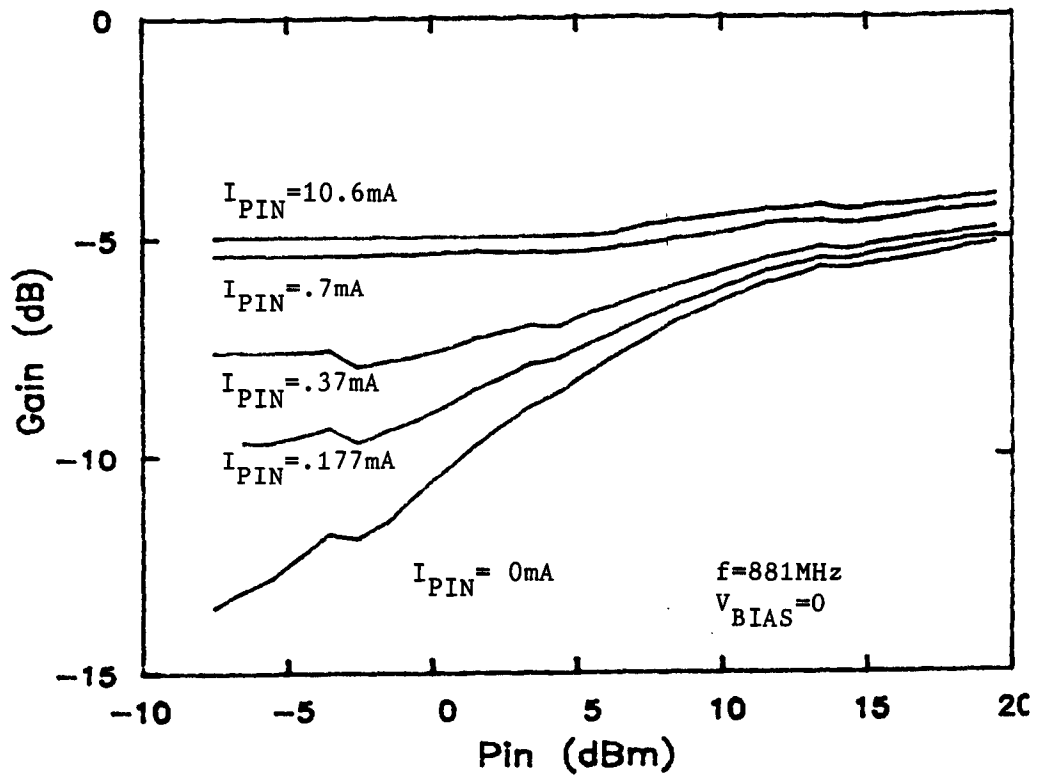


Figure 6.1. Predistorter amplitude characteristic, PIN current varying.

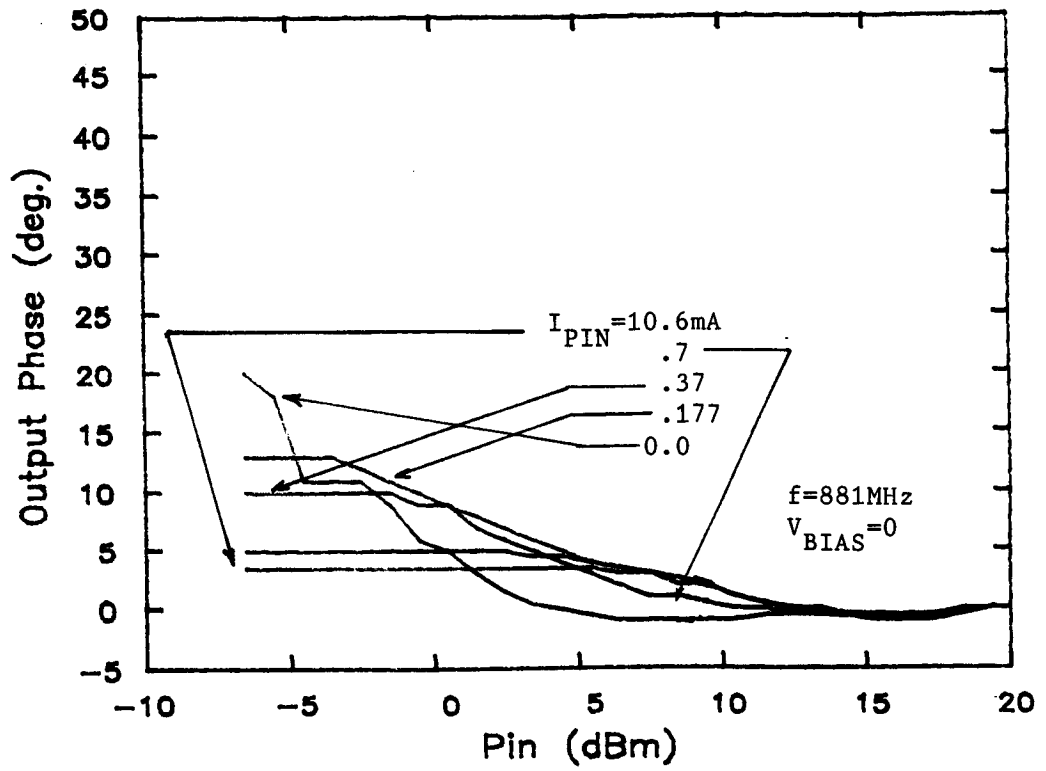


Figure 6.2. Predistorter phase characteristic, PIN current varying.

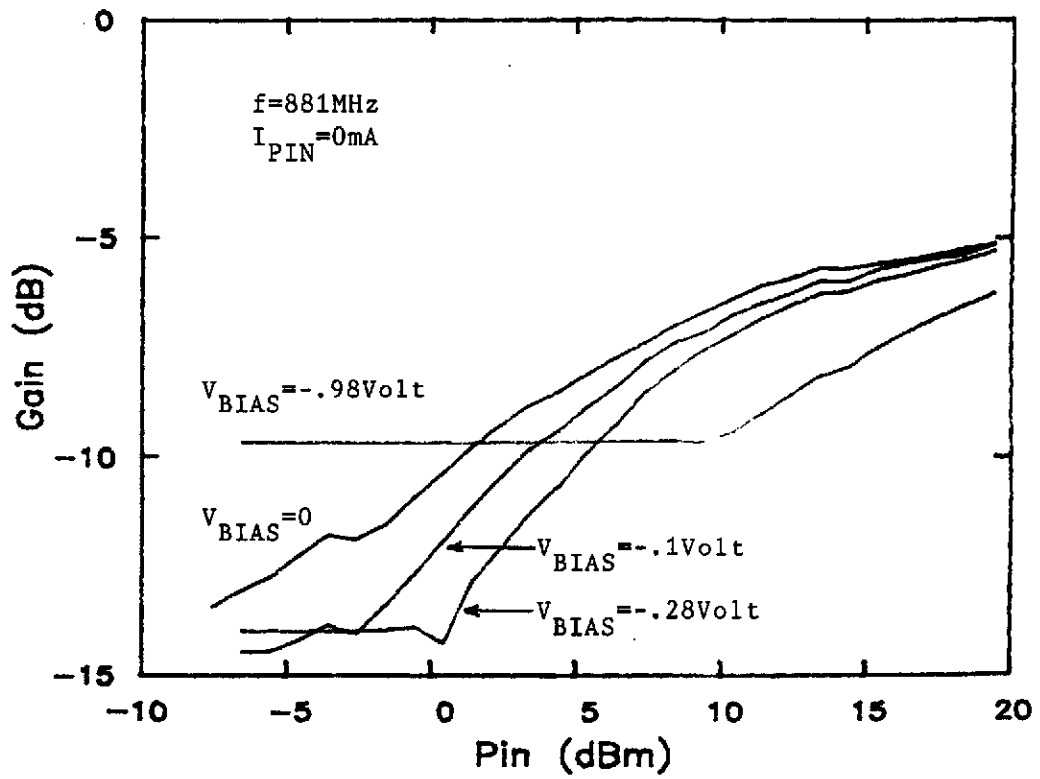


Figure 6.3. Predistorter amplitude characteristic, V_{BIAS} varying.

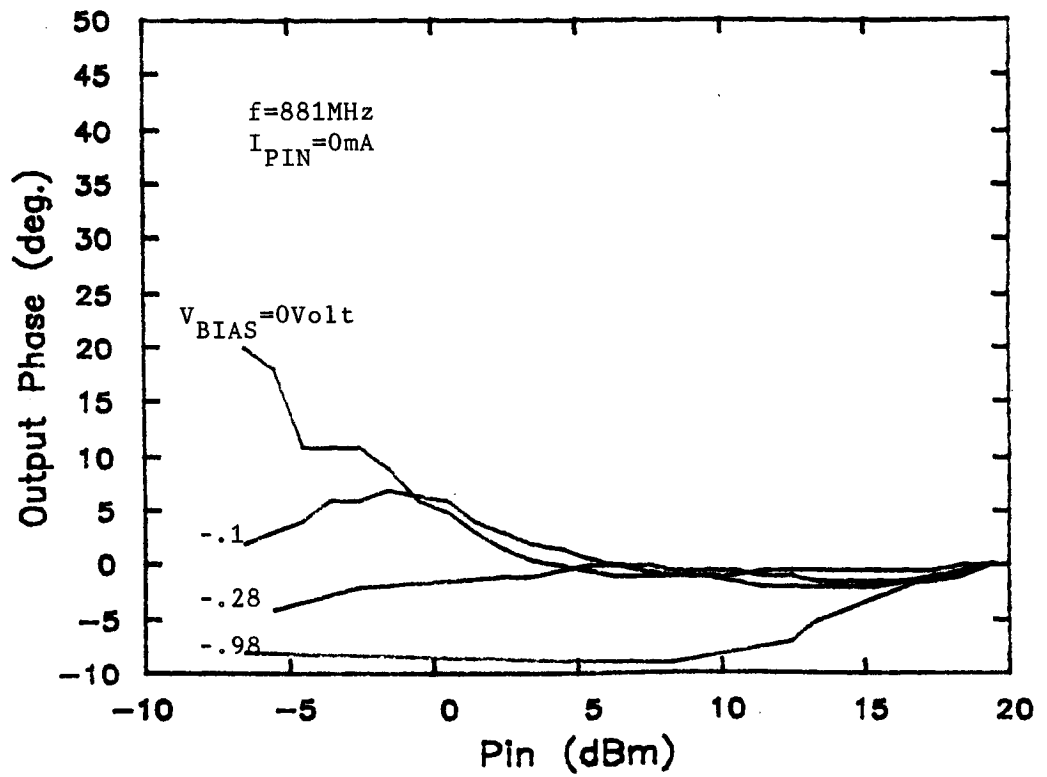


Figure 6.4. Predistorter phase characteristic, V_{BIAS} varying.

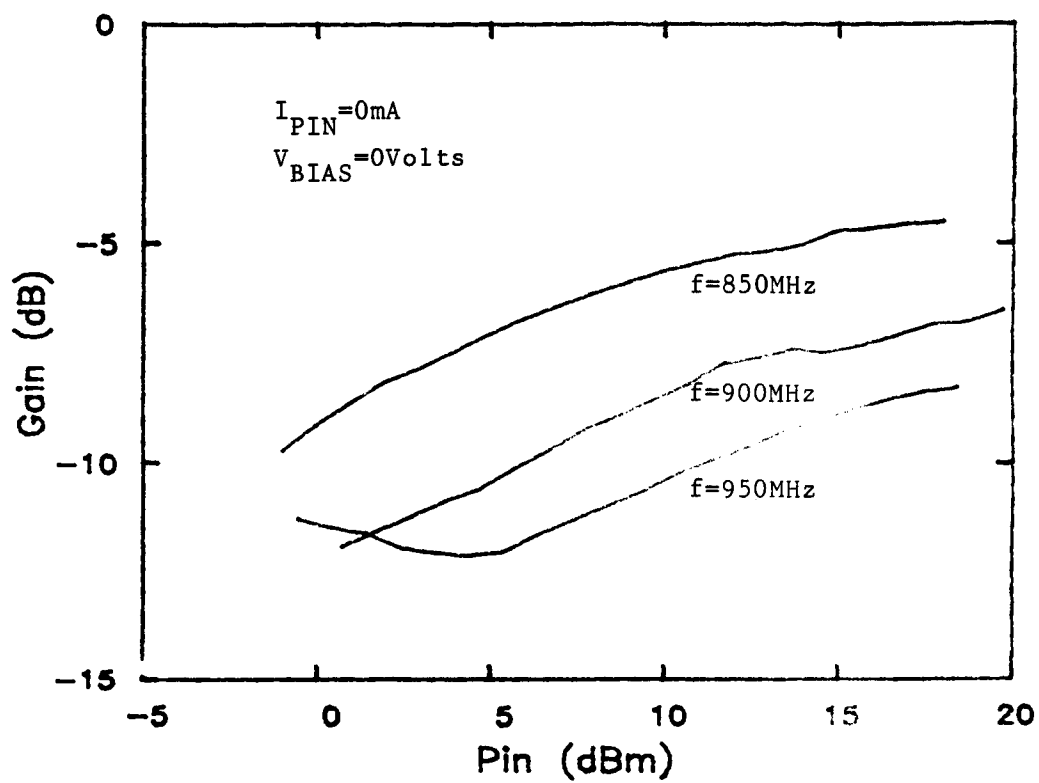


Figure 6.5. Predistorter amplitude characteristic, frequency varying.

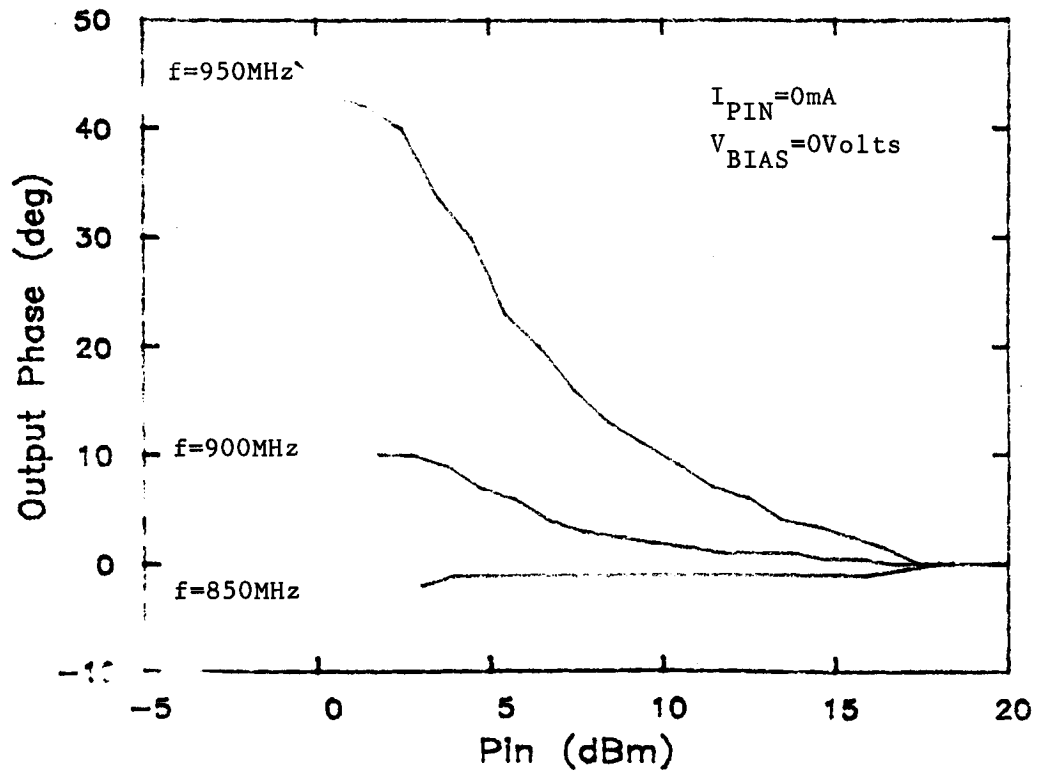


Figure 6.6. Predistorter phase characteristic, frequency varying.

The question of power dissipation in the diodes should be addressed. Dissipation is a function of both the input power and reflection coefficient, as evident from equation (150). An approximate value for the maximum dissipation can be obtained from Figure 6.1. For an input power of 20 dBm, the return loss approximates -5 dB, hence 68 percent of input power is absorbed. This corresponds to 68 mW. Data sheets for the RF diodes utilized can be found in Appendix 3 and indicate maximum allowable dissipations of 250 mW, therefore dissipation is well within allowable limits and "burn-out" is not a possibility.

6.3 HPA Characteristics

The HPA employed for the linearizing experiments was a broadband, solid-state linear amplifier, useable over a frequency range from 500 MHz to 1GHz, see Appendix 5. Static AM-to-AM and AM-to-PM transfer characteristics for the amplifier are presented in Figures 6.7 and 6.8 at a frequency of 890 MHz. The amplitude characteristic remains linear up to an output power of 29 dBm, however, the AM-to-PM characteristic is extremely erratic with significant AM-to-PM conversion exhibited even over the linear amplitude region. As such, the amplifier is an extremely challenging candidate for predistortion compensation. Amplitude compensation must occur over the region of amplifier compression without degrading performance of the amplifier over its inherently linear region ($P_{OUT} < 29$ dBm). In addition, the erratic AM-to-PM characteristic should be minimized over the full range of operation. The curves of Figures 6.7 and 6.8 are sufficient for the characterization of the non-

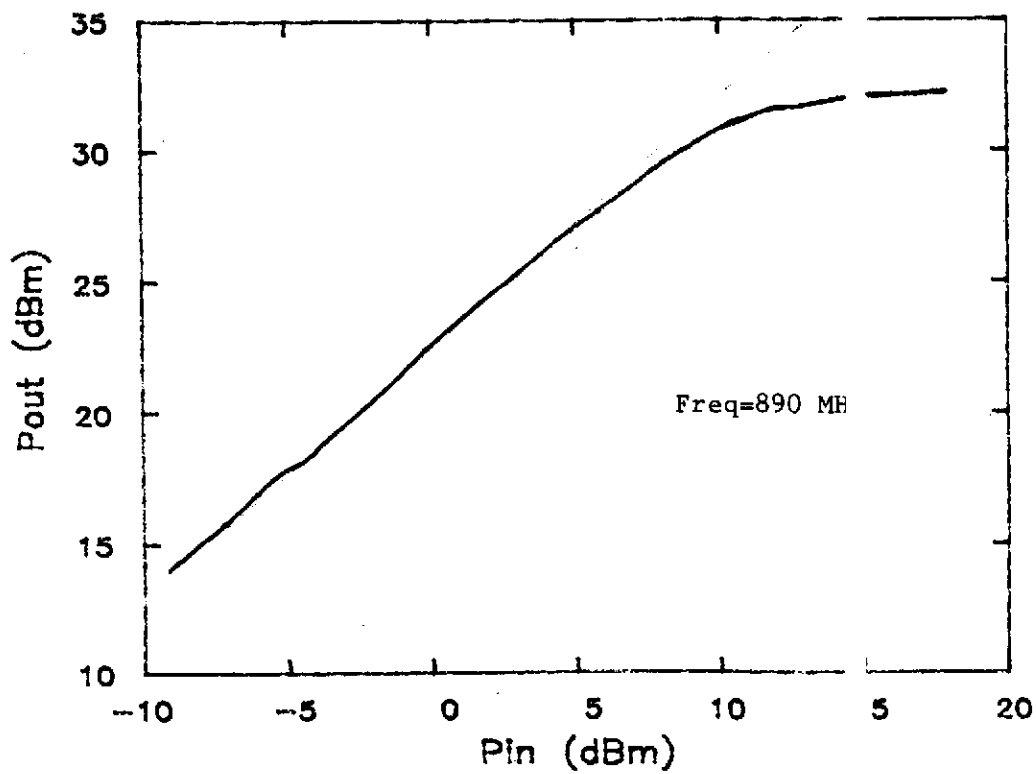


Figure 6.7. Static AM-to-AM HPA transfer characteristic.

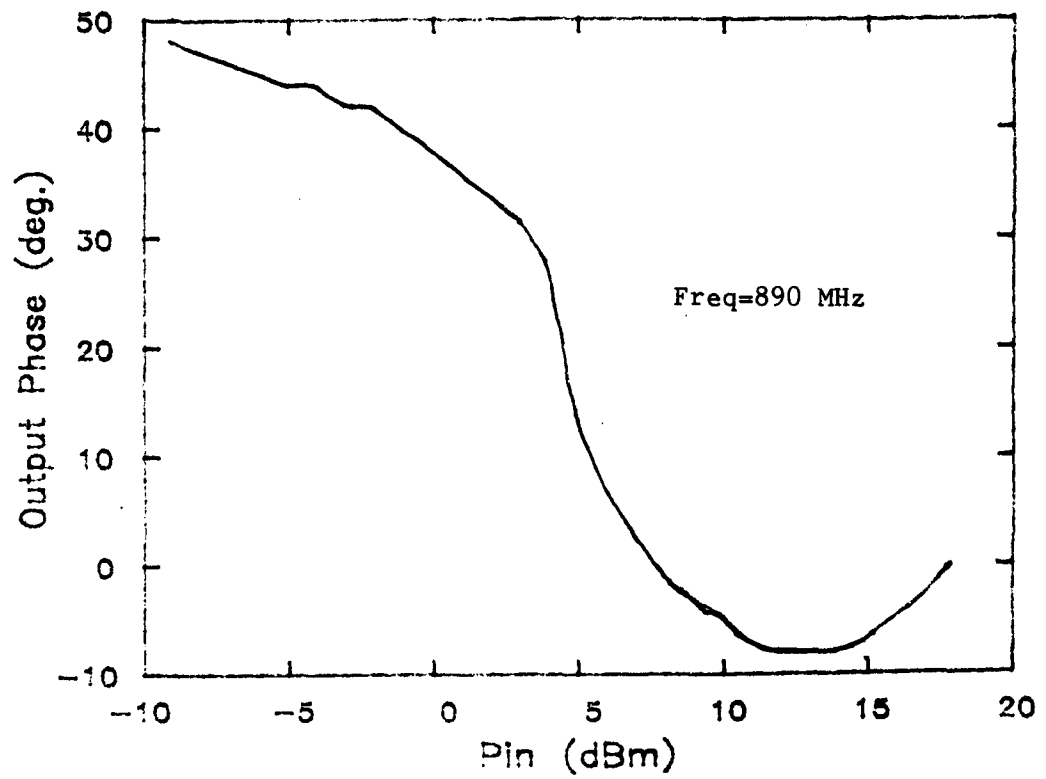


Figure 6.8. Static AM-to-PM HPA transfer characteristic.

linear HPA characteristics over a wide bandwidth on account of the amplifier's broadband capability. The HPA then appears to be "nonlinear, effectively without memory" if operation is restricted to a relatively narrow band.

It should be understood that amplitude predistortion compensation can only occur up to the point of amplifier saturation. No improvement in linearity can be gained after this point. This is most readily demonstrated through equation (99) which indicates that the predistorter must generate a transfer characteristic which is formulated from the inverse of the amplifier characteristic. If the amplifier has saturated (a slope of zero), then at that point the predistorter must have infinite slope. Obviously, this is a practical impossibility.

6.4 Predistortion System Performance

A combination of tests is necessary to evaluate the success of the linearization system. These include:

- (1) Static AM-to-AM transfer characteristics
- (2) Static AM-to-PM transfer characteristics
- (3) Two-tone intermodulation tests
- (4) Three-tone intermodulation tests .

The first three tests indicate the degree of linearity of the system over a narrow bandwidth. The three-tone intermodulation test was employed to simulate a multi-carrier wider band input spectrum.

Since the system is designed to train the predistorters at a particular amplifier output power, several of these output power linearization points should be attempted. For example, one should not attempt to train the system at an amplifier output power beyond saturation as predistortion is unable to compensate for amplifier compression, although the resultant intermodulation products will likely be reduced. This reduction would be due to increased amplifier linearity before compression. Similarly, it would be unwise to train the predistorter over a region of the amplifier's inherent linearity as nothing is to be gained. Consequently, predistorter training should occur over some region of the nonlinear amplifier characteristics before saturation. For this thesis, two linearization points were selected; a "low power" of 27 dBm and a "high power" of 30 dBm. These powers represent two practical extremes for the linearization system. The lower power linearization simulates a system where the goal is an improvement in linearity of a "linear" amplifier. The high power optimization more closely models the situation where one would attempt to compensate for a nonlinear HPA. Linearization results follow.

6.4.1 System performance; optimization at 27 dBm

Predistortion performance for system optimization at 27 dBm is now presented.

Figure 6.9 illustrates the static, single-carrier amplitude transfer characteristics for both the amplifier and the linearized amplifier.

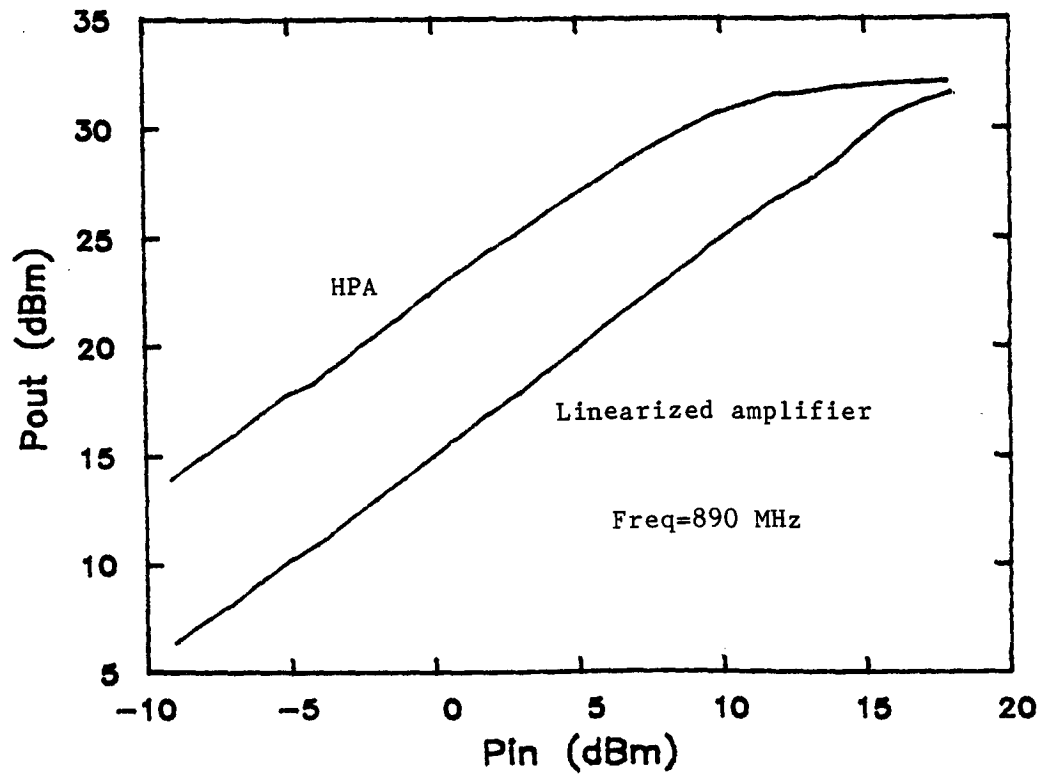


Figure 6.9. Static amplitude characteristics.

A clear improvement in linearity has been obtained up to the point of amplifier compression; the cost of this linearity is a loss of approximately 8 dB in overall system gain. Note that this loss is the minimum that could possibly be incurred by a passive predistorter as gain compression approximates 8 dB at the point of saturation. It is important to realize that this 8 dB loss could be regained simply by adding 8 dB of amplifier gain anywhere in the system. For example, since it is relatively simple to construct low-level, small-signal amplifiers, one would most likely regain the 8 dB before any high level amplification. The gain of the HPA has in no way been affected. This contrasts to the situation of negative feedback linearization where the net effect may be an 8 dB loss in system gain, but this 8 dB loss would be in HPA gain. The feedback amplifier will not be able to obtain the same "linear" output power as the pre-distortion system. Figure 6.10 shows the static AM-to-PM transfer characteristic of the amplifier and the compensated amplifier. There is no significant improvement here for output powers less than 26 dBm (the phase characteristics become identical) and only a minor improvement for powers above this threshold. Evidently, in this case, the predistortion system was best able to minimize intermodulation products by linearizing the amplifier characteristic while ignoring the phase nonlinearities.

Figures 6.11 and 6.12 demonstrate the carrier-to-intermodulation (C/I) performance of the amplifier for a two-tone test. As expected, the third-order products were found to be lower for the linearized system with best performance observed for output powers in the vicinity of

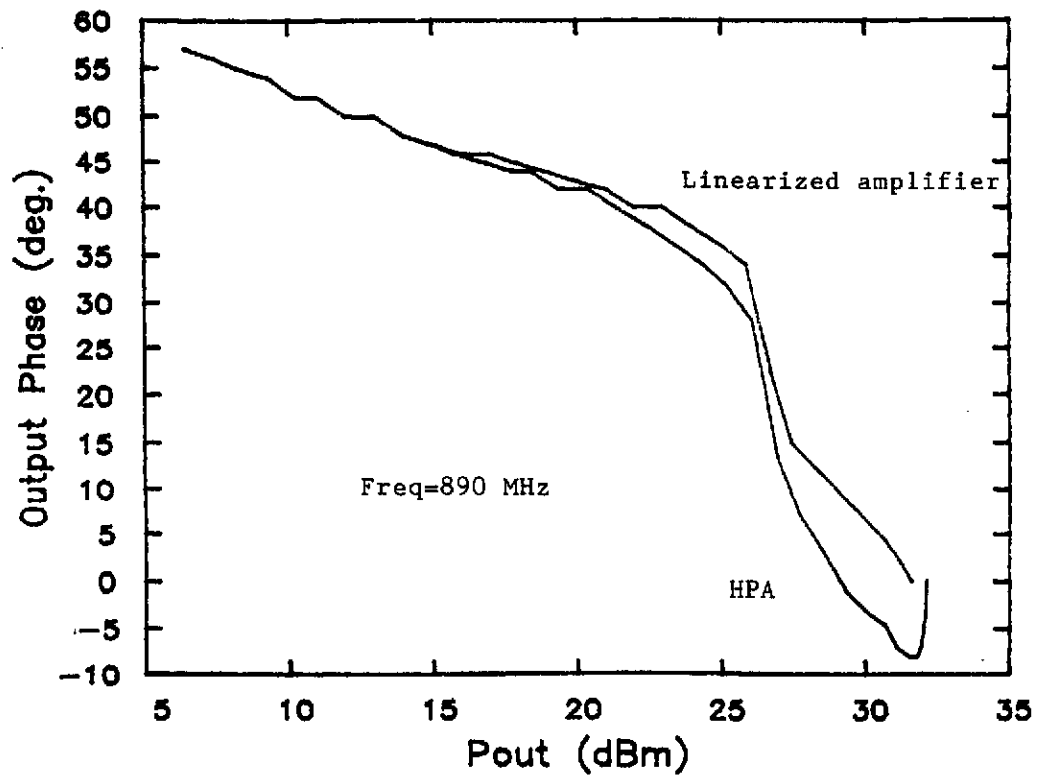


Figure 6.10. Static phase characteristics.

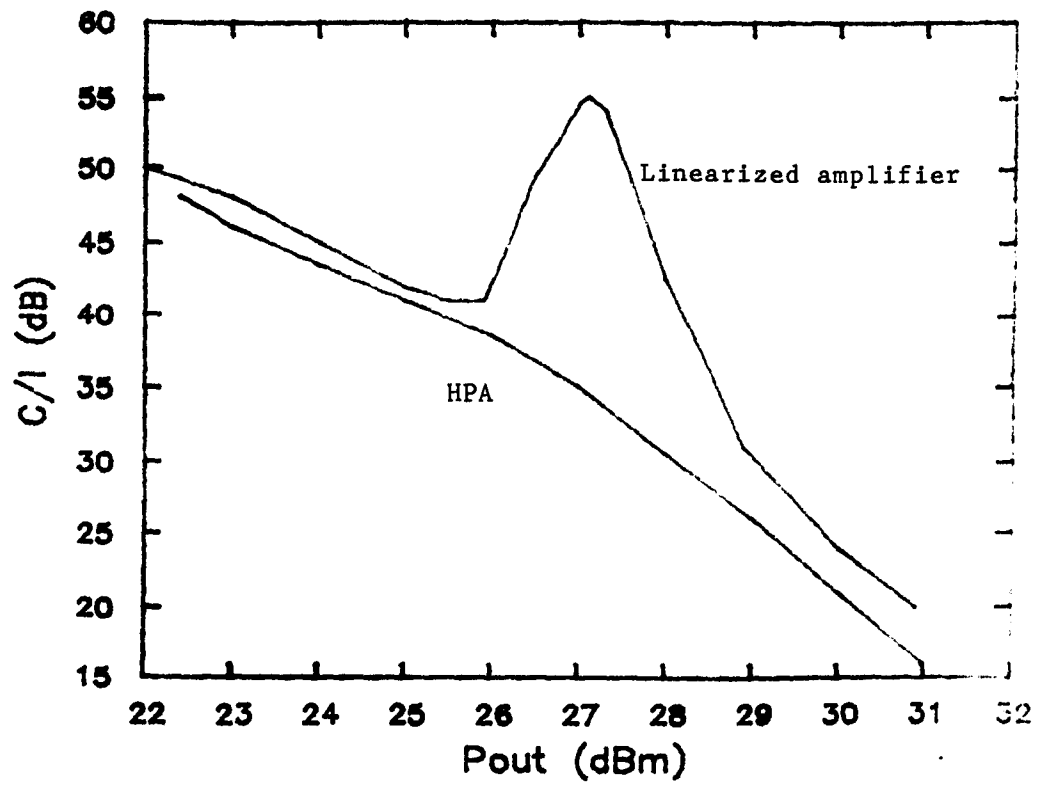


Figure 6.11. Third-order carrier to intermodulation ratios.

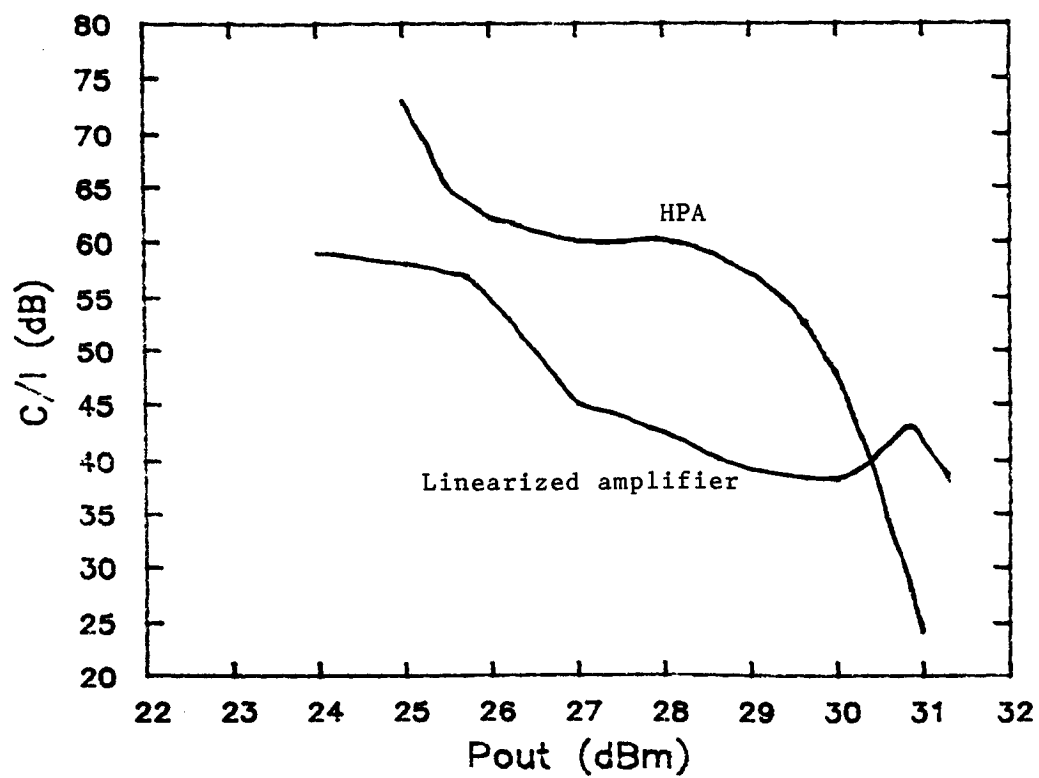


Figure 6.12. Fifth-order carrier to intermodulation ratios.

system optimization. The maximum improvement in the C/I ratio is approximately 20 dB. This improvement is achieved at the cost of poorer fifth-order C/I performances. However, fifth-order products are usually of such low amplitude that an increase in this level is tolerable.

Figures 6.13 and 6.14 present typical output spectra for the unlinearized and linearized amplifier respectively. Note the increase in higher-order products for the predistorted amplifier, as predicted in Section 3.2.5.

6.4.2 System performance; optimization at 30 dBm

Referring to Figure 6.15, one can again see the improvement in amplitude linearity provided by the predistorter. The characteristic is similar to that of Figure 6.9, although not quite as linear.

A significant improvement in the phase nonlinearity has been obtained, however, as demonstrated by Figure 6.16. The AM-to-PM coefficient, (the slope of Figure 6.16), is much lower after amplifier linearization than for the HPA over the entire range of output power. The important increase in phase linearity occurs in the region of output powers from 26 dBm to 31 dBm. Here the linearized AM-to-PM coefficient is approximately 1 deg./dB as opposed to 7 deg./dB for the HPA.

Figures 6.17 and 6.18 present the third and fifth-order C/I results for the 30 dBm optimized system. Again, optimum third order C/I ratios occur close to the optimization point; the improvement is seen to be approximately 15 dB.

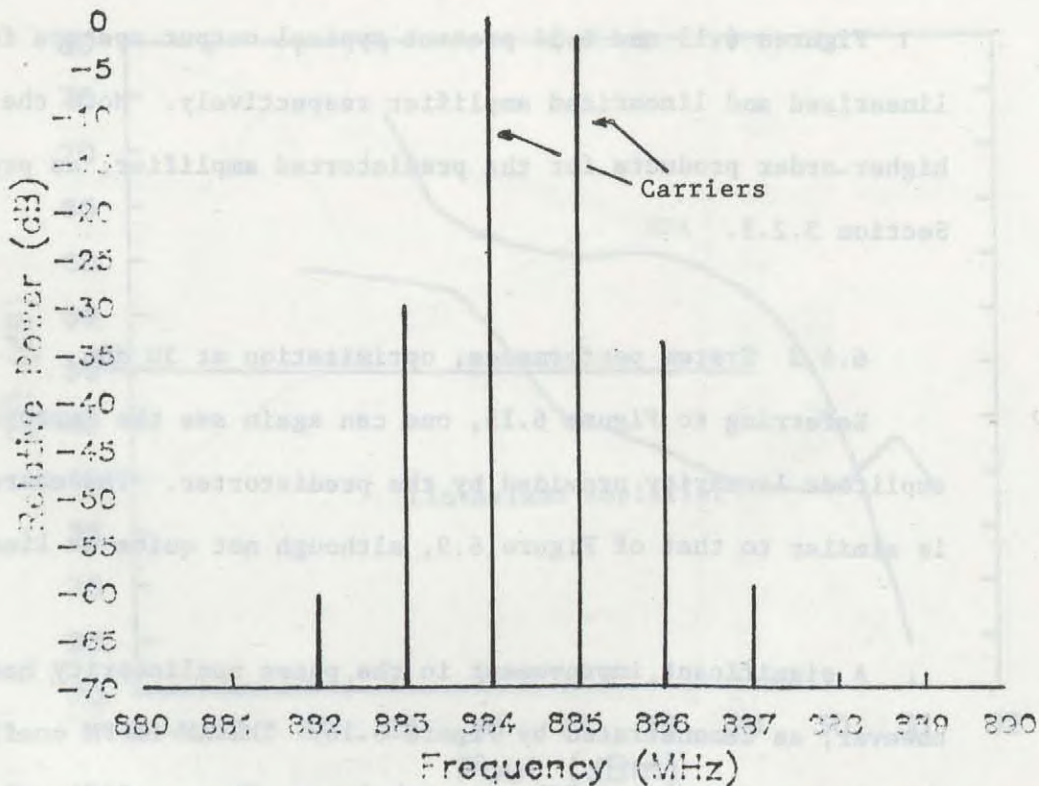


Figure 6.13. Two-tone intermodulation spectrum for the HPA.
Output power= 27.11 dBm.

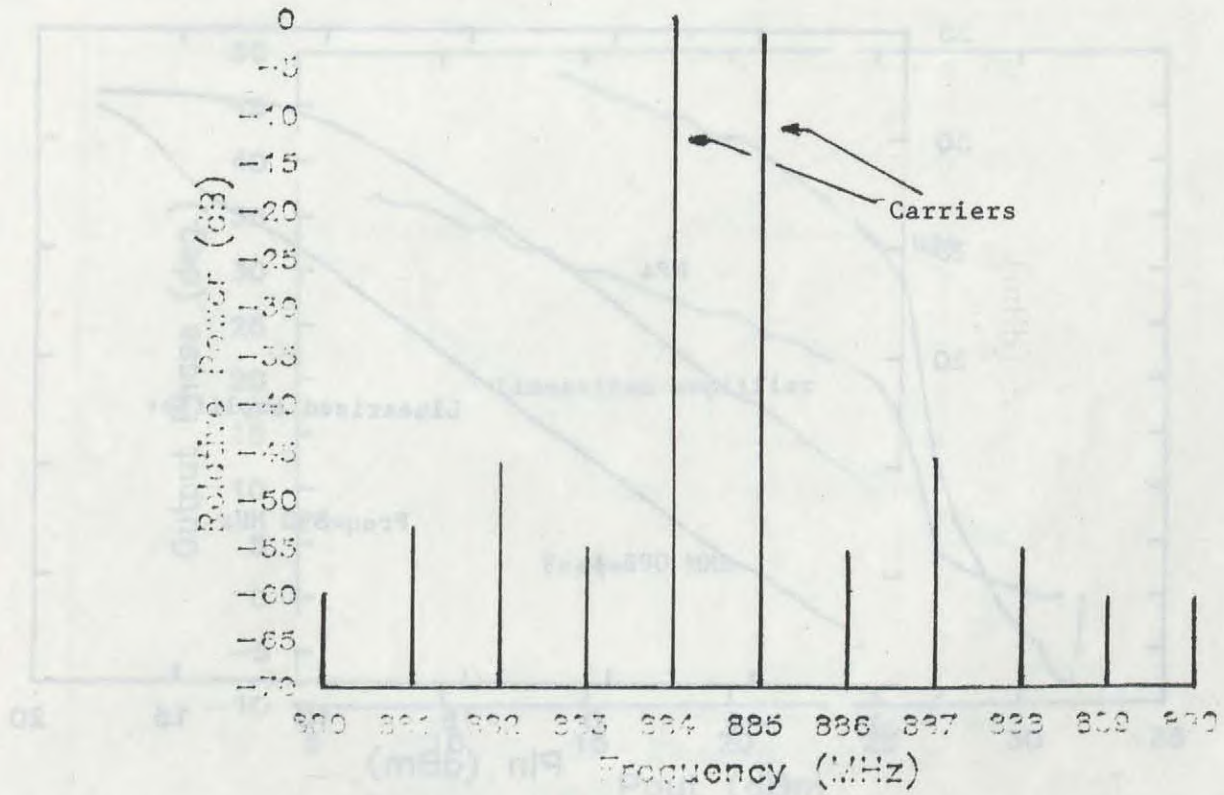


Figure 6.14. Two-tone intermodulation spectrum for the linearized HPA.

Output power= 27.11 dBm.

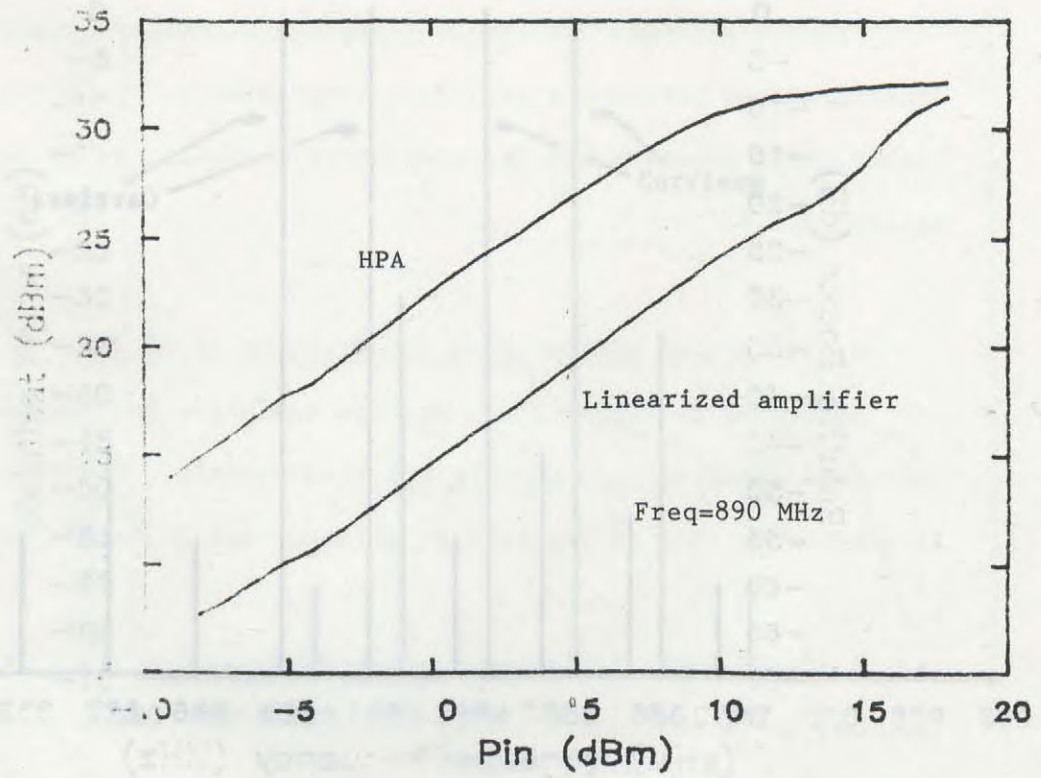


Figure 6.15. Static amplitude characteristics.

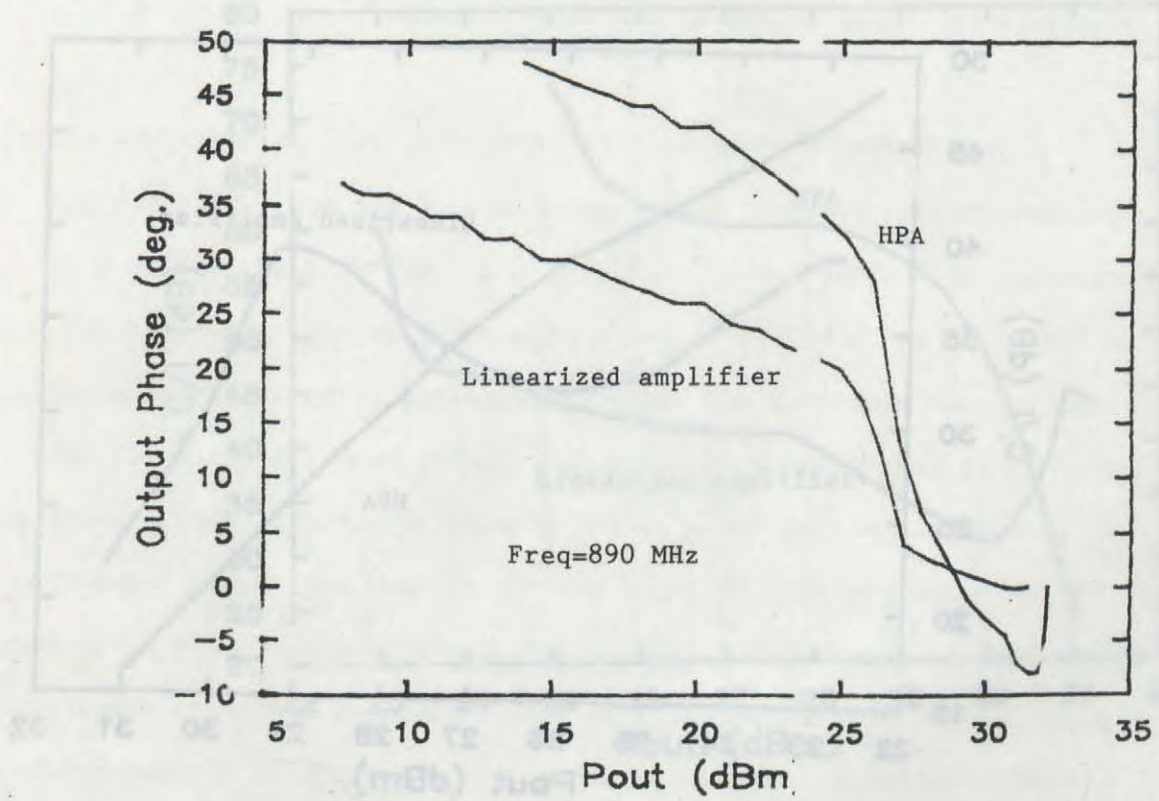


Figure 6.16. Static phase characteristics.

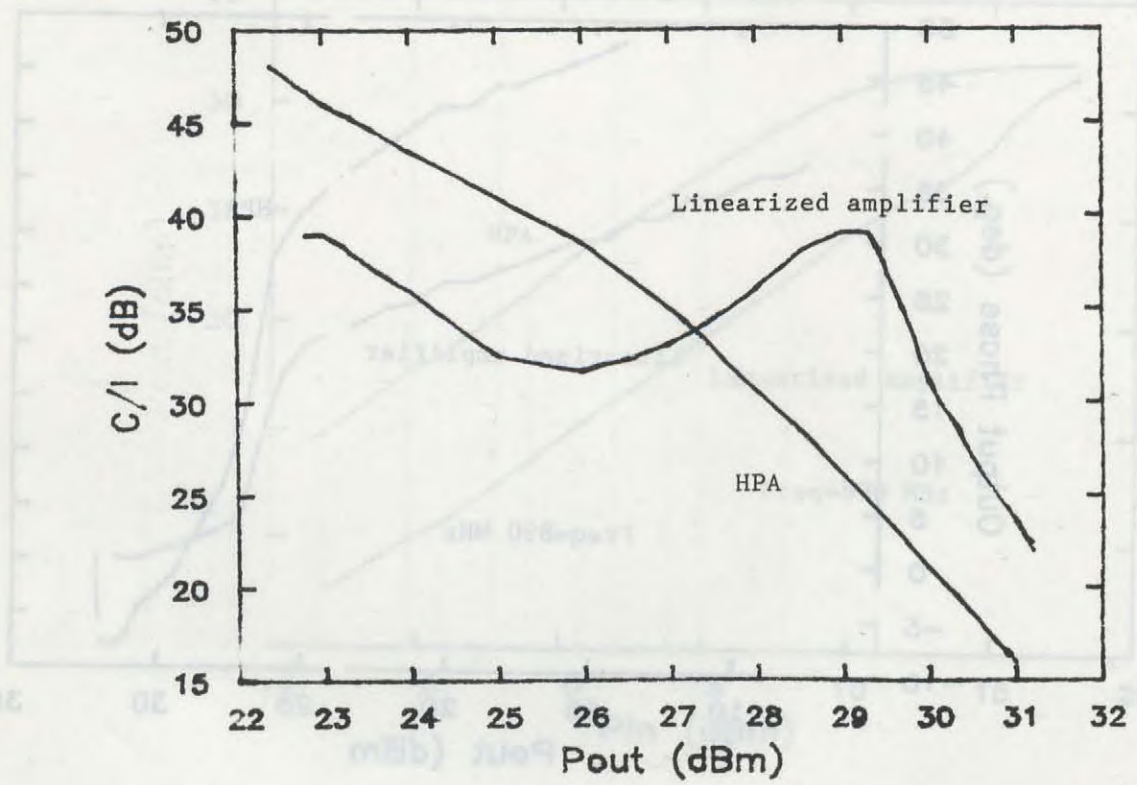


Figure 6.17. Third-order carrier to intermodulation ratios.

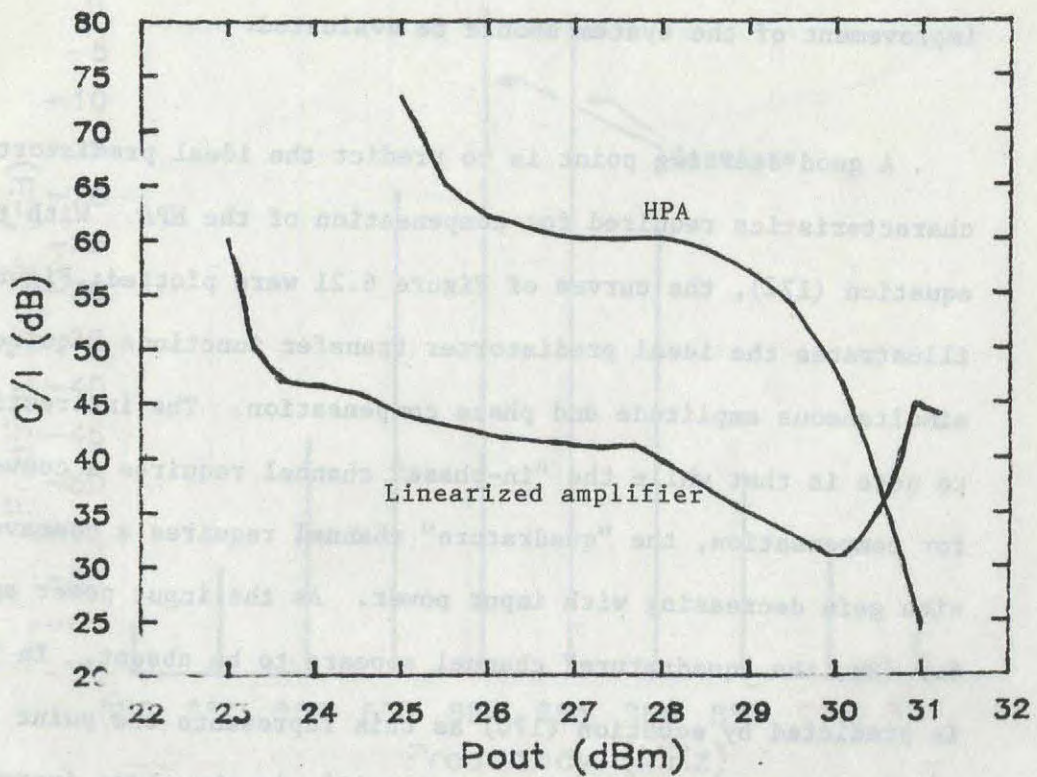


Figure 6.18. Fifth-order carrier to intermodulation ratios.

Sample output spectra are presented in Figures 6.19 and 6.20 for the unlinearized and linearized amplifier respectively.

6.4.3 Ideal predistorter transfer characteristics

Having seen the results of the previous sections, mechanisms for improvement of the system should be evaluated.

A good starting point is to predict the ideal predistorter transfer characteristics required for compensation of the HPA. With the aid of equation (171), the curves of Figure 6.21 were plotted; Figure 6.21 illustrates the ideal predistorter transfer functions required for simultaneous amplitude and phase compensation. The interesting point to note is that while the "in-phase" channel requires a convex function for compensation, the "quadrature" channel requires a concave function, with gain decreasing with input power. As the input power approaches 6.5 dBm, the "quadrature" channel appears to be absent. In fact, this is predicted by equation (170) as this represents the point where the amplitude dependent phase approaches 45° . As the phase increases past this point, the "quadrature" channel is required to produce a component 180° out of phase with the components that are required for lesser phase shifts (on a voltage basis, this signified a negative voltage component).

Several limitations of the system are now evident. First, certain compensation situations may require both convex and concave linearizers

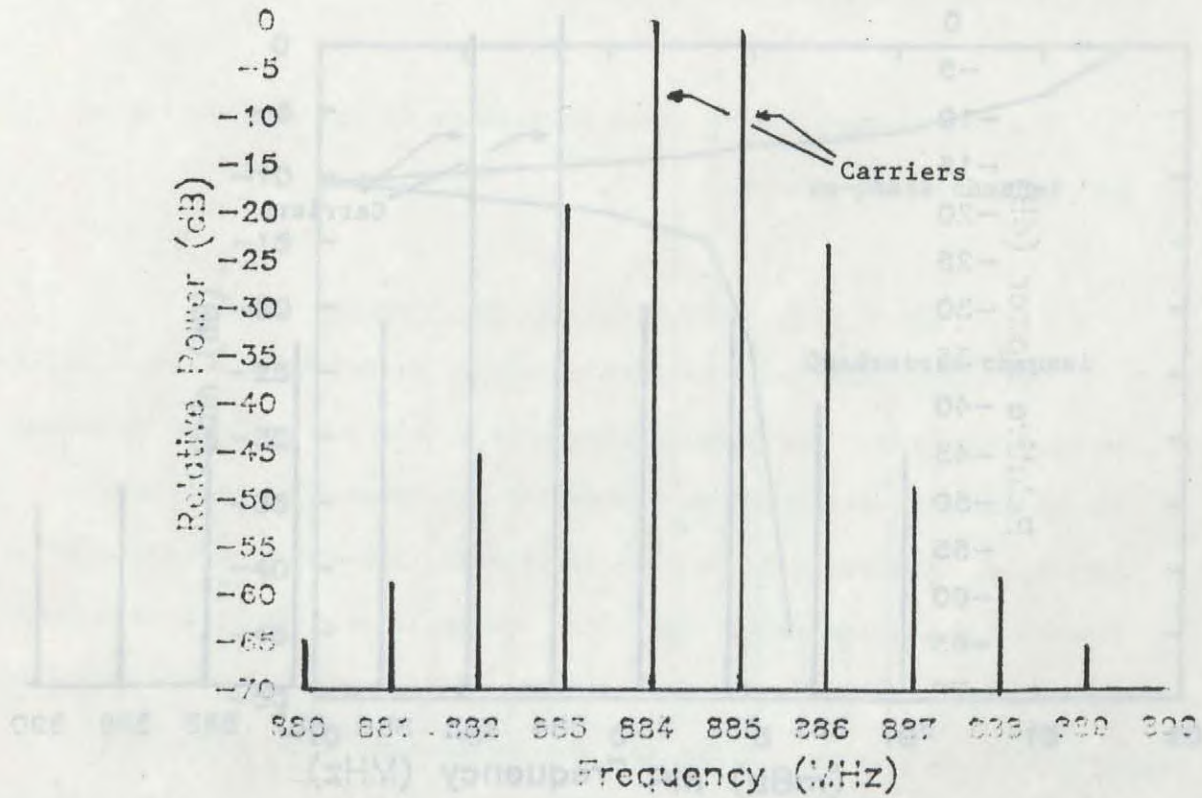


Figure 6.19. Two-tone intermodulation spectrum for the HPA.

Output power= 29.79 dBm.

Sample output spectra are presented in Figures 6.19 and 6.20 for the unlinearized and linearized amplifier respectively.

6.4.3 Ideal pre-distorter transfer characteristics

Having seen the results of the previous sections, mechanisms for

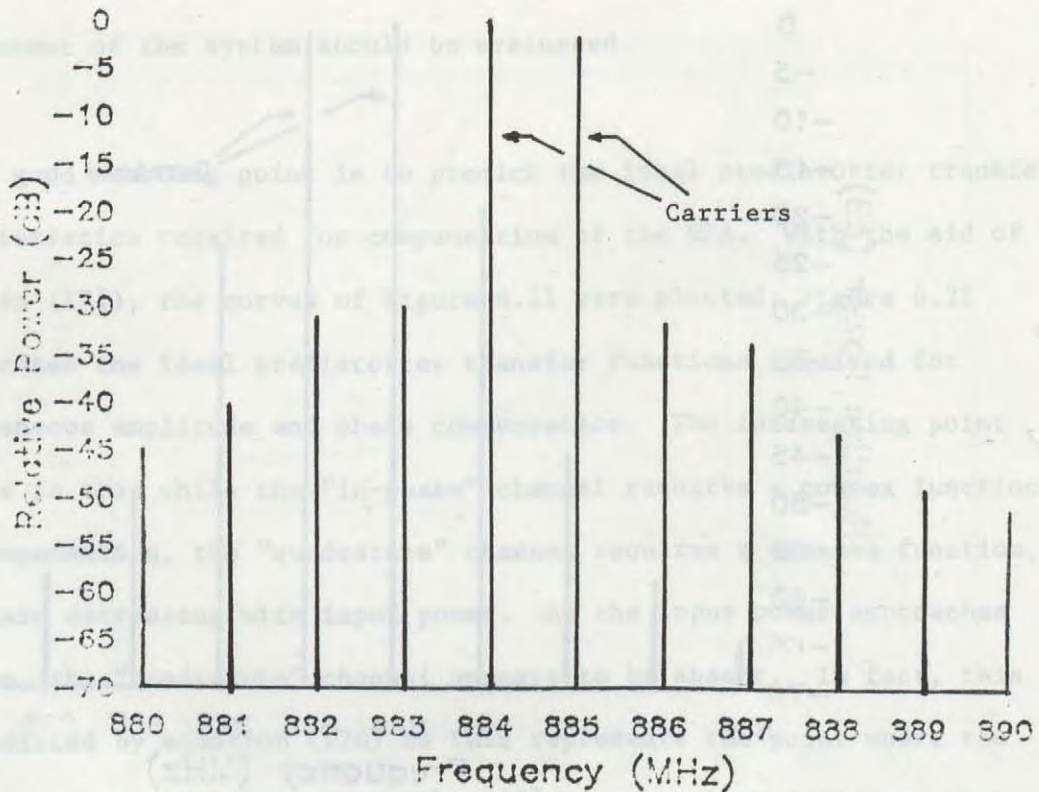


Figure 6.20. Two-tone intermodulation spectrum for the linearized HPA.

Output power = 29.79 dBm.

Several limitations of the system are now evident. First, certain compensation situations may require both convex and concave linearizers

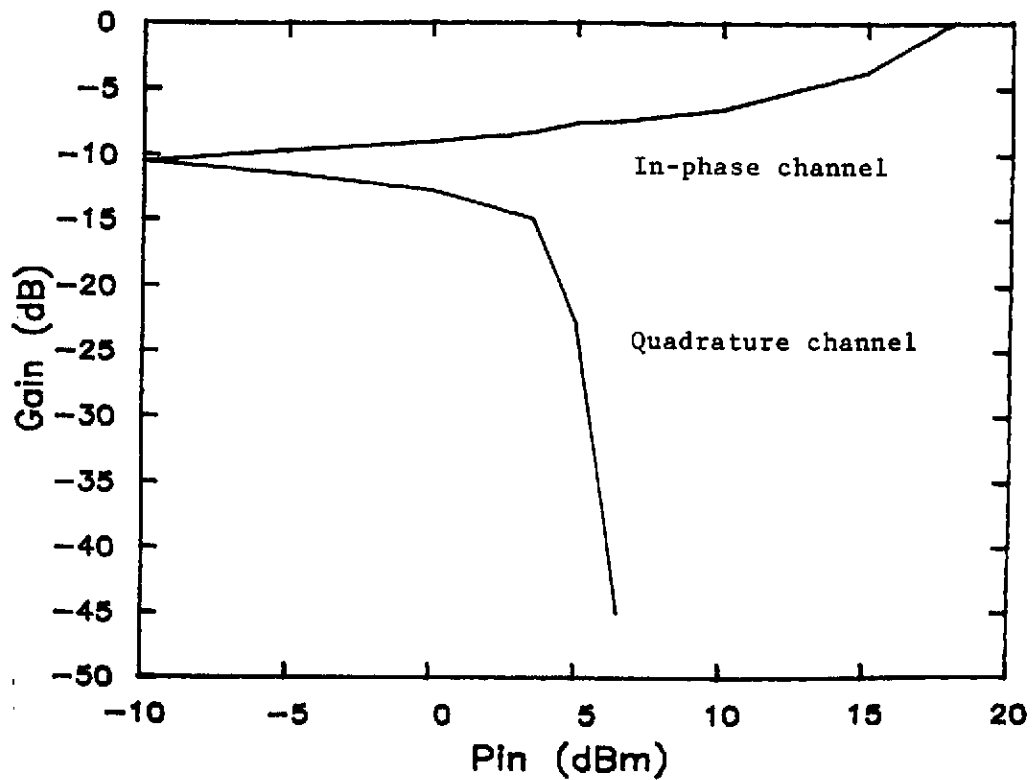


Figure 6.21. Ideal predistorter characteristics.

to be utilized. Second, the present predistortion system has no facility for correcting for phases greater than $\pm 45^\circ$ from the linear phase reference. Recall that the predistorters were required to produce negligible phase shifts and that a considerable effort was made to minimize the generation of significant AM-to-PM conversion by these circuits.

The two factors listed above contribute to the degradation of performance of the system.

6.4.4 Three-tone intermodulation performance

The three-tone intermodulation test is useful to simulate a multi-carrier spectrum. For this system, such a test was employed to demonstrate the degradation in predistortion performance as bandwidth is increased. Figures 6.22 to 6.29 illustrate three-tone intermodulation spectra for various bandwidths. The system is seen to be less effective for wideband intermodulation reduction; for Figures 6.28 and 6.29, the bandwidth approaches 200 MHz and the improvement provided by the predistorter is minimal. This was expected, as the system can no longer be classified as "nonlinear effectively without memory". Wideband predistortion requires a "full memory" compensation system.

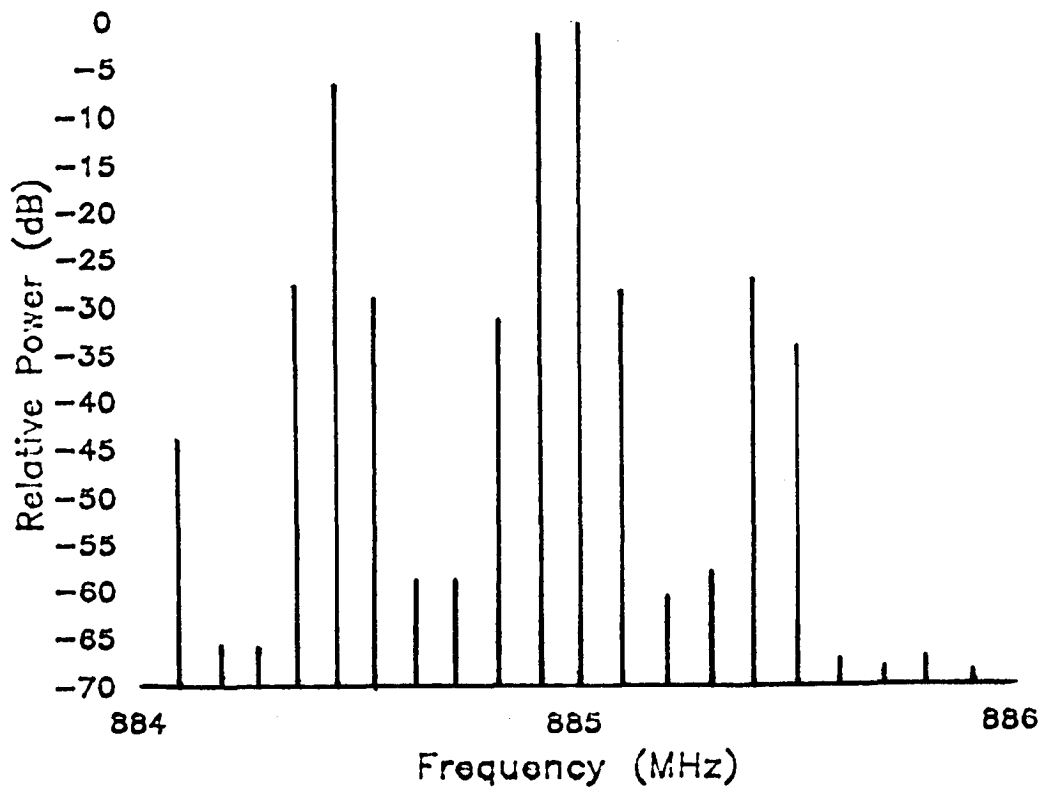


Figure 6.22. HPA three-tone intermodulation spectrum.
Output power = 27.09 dBm. (See also Fig. 6.23.)

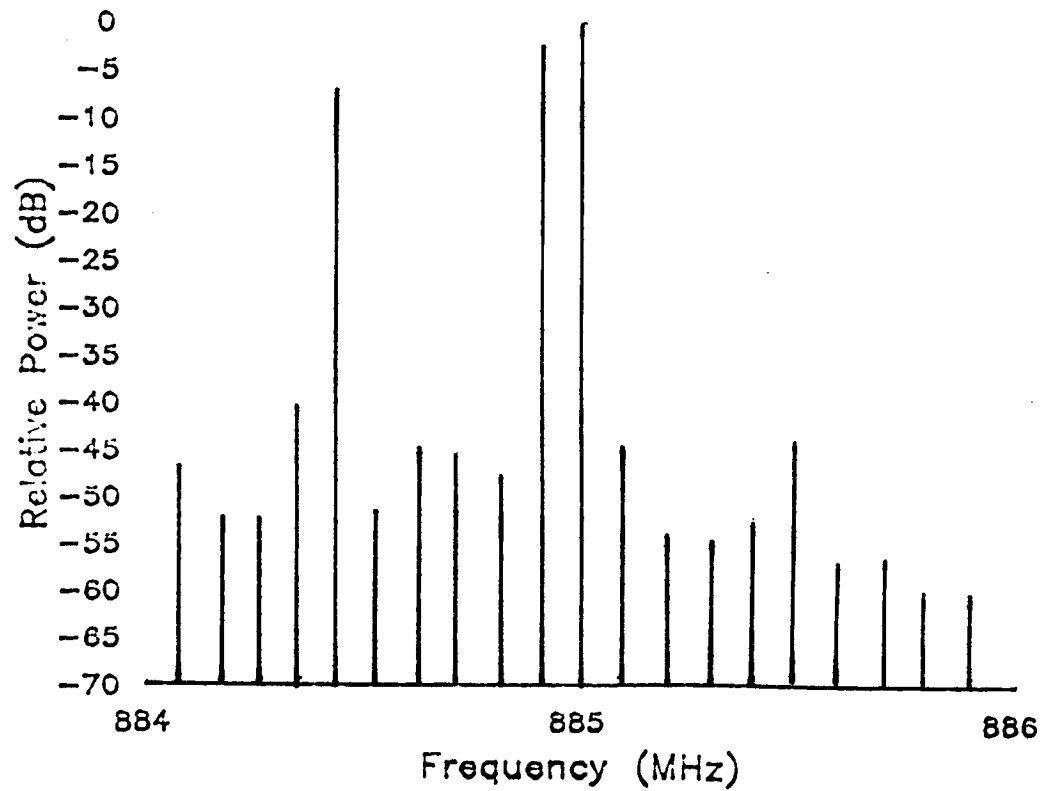


Figure 6.23. Linearized three-tone intermodulation spectrum. Output power = 27.09 dB_m. (See also Fig. 6.22.)

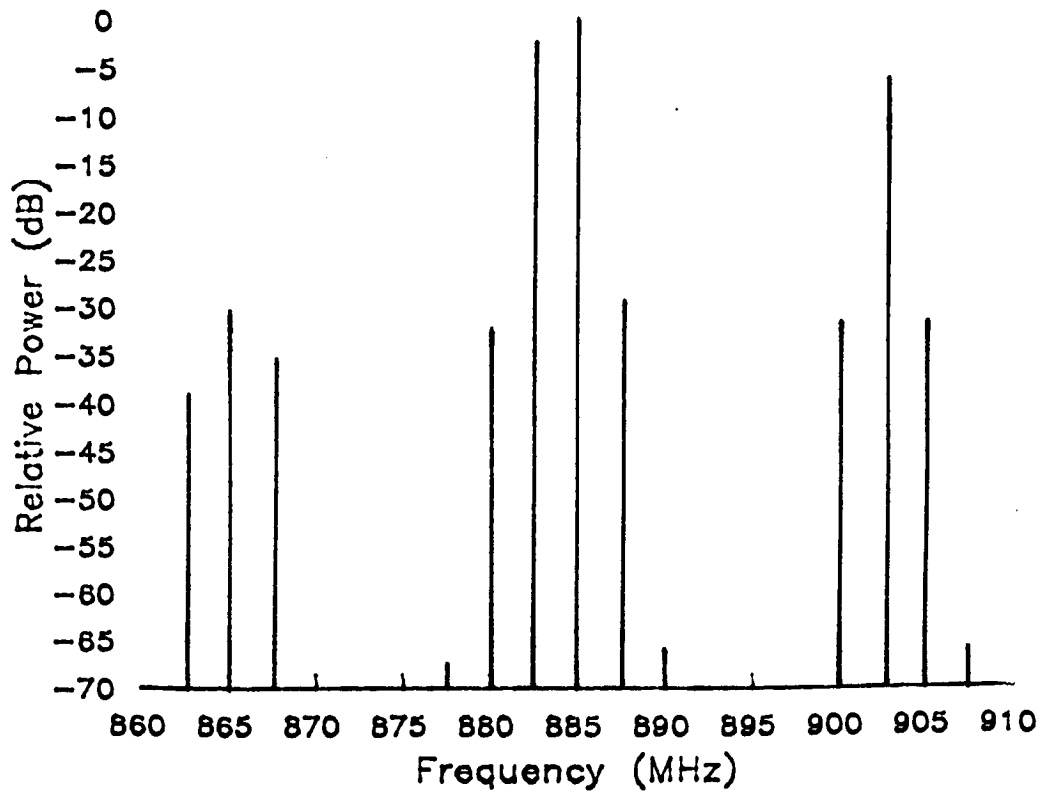


Figure 6.24. HPA three-tone intermodulation spectrum.
Output power = 27.25 dBm. (See also Fig. 6.25.)

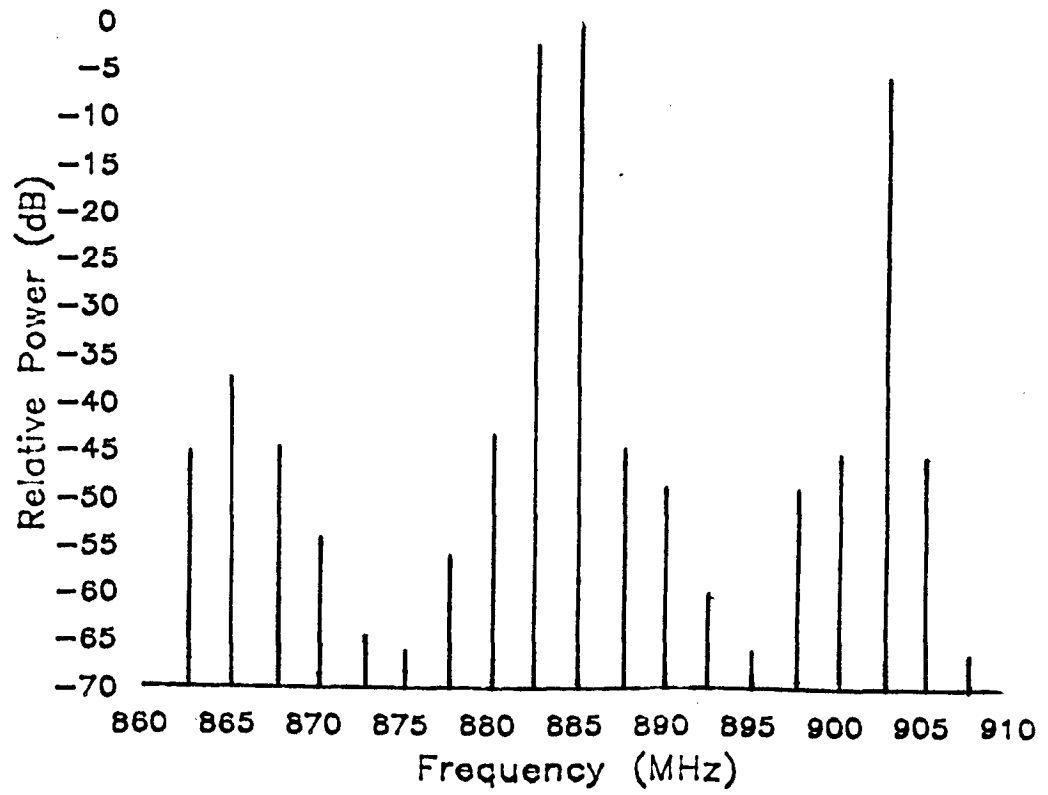


Figure 6.25. Linearized three-tone intermodulation spectrum.
Output power = 27.25 dBm. (See also Fig. 6.24.)

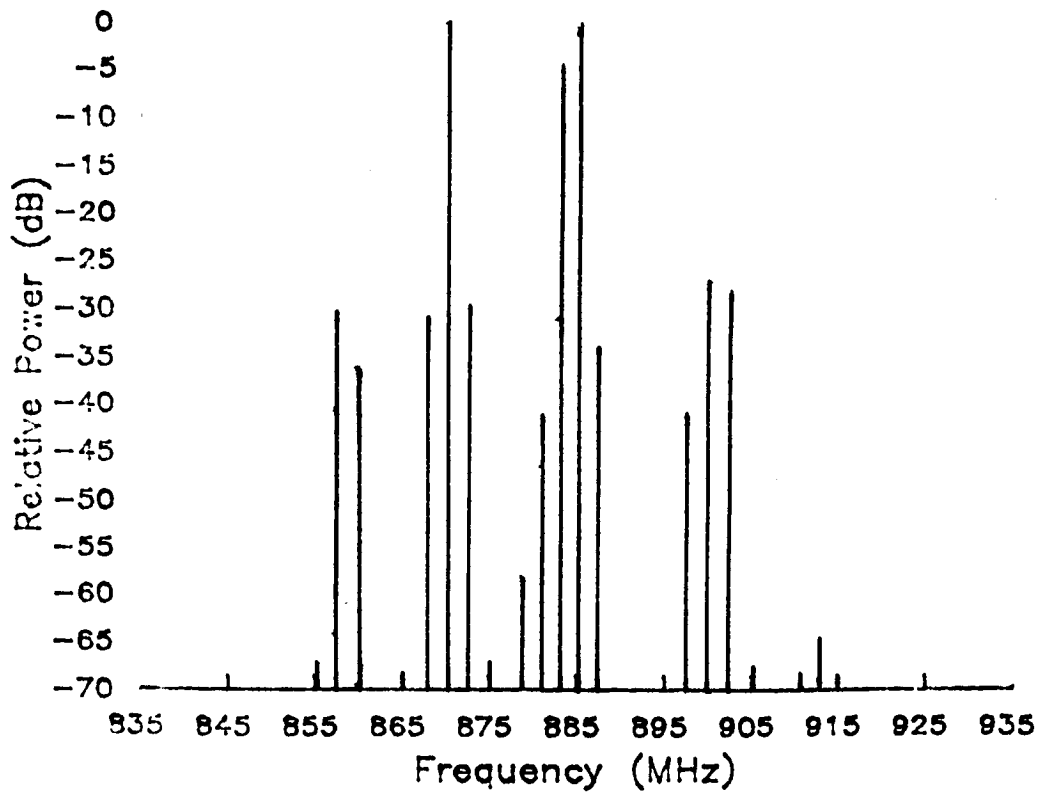


Figure 6.26. HPA three-tone intermodulation spectrum.
Output power = 27.66 dBm. (See also Fig. 6.27.)

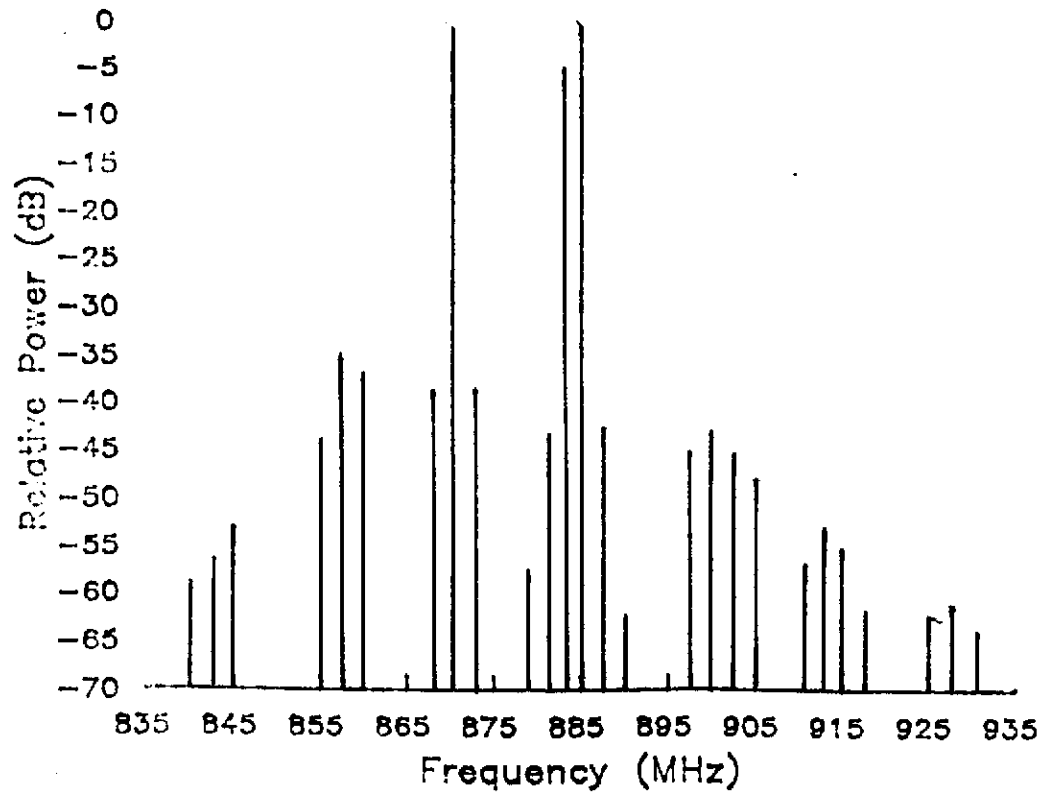


Figure 6.27. Linearized three-tone intermodulation spectrum.
Output power = 27.66 dBm. (See also Fig. 6.26.)

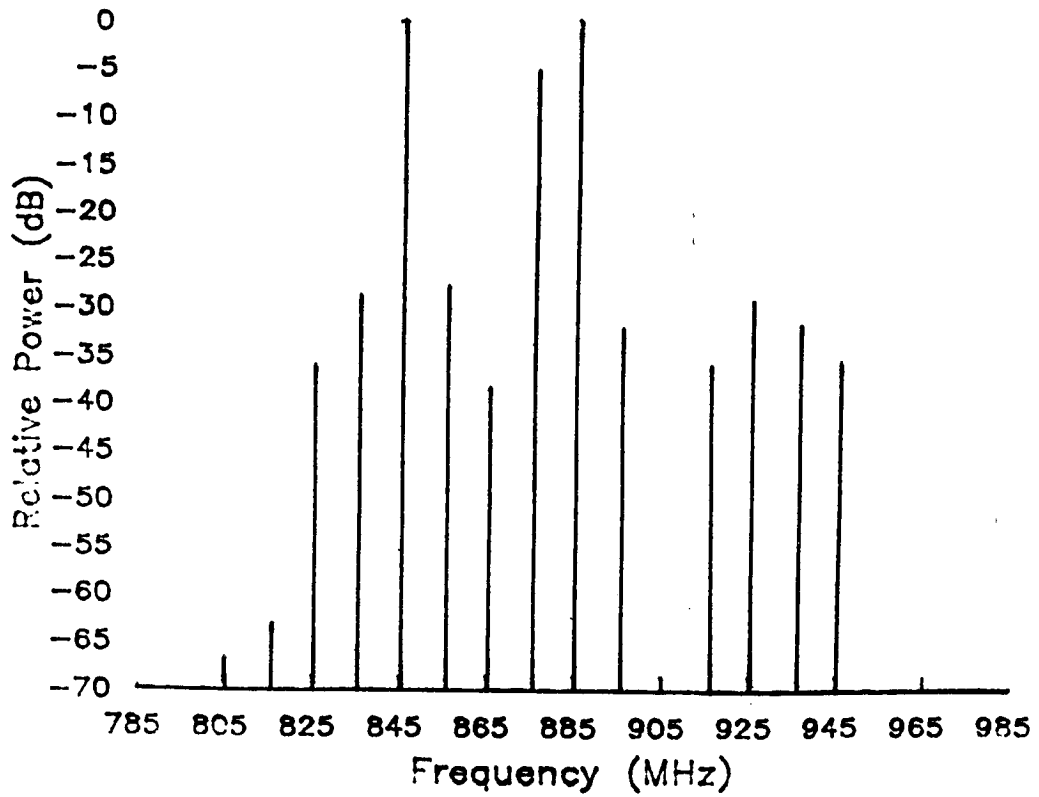


Figure 6.28. HPA three-tone intermodulation spectrum.
Output power = 27.53 dBm. (See also Fig. 6.29.)

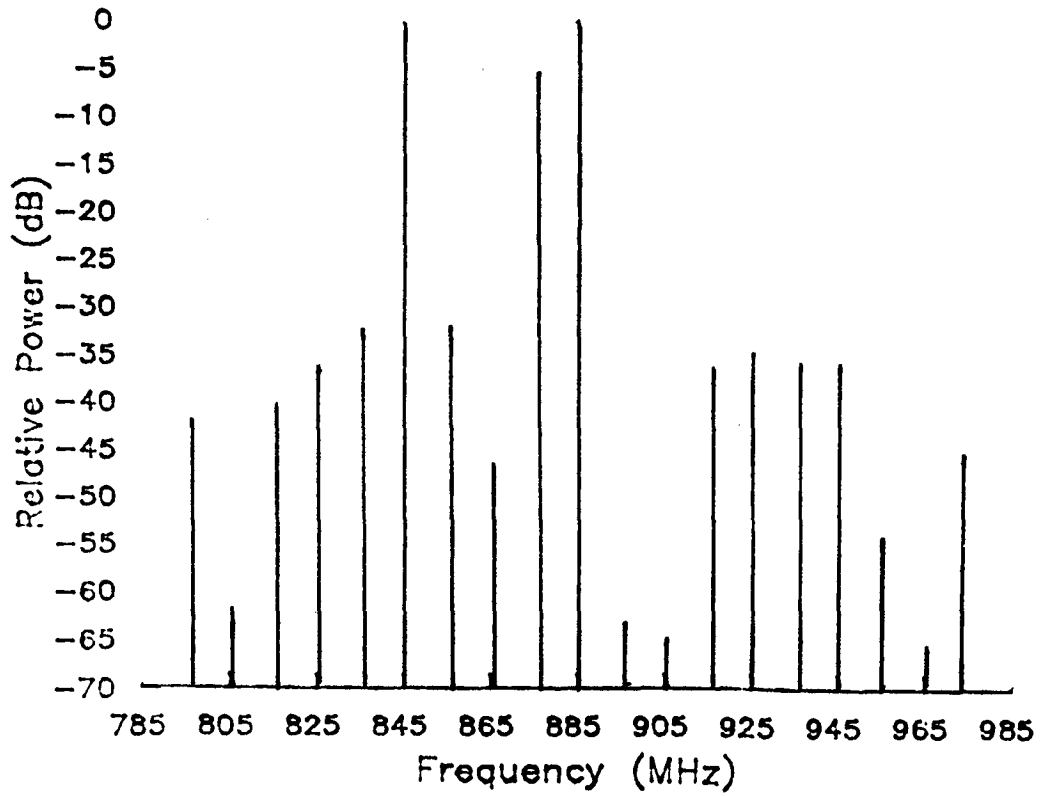


Figure 6.29. Linearized three-tone intermodulation spectrum.
Output power = 27.53 dBm. (See also Fig. 6.28.)

CHAPTER 7

CONCLUSIONS AND RECOMMENDATIONS FOR FUTURE WORK

o A practical, 900 MHz adaptive RF predistortion system was designed and implemented. A significant improvement in amplifier linearity was obtained, with two-tone carrier-to-intermodulation ratios being improved by an average of 15 to 20 dB. Static AM-to-PM and AM-to-PM transfer characteristics were also seen to be linearized.

Adaptive control allowed a totally autonomous system that could initially train the predistorter for optimum linearity, and maintain this linearity, correcting for long term aging and temperature drifts.

A unique RF predistorter was devised. This predistorter was based on nonlinear reflection so as to minimize amplitude-dependent phase shifts. This RF circuit also readily lends itself to adaptive control.

Predistortion performance can be improved through increased circuit complexity.

As presented in Chapter 6.4.3, ideal predistortion for certain amplifiers might require the generation of both convex, as well as a concave nonlinearity. Hence, the proposed RF circuit of Chapter 4.3 should be further developed and implemented.

Certain authors, [25], [27], have utilized equalizers to correct for linear distortion in conjunction with nonlinear predistortion systems. The linear equalizers improve wideband predistortion performance by increasing the frequency limits over which the HPA can be classified as "effectively without memory". For predistortion systems where amplifier operation must occur over a wide bandwidth, the proposed topology of Figure 7.1 could be implemented. Here, linear filters provide the frequency response required for compensation of "full memory" nonlinearities. Each predistortion subsection is required to compensate for only a narrow range of frequencies and each predistorter would generate a different complex transfer function, as required for linearization in that narrow frequency range.

In summary, direct RF adaptive predistortion has been shown to be effective for system linearization. Adaptive control allows for an autonomous system with the ability to train to the HPA transfer functions and maintain linearization conditions, compensating for aging and temperature effects.

Advancements have also been made in the analysis of nonlinear systems; these advancements are summarized in Section 3.3.

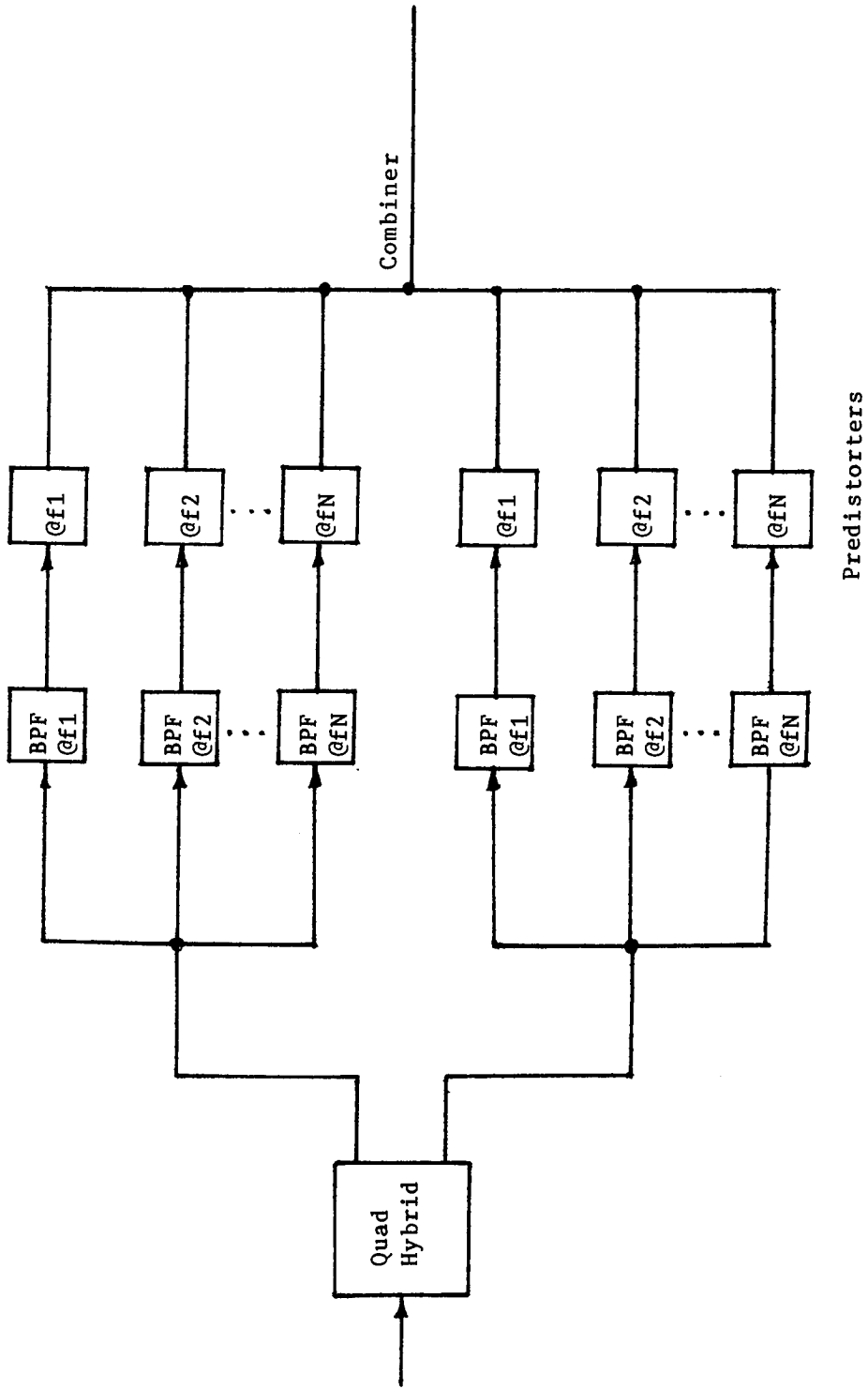


Figure 7.1. Proposed predistortion system.

APPENDIX 1

NOTES ON LINEAR INDEPENDENCE

A class of random processes, $[X_{t_1}, X_{t_2}, \dots, X_{t_n}]$, is considered to be linearly independent if

$$C_{xx}(t_1, t_2) = R_{xx}(t_1, t_2) - E(X_{t_1})E(X_{t_2}) = 0. \quad [37], [38] \quad (A1-1)$$

Here $C_{xx}(t_1, t_2)$ is the covariance function, $R_{xx}(t_1, t_2)$ is the correlation function and $E(X_t)$ is the expected value.

If these processes are zero mean, then linear independence implies

$$R_{xx}(t_1, t_2) = 0. \quad (A1-2)$$

For the system with "in-phase/quadrature" components the objective is to see under which conditions the two signal paths are linearly independent, see Figure A1.1. Denote the output as $z(t)$, the $\cos \omega t$ component as $x(t)$, and the $\sin \omega t$ component as $y(t)$. Now

$$z(t) = x(t) + y(t) \quad (A1-3)$$

In order to determine the output spectrum, one must first obtain the

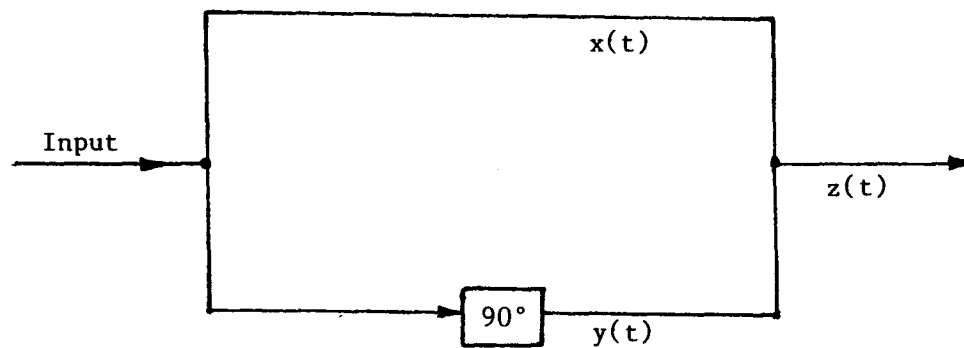


Figure A1.1. Quadrature signal path.

correlation function of $z(t)$, $R_{zz}(t_1, t_2)$. Assuming a stationary process

$$\begin{aligned} R_{zz}(t_1, t_2) &= R_{zz}(\tau) = E[z(t) z(t+\tau)] = E[(x(t)+y(t)) (x(t+\tau)+y(t+\tau))] \\ &= R_{xx}(\tau) + R_{yy}(\tau) + R_{xy}(\tau) + R_{yx}(\tau) \end{aligned} \quad (A1-4)$$

where $\tau = t_2 - t_1$. The resultant spectral density, $S_{zz}(\omega)$ is therefore

$$S_{zz}(\omega) = S_{xx}(\omega) + S_{yy}(\omega) + S_{xy}(\omega) + S_{yx}(\omega). \quad (A1-5)$$

In order to be able to add $S_{xx}(\omega)$ and $S_{yy}(\omega)$ to obtain $S_{zz}(\omega)$, we must have

$$S_{xy}(\omega) = S_{yx}(\omega) = 0 \quad (A1-6)$$

and

$$R_{xy}(\tau) = R_{yx}(\tau) = 0. \quad (A1-7)$$

Now assume a random envelope, $A(t)$. Then

$$\begin{aligned} R_{xy}(\tau) &= E[A(t) \cos \omega t \quad A(t+\tau) \cos \omega(t+\tau)] \\ &= E[A(t) A(t+\tau)] \quad E[\cos \omega t \cos \omega(t+\tau)] \\ &= R_{AA}(\tau) \cos \omega \tau. \end{aligned} \quad (A1-8)$$

Since $\tau = T/4$ (90°), one readily sees that

$$R_{xy}(\tau) = 0. \quad (A1-9)$$

A similar result can be obtained for $R_{yx}(\tau)$. Hence for narrowband results, the two quadrature signal paths are linearly independent and the resultant power spectrum can be obtained through the addition of the individual spectra.

APPENDIX 2

SELECTED CHEBYSHEV TRANSFORMS

Selected Chebyshev transforms are now presented, [6].

We define a narrowband input waveform,

$$u(t) = a(t) \cos[2\pi ft + \alpha(t)]. \quad (\text{A2-1})$$

The output is a function, $v(u)$, of the input, hence

$$v_{\text{out}} = v(a(t) \cos[2\pi ft + \alpha(t)]). \quad (\text{A2-2})$$

Denote the m^{th} -order frequency component of the output to be $v_m(a)$.

The Chebyshev transform evaluates $v_m(a)$ for any given $v(u)$.

Table A2-1 presents several relevant transform pairs.

TABLE A2-1

$v(u)$	$v_m(a)$	Blachman's transform number, [6]
$u^n; n=0,1,2,\dots$	$2 \binom{n}{1/2(n-m)} (a/2)^n$ $m=n, n-2, n-4, \dots, 0$ 0 Otherwise	T5
$\sin u$	$(-1)^{(m-1)/2} 2 J_m(a)$ $m \text{ Odd}$ 0 Otherwise	T7
$\sinh u$	$2 I_m(a)$ $m \text{ Odd}$ 0 Otherwise	T10

**The binomial coefficient $\binom{n}{r}$ is generalized as

$$\frac{\Gamma(n+1)}{\Gamma(r+1) \Gamma(n-r+1)}$$


It vanishes whenever r is a negative integer.

APPENDIX 3

5082-3080 PIN DIODE SPECIFICATIONS

HEWLETT  PACKARD
COMPONENTS

PIN DIODES FOR RF SWITCHING AND ATTENUATING

5082-3001/02
HPND-4165/66 
5082-3039(1N5719)
5082-3042/43
5082-3077
5082-3080 (1N5767)
5082-3081
5082-3168/88

Features

- LOW HARMONIC DISTORTION
- LARGE DYNAMIC RANGE
- LOW SERIES RESISTANCE
- LOW CAPACITANCE
- LOW TEMPERATURE COEFFICIENT
- Typically Less Than 20% Resistance Change from 25°C to 100°C

Description / Applications

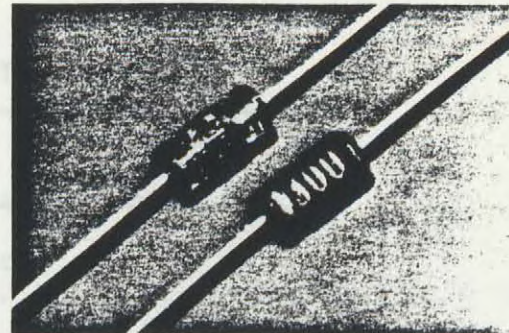
These general purpose switching diodes are intended for low power switching applications such as RF duplexers, antenna switching matrices, digital phase shifters, and time multiplex filters. The 5082-3168/3188 are optimized for VHF/UHF bandswitching.

The RF resistance of a PIN diode is a function of the current flowing in the diode. These current controlled resistors are specified for use in control applications such as variable RF attenuators, automatic gain control circuits, RF modulators, electrically tuned filters, analog phase shifters, and RF limiters.

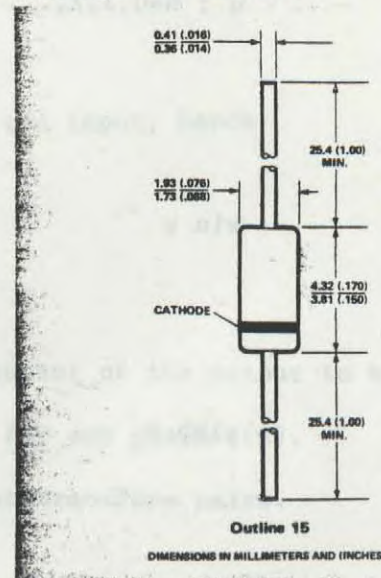
	Lead Finish	Body Finish
5082-3001/02	Tin	Painted
HPND-4165/66	Tin	Painted
5082-3039 (1N5719)	Tin	Painted
5082-3042/43	Gold	Painted
5082-3077	Tin	Clear
5082-3080 (1N5767)	Tin	Clear
5082-3081	Tin	Clear
5082-3168/88	Tin	Clear

Mechanical Specifications

The HP Outline 15 package has a glass hermetic seal with dumet leads. The leads on the Outline 15 package should be restricted so that the bend starts at least 1/16 inch (1.6mm) from the glass body. With this restriction, Outline 15 package will meet MIL-STD-750, Method 2036, Conditions A (4 lbs., 1.8 kg.), tension for 30 minutes; and E. The maximum soldering temperature is 230°C for five seconds. Typical package inductance and capacitance are 2.5 nH and 0.13pF, respectively. Marking is by digital coding with a cathode band.



Package Dimensions



Maximum Ratings at $T_{CASE} = 25^{\circ}C$

Junction Operating and Storage

Temperature Range -65°C to +150°C

Operation of these devices within the above temperature ratings will assure a device Mean Time Between Failure (MTBF) of approximately 1×10^7 hours.

Power Dissipation 250mW
(Derate linearly to zero at 150°C)

Peak Inverse Voltage (PIV) V_{BR}

RF Current Controlled Resistor Diodes Electrical Specifications at $T_A = 25^\circ\text{C}$

Part Number	Minimum Effective Carrier Lifetime τ	Minimum Breakdown Voltage V_{BR}	Maximum Residual Series Resistance R_S	Maximum Total Capacitance C_T	High Resistance Limit, R_H		Low Resistance Limit, R_L		Maximum Difference in Resistance vs. Bias Slope, Δx
					Min.	Max.	Min.	Max.	
HPND-4165	100	100	1.5	0.3	1100	1660	16	24	.04
HPND-4166	100	100	1.5	0.3	830	1260	12	18	.04
5082-3080*	1300(typ)	100	2.5	0.4	1000	—	—	8**	—
5082-3081	2000(typ)	100	3.5	0.4	1600	—	—	8**	—
Units	ns	V	Ω	pF	Ω	Ω	Ω	Ω	—
Test Conditions	$I_F = 50\text{mA}$ $I_F = 250\text{mA}$	$V_R = V_{BR}$, Measure $I_F < 10\mu\text{A}$	$I_F = 100\text{mA}$ $f = 100\text{MHz}$	$V_R = 50\text{V}$ $f = 1\text{MHz}$	$I_F = 0.01\text{mA}$ $f = 100\text{MHz}$	$I_F = 1.0\text{mA}$ ** $I_F = 20\text{mA}$ $f = 100\text{MHz}$	Batch Matched $I_F = 0.01\text{mA}$ and 1.0mA $f = 100\text{MHz}$		

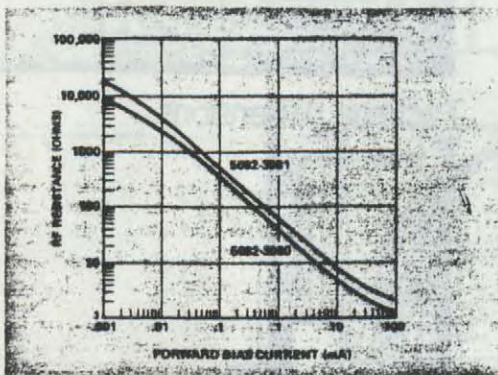


Figure 5. Typical RF Resistance vs. Forward Bias Current.

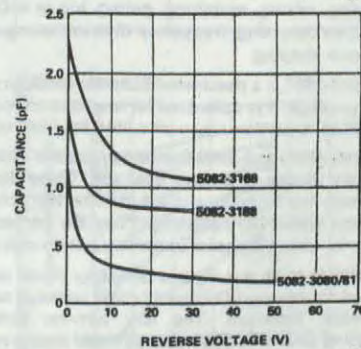


Figure 7. Typical Capacitance vs. Reverse Voltage 5082-3080, 3081, 3168, 3188.

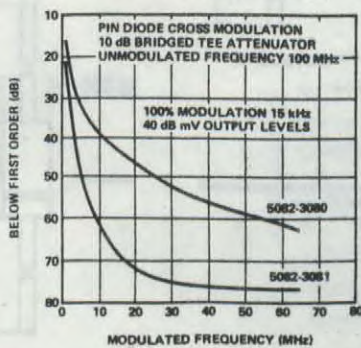


Figure 11. Typical Cross Modulation Distortion.

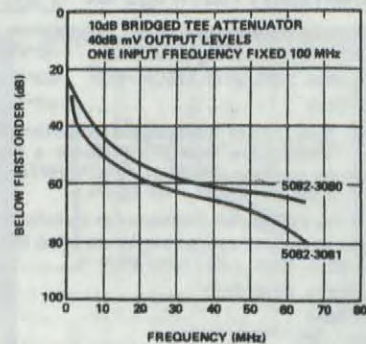


Figure 10. Typical Second Order Intermodulation Distortion.

5082-2810 SCHOTTKY DIODE SPECIFICATIONS



**SCHOTTKY BARRIER DIODES
FOR GENERAL PURPOSE
APPLICATIONS**

- 5082-2301/02/03/05
- 5082-2800(1N5711)
- 5082-2810(1N5712)
- 5082-2811(1N5713)
- 5082-2835
- 5082-2900
- HSCH-1001(1N6263)

Features

- LOW TURN-ON VOLTAGE: .34V AT 1mA**
- PICO-SECOND SWITCHING SPEED**
- HIGH BREAKDOWN VOLTAGE: UP TO 70V**
- UNIFORM FORWARD TRACKING**

Description/Applications

The 5082-2800, 2810, 2811 are passivated Schottky barrier diodes which use a patented "guard ring" design to achieve a high breakdown voltage. They are packaged in a low cost glass package. They are well suited for high level detecting, mixing, switching, gating, log or A-D converting, video detecting, frequency discriminating, sampling and wave shaping.

The 5082-2835 is a passivated Schottky diode in a low cost glass package. It is optimized for low turn-on voltage. The 5082-2835 is particularly well suited for UHF mixing.

The 5082-2300 and 2900 Series devices are unpassivated Schottky diodes in a glass package. These diodes have extremely low 1/f noise and are ideal for low noise mixing, and high sensitivity detecting. They are particularly well suited for use in Doppler or narrow band video receivers.

The HSCH-1001 is a Hybrid Schottky diode sealed in a rugged double stud Outline 12 glass package suitable for automatic insertion. The low turn-on voltage, fast switching speed, and low cost of these diodes make them ideal for general purpose switching.

Application Bulletins 13, 14, 15, and 16 describe applications in which these diodes are used for speed up of a transistor, clipping, clamping, and sampling, respectively.

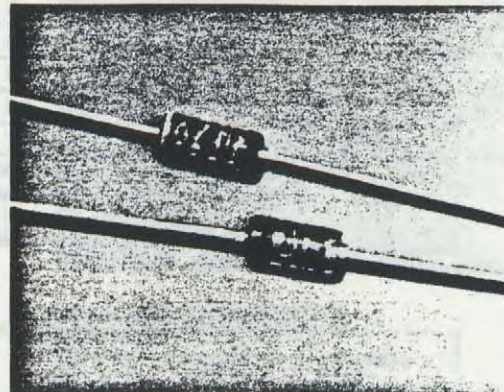
Maximum Ratings at T_{CASE} = 25°C

Junction Operating and Storage Temperature Range	
5082-2305, 2301, 2302, 2303, 2900	-60°C to +125°C
5082-2800, 2810, 2811, HSCH-1001	-65°C to +200°C
5082-2835	-60°C to +150°C

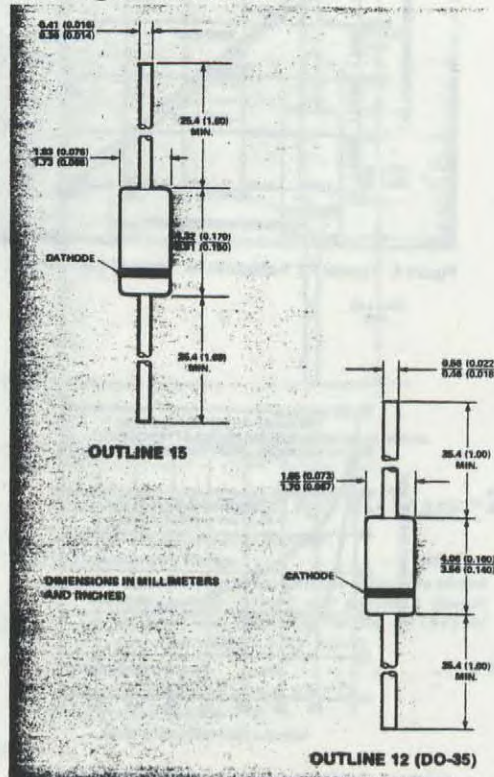
Operation of these devices within the above temperature ratings will assure a device Mean Time Between Failure (MTBF) of approximately 1 x 10⁷ hours.

DC Power Dissipation (Measured in an infinite heat sink)	
Derate linearly to zero at maximum rated temperature	
5082-2305, 2301, 2302, 2303, 2900	125 mW
5082-2800, 2810, 2811	250 mW
5082-2835	150 mW
HSCH-1001	400 mW

Peak Inverse Voltage V_{BR}



Package Dimensions



SCHOTTKY BARRIER DIODES & HIGH CONDUCTANCE DIODES

Electrical Specifications at $T_A=25^\circ\text{C}$

Part Number 5082-	Package Outline	Minimum Breakdown Voltage V_{BR} (V)	Maximum Forward Voltage V_F (mV)	$V_F=1\text{V}$ Max at Forward Current I_F (mA)	Maximum Reverse Leakage Current		Maximum Capacitance C_T (pF)
					I_R (nA)	at V_R (V)	
2800 ✓	15	70	410	15	200	50	2.0
1N5711(1)	15	70	410	15	200	50	2.0
2305	15	30	400	75	300	15	1.0
2301(2)	15	30	400	50	300	15	1.0
2302(2)	15	30	400	35	300	15	1.0
2303(2)	15	20	400	35	500	15	1.0
2810 ✓	15	20	410	35	100	15	1.2
1N5712(1)	15	20	550	35	150	16	1.2
2811	15	15	410	20	100	8	1.2
1N5713(1)	15	15	410	20	100	8	1.2
2900	15	10	400	20	100	5	1.2
2835	15	5*	340	10†	100	1	1.0
H5CH-1001(1) (1N6263) ✓	12 (DO-35)	60	410	15	200	50	2.2
Test Conditions		$I_R = 10 \mu\text{A}$ * $I_R = 100 \mu\text{A}$	$I_F = 1 \text{ mA}$	† $V_F = .45\text{V}$			$V_R = 0 \text{ V}$ $f = 1.0 \text{ MHz}$

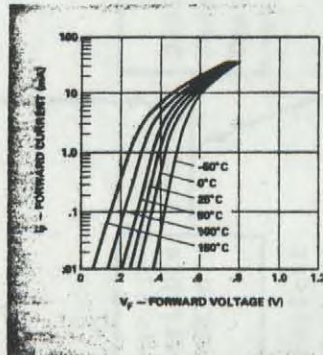


Figure 5. I-V Curve Showing Typical Temperature Variation for the 5082-2810 or 1N5712 Schottky Diode.

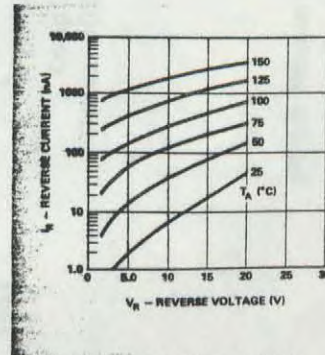


Figure 6. (5082-2810 or 1N5712) Typical Variation of Reverse Current (I_R) vs. Reverse Voltage (V_R) at Various Temperatures.

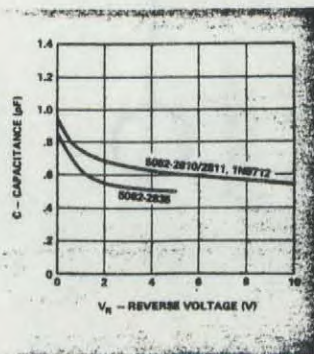


Figure 13. Typical Capacitance (C) vs. Reverse Voltage (V_R).

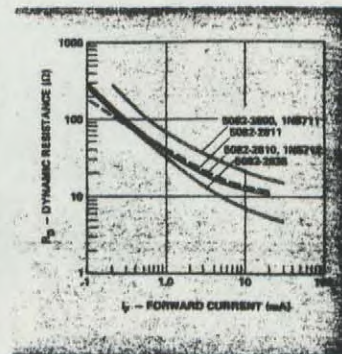
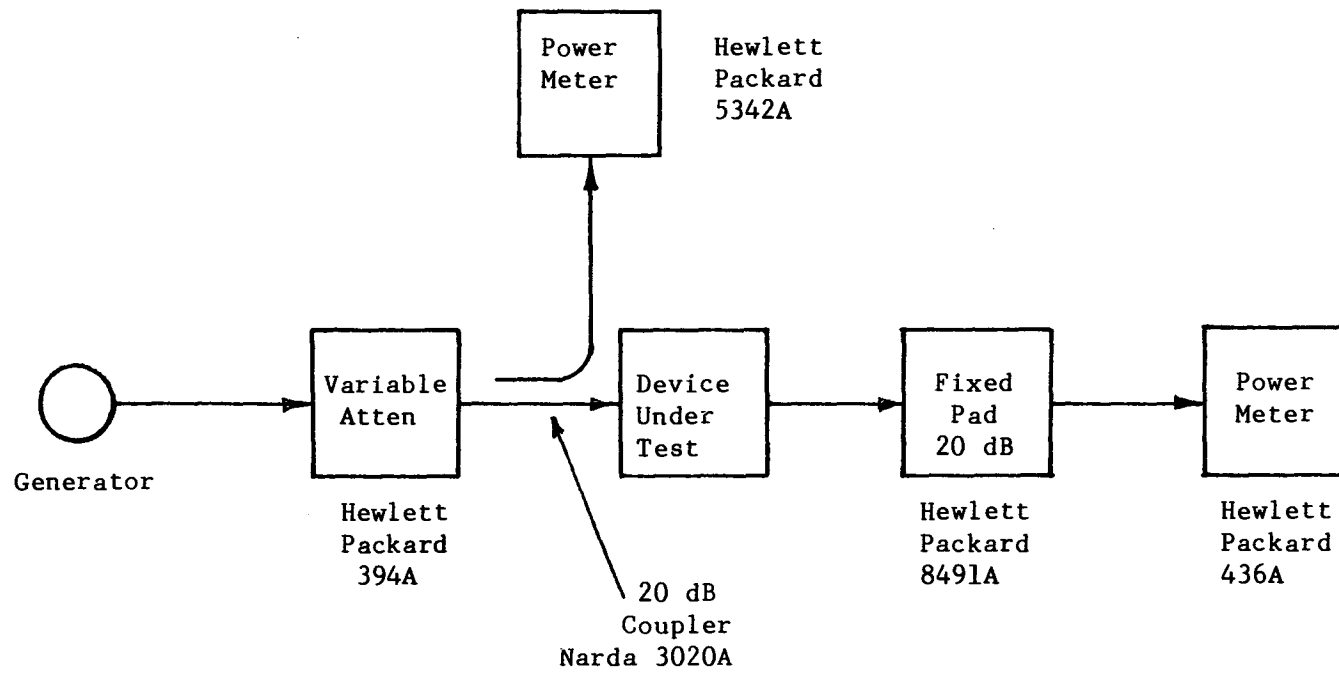


Figure 14. Typical Dynamic Resistance (R_D) vs. Forward Current (I_F).

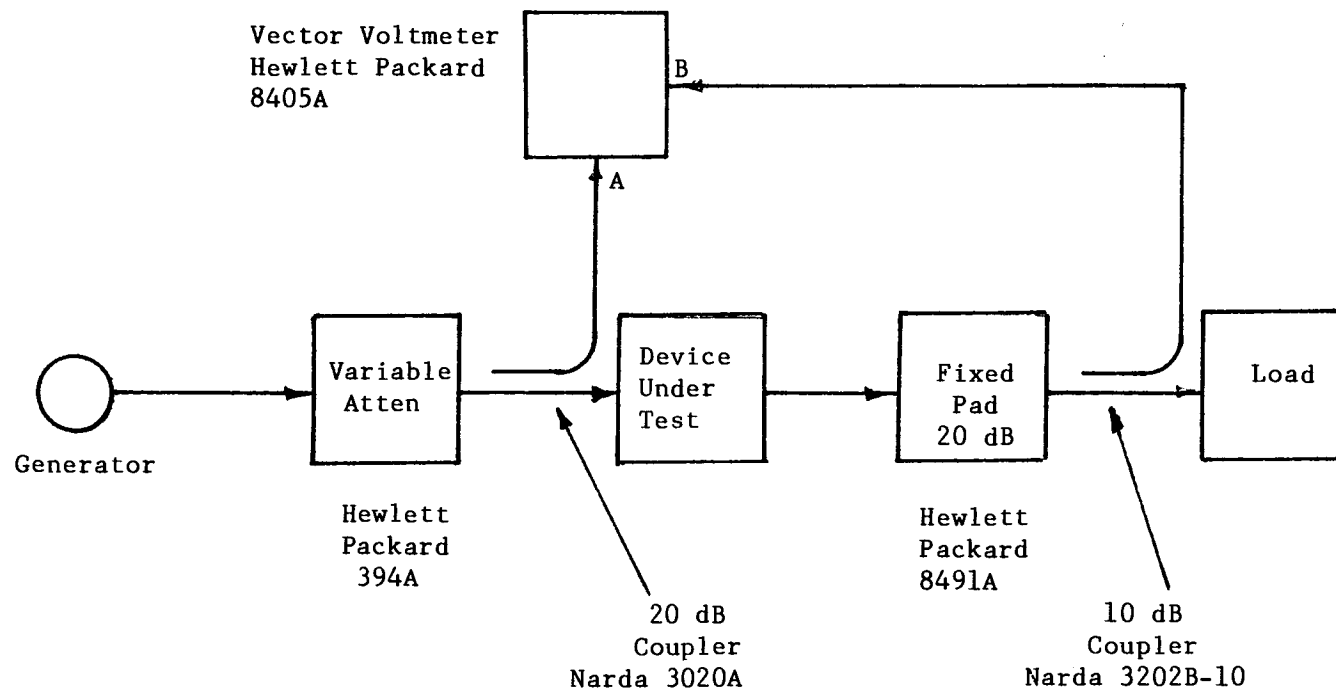
Mechanical Specifications

	<u>Outline 15</u>	<u>Outline 12 (DO-35)</u>
Lead Material:	Dumet	Dumet
Lead Finish:	2800 Series: Tin 2300, 2900 Series: Gold	Tin
Maximum Soldering Temperature:	230° C for 5 sec.	260° C for 10 sec.
Minimum Lead Strength:	4 lb. Pull	10 lb. Pull
Typical Package Inductance:	2800 Series: 2.0 nH 2300, 2900 Series: 3.0 nH	1.8 nH
Typical Package Capacitance:	2800 Series: 0.2 pF 2300, 2900 Series: 0.07 pF	0.25 pF

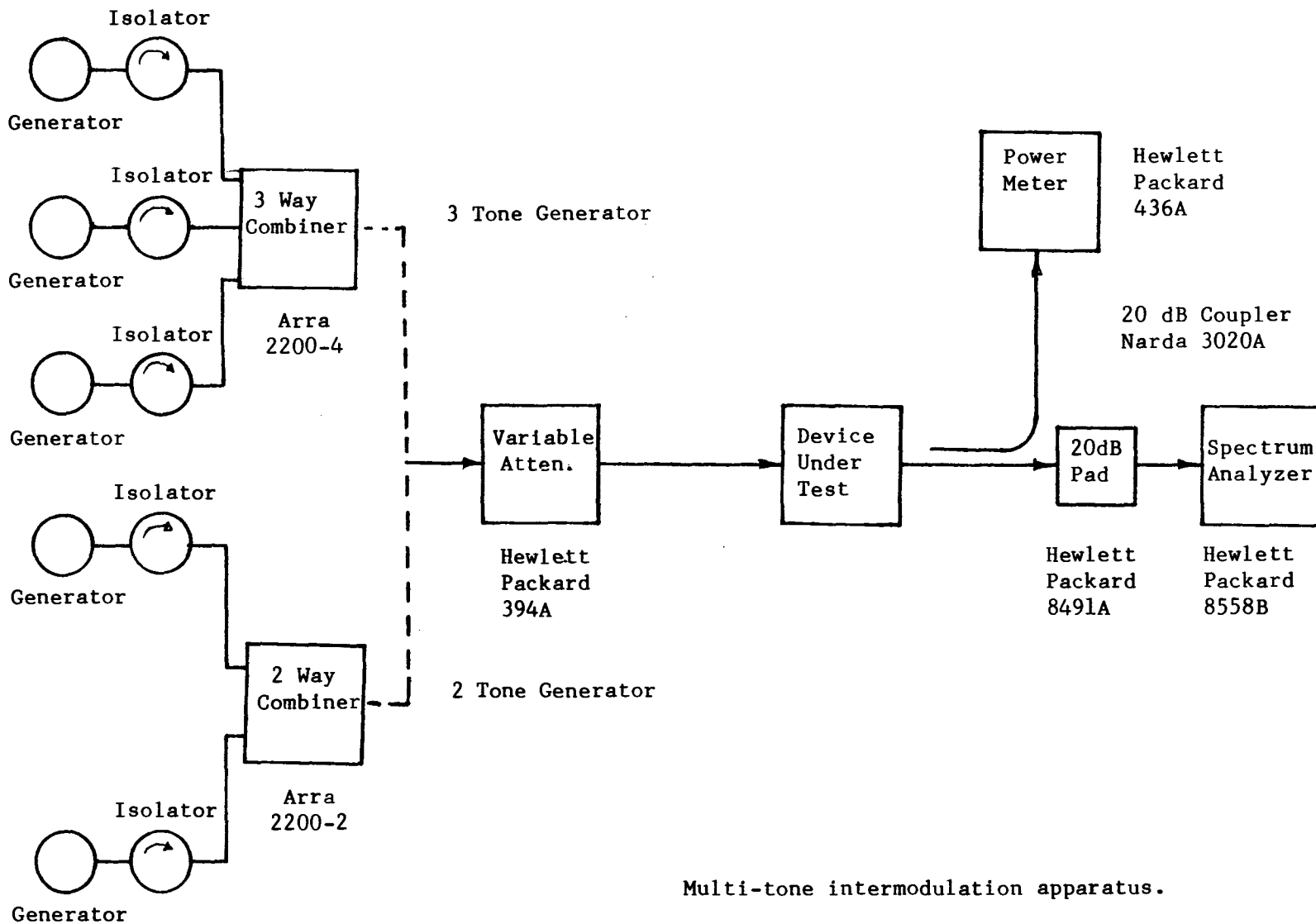
The leads on the Outline 15 package should be restricted so that the bend starts at least 1/16 inch from the glass body.



AM-AM Measurement Apparatus.



AM-PM Measurement Apparatus.



Multi-tone intermodulation apparatus.

APPENDIX 5

AMPLIFIER SPECIFICATIONS

Amplifiers, Broadband

High Power (+ 30 dBm)



ZHL SERIES

ZHL-A SERIES

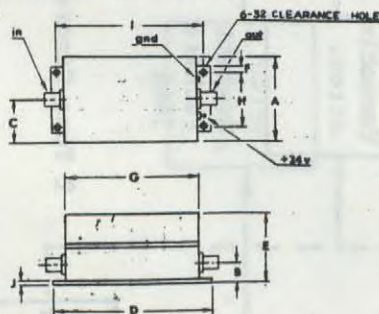
MODEL	FREQUENCY	Z (Ohms)	COST
ZHL-1A	2 MHz - 500 MHz	50	\$199 (1-9)
ZHL-2	10 MHz - 1000 MHz	50	\$349 (1-9)
ZHL-2-8	10 MHz - 1000 MHz	50	\$449 (1-9)
ZHL-2-12	10 MHz - 1200 MHz	50	\$524 (1-9)
ZHL-3A	0.4 MHz - 150 MHz	50	\$199 (1-9)
ZHL-32A	50 KHz - 130 MHz	50	\$199 (1-9)

DESCRIPTION — The ZHL RF power amplifiers are capable of providing approximately 1 watt of power output over a broad frequency range from 50 KHz to 1200 MHz. Using an ultra linear Class A design, these amplifiers are offered with a wide selection of gain, 16dB to 27dB minimum, over their full frequency range. Gain flatness is typically within ± 0.5 dB.

The ZHL is unconditionally stable and can be connected to any load impedance without amplifier damage or oscillation. Having a two or three stage design, and incorporating a highly reliable power output transistor enables the ZHL to be designed for reliability of performance.

BNC connectors are supplied. Housed in a $\frac{3}{16}$ inch thick aluminum case, the ZHL is constructed to withstand tough environments. This rugged case includes a hefty heat sink as an integral part of the case construction.

The high performance ZHL is offered at a remarkable price of $\frac{1}{2}$ to $\frac{1}{3}$ the cost of competitive units.

DIMENSIONS AND CONNECTIONS**ZHL**

ZHL	A	B	C	D	E	F	G	H	I	J
IN.	2.60	.58	1.30	4.75	2.21	.23	4.00	1.54	4.375	.09
CM.	6.60	1.47	3.30	12.07	5.61	.58	10.16	3.91	11.113	.23

BNC (std), SMA on request, add \$10 to unit cost.

WEIGHT:

ZHL 400 grams .88 lbs.

NATIONAL STOCK NO.MCL MODEL NSN
ZHL-1A 6130-01-088-2322**FEATURES**

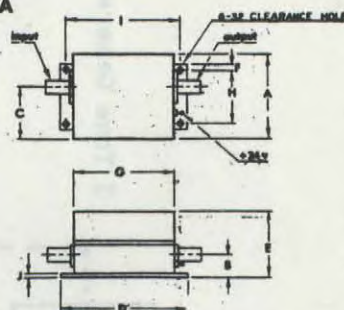
- High Power: 1 watt output
- Broadband: 50 KHz to 1200 MHz
- Compact
- Connectors: BNC (SMA Add \$10 to unit price)
- Price: From \$199 (1-9)
- Very Flat Frequency Response: ± 0.5 dB ty
- Self Contained Heat Sink

APPLICATIONS

- Increase the output power of signal generator
- Intermodulation testing of components
- Broadband, high level isolators
- Provide linear gain in signal processing systems

ABSOLUTE MAXIMUM RATINGS

- Total Input Power: +20 dBm when output loaded, +10 dBm when output not loaded.
- DC Supply Voltage: +24V
- Operating Temperature: 0°C to +65°C
- Storage Temperature: -55°C to +100°C

ZHL-A

ZHL-A	A	B	C	D	E	F	G	H	I	J
IN.	2.60	.665	1.60	3.75	1.84	.187	3.00	1.625	3.375	.09
CM.	6.60	1.69	4.06	9.52	4.67	.47	7.62	4.13	8.57	.23

Connectors: BNC (std), SMA on request, add \$10 to unit cost.

WEIGHT:

ZHL-A 220 grams 49 lbs.

Mini-Circuits 2525 E. 74th St., Brooklyn, NY 11220 (718) 794-2200 Fax: (718) 794-2201
M-38

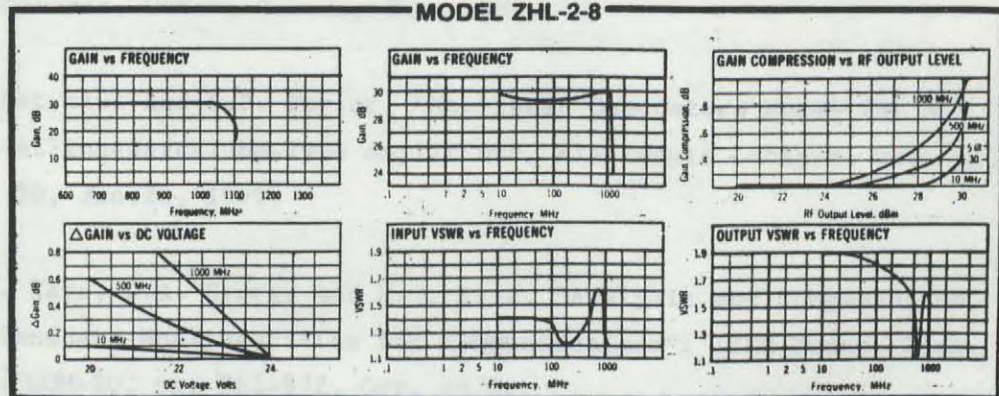
Amplifiers, Broadband

High Power (+ 30 dBm)

Model No.	Frequency Range MHz	Gain dB	Gain Flatness dB	Maximum Power Output dBm @ 1dB Compression	Noise Figure dB	Intercept Point 3rd Order	Impedance Ohms		VSWR, Max.		DC Power	
							Input	Output	Input	Output	Voltage	Current
ZHL-2-8	10-1000	27 Min.	±1.0 Max.	+29 Min.	10 Typ.	+38 Typ.	50	50	2:1	2:1	+24V	0.6A
ZHL-2-12	10-1200	24 Min.	±1.0 Max.	+29 Min.*	10 Typ.	+38 Typ.	50	50	2:1	2:1	+24V	0.75A
ZHL-3A	0.4-150	24 Min.	±1.0 Max.	+29.5 Min.	11 Typ.	+38 Typ.	50	50	2:1	2:1	+24V	0.6A
ZHL-32A	0.05-130	25 Min.	±1.0 Max.	+29 Min.	10 Typ.	+38 Typ.	50	50	2:1	2:1	+24V	0.6A

*+28.5 dBm from 1000-1200 MHz.

MODEL ZHL-2-8



REFERENCES

- [1]. X.T. Vuong and A.F. Guibord, "Modelling of Nonlinear Elements Exhibiting Frequency-Dependent AM/AM and AM/PM Transfer Characteristics", Canadian and International Satellite Communications Conference, Ottawa Canada, June 1983.
- [2]. P. Hetrakul and D.P. Taylor, "Nonlinear Quadrature Model for a Travelling-Wave-Tube-Type Amplifier", Electronic Letters, Vol. 11, pp. 50, Jan.23, 1975.
- [3]. A.R. Kaye, D.A. George and M.J. Eric, "Analysis and Compensation of Bandpass Nonlinearities for Communications", IEEE Trans. Comm., Vol. COM-20, pp. 965-972, Oct. 1972.
- [4]. D. Weiner and J. Spina, "Sinusoidal Analysis and Modelling of Weakly Nonlinear Circuits", New York, Van Nostrand Reinhold Co., 1980.
- [5]. A.A.M. Saleh, "Frequency-Independent and Frequency-Dependent Nonlinear Models of TWT Amplifiers", IEEE Trans. Comm., Vol. COM-29, No. 11, pp. 1715-1720, Nov. 1981.
- [6]. N.M. Blachman, "Detectors, Bandpass Nonlinearities, and Their Optimization: Inversion of the Chebyshev Transform", IEEE Trans. Info. Theory, Vol. IT-17, No. 4, pp. 398-404, July 1971.
- [7]. D.R. Green, "Characterization and Compensation of Nonlinearities in Microwave Transmitters", IEEE Globecomm 82, pp. 213-217.

- [8]. J. King, "The Third Generation", Orbit, pp.12-18, Nov./Dec. 1980.
- [9]. H. Seidel, "A Microwave Feed-Forward Experiment", BSTJ, Vol. 50, No. 9, pp. 2879-2916, Nov. 1971.
- [10]. T.J. Bennett and R.F. Clements, "Feedforward- an alternate approach to amplifier linearization", The Radio and Electronic Engineer, Vol. 44, No. 5, pp. 257-262, May 1974.
- [11]. A. Prochazka and R. Neumann, "Design of a Wideband Feedforward Distribution Amplifier", IEEE Trans. On Cable Television, Vol. CATV-5, No.2, pp. 72-79, April 1980.
- [12]. P. Hetrakul and D.P. Taylor, "Compensators for Bandpass Nonlinearities in Satellite Communications", IEEE Trans. On Aerospace and Electronic Systems, Vol. AES-12, No. 4, pp. 509-514, July 1976.
- [13]. L. Kahn, "Single-Sideband Transmission by Envelope Elimination and Restoration", Proc. of the IRE, Vol. 40, pp. 803-806, July 1952.
- [14]. D.C. Cox, "Linear Amplification with Nonlinear Components", IEEE Trans. Comm., Vol. COM-22, No. 12, pp. 1942-1945, Dec. 1974.
- [15]. P.T. Ho, M.D. Rubin and J.G. Wherry, "Solid-State Power Amplifiers in Communications Satellites", 7th Communications Satellite Systems Conf., San Diego, Calif., pp. 182-187, 1978.
- [16]. E.T. Ebersol, "L-Band Transistor Amplifier Dishes Out 1 kW", Microwaves, Dec. 1972.
- [17]. H.W. Bode, "Network Analysis and Feedback Amplifier Design", Van Nostrand Co., Princeton, New Jersey, 1945.

- [18]. R. Hejhall, "Systemizing RF Power Amplifier Design", Motorola Applications Note AN-282A.
- [19]. H.S. Black, U.S. Patent 1,686,792, issued October 9, 1929.
- [20]. Y.S. Cho, "Sensitivity Analysis of Feed-Forward Amplifier", Proc. Intl. Conf. Comm., pp. 3c-1 - 3c-5, 1974.
- [21]. A. Prochazka, P. Lancaster and R. Neumann, "Amplifier Linearization by Complimentary Pre- or Post-Distortion", IEEE Trans. on Cable Television, Vol. CATV-1, No. 1, pp. 31-39, Oct. 1976.
- [22]. G.W. Holbrook and W.E. Rockwell, "Pre-distortion Correction of Intermodulation Products in Single Sideband Transmitter", IEEE Intl. Electrical and Electronics Conf. Digest, Toronto, Canada, pp. 134-135, Oct. 1971.
- [23]. G.W. Holbrook and L.A. Buckler, "Reduction of Distortion in Broad-Band and Narrow-Band Amplifiers by Complimentary Methods", Trans. Engineering Institute of Canada, EIC-70-CE&A, Vol. 13, pp. I-VII, June 1970.
- [24]. A. Egger, M. Horn, T. Vien, "Broadband Linearization of Microwave Power Amplifiers", European Microwave Conference, pp. 490-494, 1980.
- [25]. C. Bremenson, M. Palazo and R. Neyer, "Linearizing T.W.T. Amplifiers in Satellite Transponders- System Aspects and Practical Implementation", 8th Communications Satellite Systems Conf., Orlando, Fla., pp. 80-89, April, 1980.
- [26]. X.T. Vuong and H.J. Moody, "Realization of Predistortion Compensators of Memoryless Nonlinear Devices", IEEE Intl. Conf. on Comm., Seattle, U.S.A., pp. 33.7.1-33.7-5, June 1980.

- [27]. G. Sato, H. Shibazaki, T. Asai, T. Kurokawa, "A Linearizer for Satellite Communications", IEEE Intl. Conf. on Comm., Seattle, U.S.A., pp. 33.3.1-33.3.4, June 1980.
- [28]. L.F. Gray and J. Van Alstyne, "Application of Broadband Linearizers to Satellite Earth Stations", IEEE Intl. Conf. on Comm., Seattle, U.S.A., pp.33.4.1-33.4.5, June 1980.
- [29]. T. Nojima and Y. Okamoto, "Predistortion Nonlinear Compensator for Microwave SSB-AM System", IEEE Intl. Conf. on Comm., Seattle, U.S.A., pp. 33.2.1-33.2.6, June 1980.
- [30]. R.P. Hecken and R.C. Heidt, "Predistortion Linearization of the AR 6A Transmitter", IEEE Intl. Conf. on Comm., Seattle, U.S.A., pp. 33.1.1-33.1.6, June 1980.
- [31]. L. Couch and J. Walker, "A VHF LINC Amplifier", IEEE Southeastcon, Destin, Florida, pp.122-125, April 1982.
- [32]. D.C. Cox and R.P. Leck, "Component Signal Separation and Recombination for Linear Amplification with Nonlinear Components", IEEE Trans. Comm., Vol. COM-23, No. 11, pp. 1285-1287, Nov. 1975.
- [33]. S.Y. Liao, "Microwave Devices and Circuits", Englewood Cliffs, New Jersey, Prentice-Hall Inc., 1980.
- [34]. D.V. Morgan and M.J. Howes, "Microwave Solid State Devices and Applications", New York, Peter Peregrinus Ltd., 1980.
- [35]. Hewlett Packard application note, "Applications of PIN Diodes", Application note 922.
- [36]. E.J. Wilkinson, "An N-Way Hybrid Power Divider", IRE Trans. MTT, pp. 116-119, Jan. 1960.
- [37]. A. Papoulis, "Probability, Random Variables, and Stochastic Processes", New York, Mc Graw-Hill Book Co., 1965.

- [38]. W.B. Davenport and W.L. Root, "Random Signals and Noise",
New York, Mc Graw-Hill Book Co., 1958.

10. 11. 1911

